Evaluation of Criteria and Investigation of Fatigue Failure Characteristics of Precast Unreinforced Concrete Arch Panel Decks

by

Dennis D. Sargent, P.Eng.
B.A.Sc. University of British Columbia, 1983

A Thesis Submitted in Partial Fulfillment of the Requirements for the Degree of

MASTER OF APPLIED SCIENCE

in the Department of Mechanical Engineering

We accept this thesis as conforming
to the required standard

© Dennis D. Sargent, P.Eng. 2004
University of Victoria

All rights reserved. This thesis may not be reproduced in whole or in part, by photocopy or other means, without the permission of the author.

Supervisor: Dr. James W. Provan

ABSTRACT

Unreinforced concrete arch panel bridge decks have recently been introduced to the highway transportation system in Canada. A common feature of these decks is the development of longitudinal cracks at the midspan between supports. Questions arise concerning the source of these cracks, the integrity of the slabs once the cracks develop and the potential life expectancy of slabs under both service and ultimate loading conditions.

In this study a Forestry Bridge deck consisting of precast unreinforced concrete arch panels is monitored for fatigue loading from logging truck traffic during its first 5 years of service. Coincident with the first year of service, laboratory fatigue loading experiments on a deck simulation of the Forestry Bridge were also conducted. A reliability assessment procedure based upon a damage accumulation algorithm involving Crack Mouth Opening Displacement (CMOD) is proposed. The method demonstrates a rational approach to monitoring which could be adopted in other areas of structural engineering.

Evaluation of Criteria and Investigation of Fatigue Failure Characteristics of Precast Unreinforced Concrete Arch Panel Decks

Dennis D. Sargent, P.Eng.

Table of Contents

Evaluation of Criteria and Investigation of Fatigue Failure Characteristics of Precast Unreinforced Concrete Arch Panel Decks

Dennis D. Sargent, P.Eng.

List of Tables

Evaluation of Criteria and Investigation of Fatigue Failure Characteristics of Precast Unreinforced Concrete Arch Panel Decks

Dennis D. Sargent, P.Eng.

List of Figures or Illustrations

Evaluation of Criteria and Investigation of Fatigue Failure Characteristics of Precast Unreinforced Concrete Arch Panel Decks

Dennis D. Sargent, P.Eng.

Nomenclature

AASHTO	American Association of State Highway and Transportation Officials
CMOD	crack mouth opening displacement
FERIC	Forest Engineering Research Institute of Canada
FRC	fibre-reinforced concrete
FSBDC	Forest Service Bridge Design and Construction
ISIS	Intelligent Sensing for Innovative Structures. A Canadian Network of Centres of Excellence
LRFD	load and resistance factor design
LVDT	linear variable displacement transducer
NSERC	Natural Sciences and Engineering Research Council of Canada
UBC	University of British Columbia
VLSSI	Vaughan Load Supporting Structures Incorporated
C	coefficient of the bridge's concrete
C_c	$aver(\log C_i')$
C'	$C\ \pi^{m/2}\ D^{m/2}$
C_i'	a specific crack's C'
D	a constant of proportionality
I1, I2	first and second inspections
R^*	a specified level of reliability; e.g., $R^* = 0.98$
R_{zz}	auto-correlation or covariance function
$X(n)$	a non-negative, stationary lognormal stochastic process
$Z(n)$	$\log(X(n))$; the normal random process based upon $X(n)$
a	half crack length
f'c	28 day compressive strength of concrete
i	the identification of a specific crack; e.g., $i = 1, \cdots, \eta,\ \eta = 23$
m	exponent of the bridge's concrete
n	index identifying each fully loaded truck axle set crossing the bridge
Δk	stress intensity factor range
$\Delta\sigma$	nominal stress range
$\Gamma(n)$	$\log\left(\Delta\sigma\sqrt{\delta(n)}\right)$
$\Psi(n)$	$\log\left(d\delta/dn\right)$
δ	crack mouth opening displacement

δ_1^i δ_2^i	CMOD of individual cracks at inspections I1 and I2
δ_K	the CMOD's knuckle dimension; e.g., δ_K = 3.6mm
$\tilde{\sigma}^2$	a stochastic process' variance
τ	number of truck axle sets crossing bridge span between the I1 and I2 inspections
ξ	correlation parameter of a stochastic process

Evaluation of Criteria and Investigation of Fatigue Failure Characteristics of Precast Unreinforced Concrete Arch Panel Decks

Dennis D. Sargent, P.Eng.

Acknowledgements

A very special acknowledgement and thanks to my supervisor, Dr. James Provan, P.Eng. for his enthusiastic encouragement and support, both during course work and preparation of the thesis. I am particularly indebted to him for his optimism and contribution of time, in spite of other more pressing responsibilities. His ability to recognize the potential for a fatigue reliability assessment of the Forestry Bridge Arch Panel deck, and his contributions to Chapters 6 and 7 and Appendix C of the thesis are greatly appreciated.

My appreciation is equally extended to Dr. Aftab Mufti, P.Eng., my co-supervisor for sharing with me the chance to participate in leading edge research, both in the laboratory and on real engineering structures. His guidance and participation during course and research work has been inspirational. In addition it was only through the concerted effort of Drs. Provan and Mufti that the opportunity was made possible for me to pursue a post-graduate degree in a field of engineering which is directly related to my work, while still maintaining my business and career. For this as well, I am very grateful.

Full acknowledgement goes to the institutions and individuals that made the research possible. These include:

- The Ministry of Forests, Resource Tenures and Engineering Branch, for support of the Arch Panel concept and for locating a bridge site at which to construct the Arch Panel Forestry Bridge. Individuals directly involved included: Ron Davis, P.Eng., Mark Frew, P.Eng., and Gary McClelland, P.Eng. A special thanks to Gary who also administered the construction contract, attended the bridge site during construction

and monitoring, and was instrumental in obtaining truck volumes for development of the load spectrums.

- The University of British Columbia Civil Engineering Department, for the opportunity to participate in observing the laboratory experiment on fatigue loading of the precast Arch Panels.
- The University of Victoria Mechanical Engineering Department which provided the basis for the Forestry Bridge monitoring and the UBC laboratory experiment to be combined into a meaningful research project.

I also wish to express my gratitude to Drs. Leslie Jaeger and Afzal Suleman for their instruction in Elementary Theory of Elastic Plates and Finite Element Analysis. Their strength in mathematics applied to engineering is most admirable and through their instruction, my ability to comprehend more advanced topics in engineering has been improved. My appreciation is extended as well to Dr. Baidar Bakht who, together with Drs. Mufti and Jaeger introduced me to their world of research in new developments, which includes the Arch Panel concept. The term "Arch Panel", which is used throughout this thesis is a registered trademark of VLSSI. Their permission to use this term is much appreciated. Thank you to Sue Stock, Matt Dybwad, E.I.T, and Dennis Mitchell for assisting with word processing and preparation of tables and figures in the thesis.

The research extended over a period of six years. Consequently, there were many people involved in the program who, unfortunately, are too numerous to be individually recognized in this document. Nevertheless, their contribution is greatly acknowledged for their efforts. These include, but are not limited to: professors and technicians, fellow researchers, design firms and designers, government employees, contractors, fabricators, forest industry personnel and trucking companies.

Last, but foremost, I would like to thank my wife Sue and my sons Michael, Dustin, Derek and David for the time I spent to undertake this Masters program; much of which would otherwise have been spent with them.

Evaluation of Criteria and Investigation of Fatigue Failure Characteristics of Precast Unreinforced Concrete Arch Panel Decks

Dennis D. Sargent, P.Eng.

Dedications

To my wife, Sue, who by being who she is, inspires me to press on. And to my sons Michael, Dustin, Derek and David.

Evaluation of Criteria and Investigation of Fatigue Failure Characteristics of Precast Unreinforced Concrete Arch Panel Decks

Dennis D. Sargent, P.Eng.

1.0 Introduction and Statement of Problems

Throughout North America, and certainly elsewhere in the developed world, large expenditures are spent annually on resurfacing steel-reinforced concrete deck slabs of bridges. A prime contributor to the need for resurfacing is the corrosion of reinforcing steel. Moisture penetrating the slab comes into contact with the reinforcing and, in combination with oxygen, provides a condition in which the corrosion process can begin. The introduction of road salts for maintenance purposes accelerates the process.

Steel expands in the order of 8 to 15 times by volume when it corrodes, thus losing its bond with the surrounding concrete and causing the concrete to deteriorate. Once the concrete breaks down, exposure to further moisture is enhanced and the problem is increased.

Numerous means have been employed to mitigate the deterioration of reinforced concrete bridge decks due to the corrosion of reinforcing steel. Some methods used in the past 20 years include:

- Increase concrete cover
- Use of higher performance concretes
- Introducing protective measures for the reinforcing (i.e. epoxy coating, galvanizing, use of stainless steel)
- Substituting alternative reinforcing materials, i.e. glass fibre reinforced polymer (GFRP) or carbon fibre reinforced polymer (CFRP)
- Liquid penetrating sealer
- Cathodic protection

These methods, all of which offer some degree of success, vary in cost and practicality. Nevertheless, in spite of attempts to reduce the problems caused by corrosion of steel deck reinforcing, it is still being utilized in large quantities throughout the continent on bridge decks and expenditures on deck resurfacing remain substantial. In British Columbia alone, deck resurfacing on average costs in the order of $5 M per annum in recent years [1]. Costs typically range from $200/m^2 to $370/m^2 of bridge deck area [2].

A 1994 study performed by the Ministry of Transportation for the 1992/93 season indicated bridges for that time period with greater than 1,000 m^2 of deck area had an average resurfacing cost of $150/m^2. For bridges with smaller deck areas the costs increased to as high as $300/m^2 to $500/m^2 [3]. Not factored into these costs is the economic loss resulting from rerouting, detaining and controlling traffic during the resurfacing process.

In recent years the conventional philosophy upon which bridge deck slabs were designed was challenged as a result of laboratory and field investigations [1]. This led first to a reduction in reinforcing steel in deck slabs, and eventually to the elimination of internal reinforcing in the slab altogether. The potential for such a shift in design philosophy is paradigm in nature [2] and could ultimately have a profound affect on the economics of the design and maintenance of bridge decks. Nevertheless, although the theory upon which this new design philosophy (referred to herein as Arch Panel design) is ultimately sound, practical field application of the technique has not been entirely without serviceability concerns. In most instances, particularly in cast-in-place applications, the concerns appear to be largely one of perception. In at least one other circumstance, that of application to precast construction, these concerns require greater attention to longer

---

[1] Private communication: Keith Kazakoff, Bridge Project Supervisor, BC Ministry of Transportation, dated March 11, 2004.
[2] Private communication: Connie Nicoletti, Senior Rehabilitation, Construction & Paving Project Manager, BC Ministry of Transportation, dated March 12 and 15, 2004.
[3] Concrete Bridge Deck Renewal, Ministry of Transportation & Highway Bridge Engineering Branch, June 1994.

term serviceability problems. In neither case should this imply that Arch Panel design philosophies should be ignored nor abandoned.

Examples abound throughout engineering history of design improvements based on previous failures. The reluctance to embrace the concept of Arch Panel design has so far been based on a perception of the significance of cracks which develop in the slab, not on the functional failure of the slabs themselves. The problem then lies in the identification of the nature of these cracks and to conceive of a method, within the intent of the design philosophy, which will aid in predicting the growth of the cracks and consequently the ultimate performance of the slabs.

A description of the research performed to that effect is the focal theme of this thesis. It is proposed that the nature of investigation, which consists of monitoring the performance of an existing structure in order to predict future behaviour and ultimate service life, can be extended to other areas of structural engineering. The preliminary research performed, which attempts to address this very problem, is the paramount theme of this thesis.

Chapter 2 reviews the existing literature and criteria pertaining to the design of Precast Unreinforced Concrete Arch Panel Deck Slabs (referred to as Precast Arch Panels). Here, the philosophy of design and behaviour under ultimate concentrated loading of the arch panel deck is described. Also discussed is the actual behaviour of traditional internal slab reinforcing relative to previously held notions of the behaviour based on bending theory. A comparison is made with the tie in to an arch panel deck.

Based upon the findings presented in Chapter 2, a detailed description of the objectives of this presentation is given in Chapter 3. Specifically, it explains the need for both investigating the behaviour of fatigue cracks propagating in precast arch panels and assessing the reliability of such structures.

Two full scale research projects are described in Chapter 4. One was conducted under laboratory conditions with controlled instrumentation to monitor loading and measure the

progression of crack growth in two arch panel deck slabs. This experiment simulated actual conditions and took place over several months. The other involved a real forestry bridge on a route travelled by logging vehicles and took place over a five year period. Both the actual loading on the bridge and the crack growth were monitored after the first and fifth years of service on eight precast arch panels. The number and types of logging trucks that used this bridge over the five year interval were also estimated. The geometric and material properties of the slabs in the two different research projects were almost identical. The results of both these investigations are presented in a concise manner under their respective sections in Chapter 4; notably the pattern of slab cracking sustained under simulated laboratory and actual field conditions following prolonged exposure to cyclic loading.

The primary objective of Chapter 5 is to develop a preliminary version of a possible "standard" deck loading signature or spectrum for loaded logging trucks. These signatures are developed on the basis of a knowledge of the loaded truck used in the experimental part of this investigation and the various types of trucks that are commonly used in the logging trucking industry.

An embryonic theory of statistically assessing the reliability of precast arch panels is presented in generic form in Chapter 6. As is shown, the procedure is in itself not limited to such decks and with further development may be applicable to a large class of civil engineering structures that are subjected to fatigue type loading. Chapter 7 presents the application of this suggested procedure to the forestry precast arch panel deck currently in use in British Columbia.

The final Chapter presents conclusions and, since a significant part of this thesis may be viewed as being exploratory, suggestions for future research.

2.0 Review of Existing Criteria Pertaining to the Design of Concrete Arch Panel Deck Slabs

2.1 Design Philosophy (failure mechanism)

It is now fairly well established that an internal arching action develops in the concrete deck slab of slab-on-girder bridges when the deck is subjected to a concentrated load perpendicular to the plane of the slab. The failure mechanism depends on the material properties, geometric properties, nature of the application of the concentrated load (ultimate static v. fatigue serviceability), degree of slab edge confinement and position of load on the slab. Assuming that the material and geometric properties are defined, the remaining variables may be discussed as follows.

2.1.1 Nature of Load

a) Ultimate Static Load

This is defined as the maximum single concentrated load which the slab can resist prior to failing. Failure can consist of either a localized (punching) mode of failure or a more global failure such as bending. In either situation, the slab is no longer capable of its former ultimate resistance under the same load application without remedial repairs.

b) Fatigue Load

Fatigue loading consists of the repetition of a concentrated load, the magnitude of which is some lesser fraction of the ultimate load. The resistance to fatigue which slabs can endure is governed by what may be considered as Serviceability Limit States. These are not as readily defined as Ultimate Limit States and can be subjective in nature. Examples include degree of cracking and deflection.

2.1.2 Slab Edge Confinement

Key to the fundamental concept of developing arching action as the primary mode of ultimate resistance to externally applied loading in a deck slab, is confinement. This has been demonstrated in numerous laboratory experiments for both cast-in-place and precast concrete panels [1], [3]. Confinement improves the in-plane flexural resistance of the slab.

The failure mode in flexure due to a concentrated load at midspan of a simply supported slab which lacks confinement is shown diagrammatically in Figure 2.1. The failure mode of a concrete deck slab with confined edges which is subjected to a concentrated load is shown in Figure 2.2. The failure surface in this instance is similar in appearance to that of a pane of glass which has been penetrated by a small high velocity projectile.

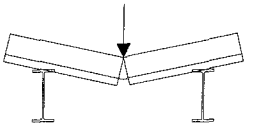

Figure 2.1 -
Bending Failure

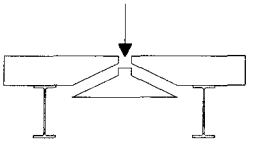

Section of Showing Failure Cone

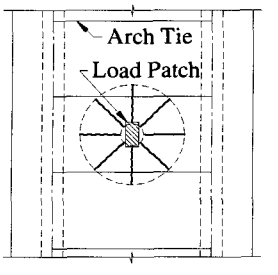

Plan of Radial Cracking Pattern

Figure 2.2 -
Punching Shear Failure

The degree to which the slab is capable of resisting an applied point load perpendicular to the plane of the slab near a free edge is also dependent on the edge restraint as described below.

a) Confined Edges

Slabs with confined edges fully compensate for the loss of in-plane flexural resistance at the free edge. This is achieved in practice by means of enhanced geometric properties at the slab edge or by connecting to laterally restrained edge beams.

b) Unconfined Edges

Slabs with unconfined edges have no provision for additional in-plane flexural reinforcement or support at the free edge. Ultimate resistance to point loading at unconfined edges is typically drastically reduced. Locations where unconfined edges may occur in practice include the ends of slabs on bridges and the free edges of adjoining precast slab panels. Figure 2.3 shows a failed reinforced concrete deck due to lack of edge confinement.

Figure 2.3 - Slab Failure at Unconfined Edge

c) Partially Confined Edges

Slabs with partial confinement are those slabs whose degree of in-plane flexural reinforcement or support at the free edge lies somewhere between being confined and being unconfined.

Confinement in the longitudinal direction of the deck of slab-on-girder bridges is provided by connecting the slab to the girders such that in-plane longitudinal stresses can be resisted by the in-plane flexual stiffness (diaphragm action) of the slab itself. When the slab is terminated, an in-plane restraint mechanism must be introduced to maintain the in-plane stiffness characteristics. Schematic diagrams showing examples of transverse edge stiffening are shown in Figure 2.4. In the transverse direction, slab edge confinement is provided through restraining the relative lateral movement of adjacent supporting girders by means of internal transverse slab reinforcing or external transverse steel straps which are anchored to the girders as described in Section 2.2.

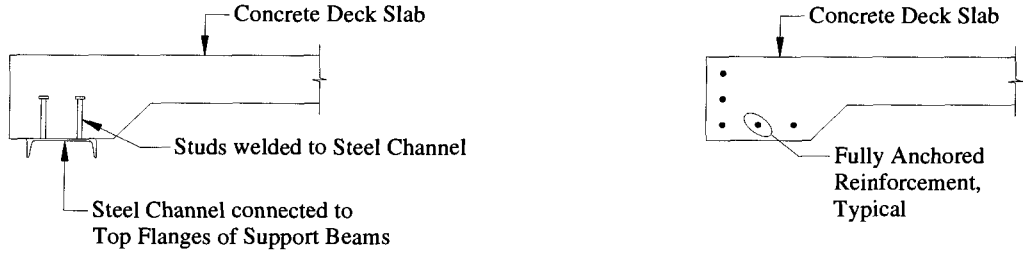

Figure 2.4 - Example Details of Transverse Edge Stiffening

2.1.3 Position of Load

a) Single Static Point Load

Positioning of a single static point load on the slab can affect the ultimate load achieved depending on, for example, its location relative to an unconfined edge, or proximity to vertical supports.

b) Repetitive Loading

Positioning of a single repetitive point load on the slab can affect the Serviceability Limited States and influence the Ultimate Limit States, again depending on its location relative to an unconfined edge or proximity to vertical supports. Behaviour of the slab becomes more complex when subjected to moving wheel loads. Nevertheless, lateral positioning of a moving wheel can influence the applied stresses.

2.2 Method of Reinforcing

2.2.1 Internal Reinforcing

As determined by Dr. Bakht, and further elaborated by Dr. Bakht and Dr. Mufti [5], [6], a reinforced concrete deck slab which is anchored to the supporting girders by means of shear connectors behaves as a tied arch. The concept is shown in Figure 2.5.

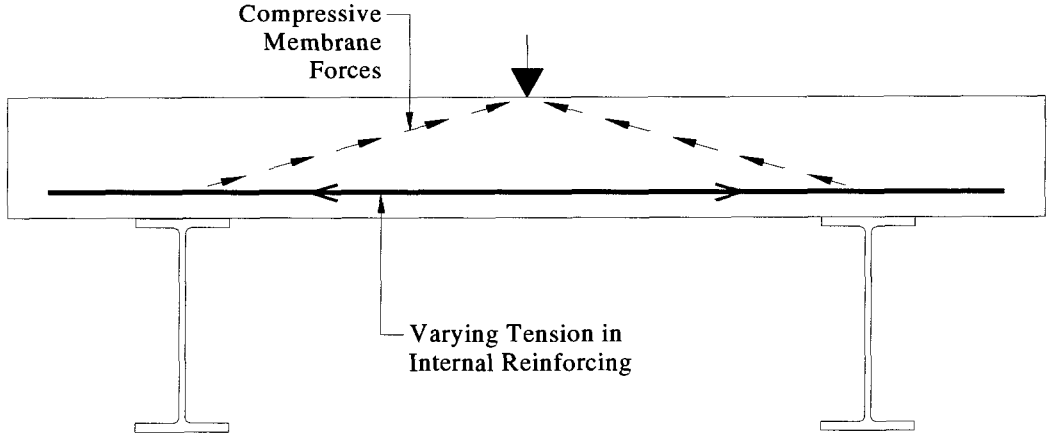

Figure 2.5 - Arching Action in a Conventionally Reinforced Concrete Deck Slab

In fact, it was demonstrated by means of strain gauges placed at intervals across the length of transverse steel reinforcing that the greatest yielding takes place near the slab supports as shown schematically in Figure 2.6. The net tensile force in the bars was gradually transferred to the concrete as the reference section moves toward midspan of the slab, resulting in the tensile force in the reinforcing becoming very small. Were the slab to behave in pure flexure, the shape of the graph would have been more like that given in Figure 2.7.

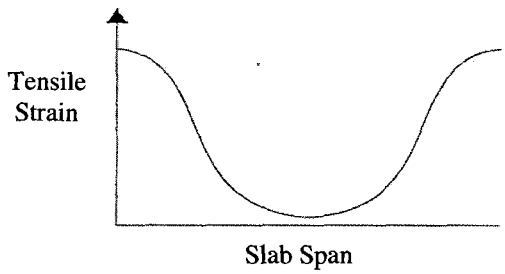

Figure 2.6 - Illustration of Reinforcing Strain in an Internally Reinforced Slab behaving as a Tied Arch

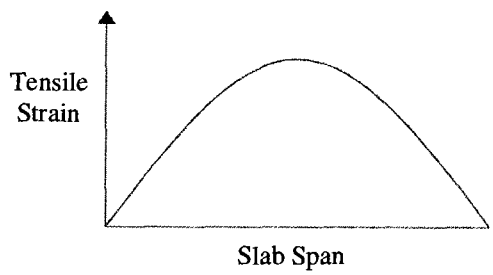

Figure 2.7 - Illustration of Reinforcing Strain in an Internally Reinforced Slab in Pure Bending

2.2.2 External Reinforcing

In recognition of the behaviour of the slab as a tied arch, Mufti et al [1] took the initiative to remove the tie completely from the slab and place it external to the slab surface. The tie is, of course, anchored at each end of the slab span in order to allow the slab to behave as a tied arch. (See Figure 2.8)

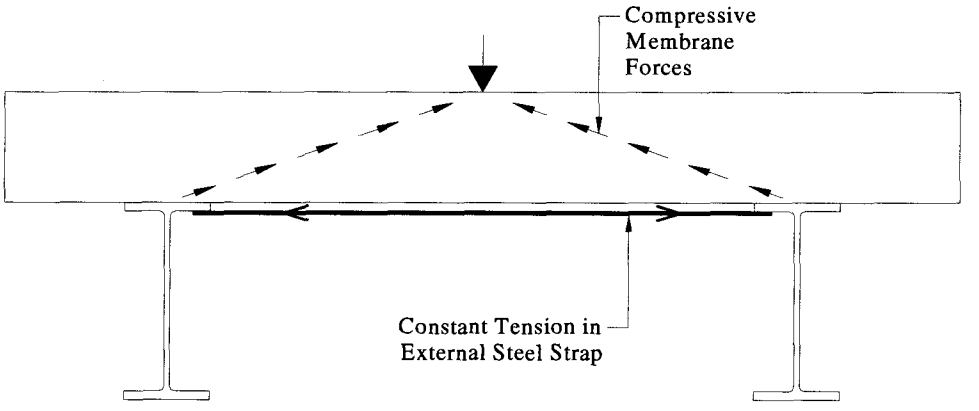

Figure 2.8 - Arching Action in an Externally Reinforced Concrete Arch Panel

The tensile strain in the tie in this situation is constant throughout the length. Various methods of anchorage have been devised to connect the straps at the slab supports. Typical methods utilized in practice include welding the straps directly to the girders or installing studs on the strap which are anchored into the concrete. In either situation both the concrete slab and the strap must be connected to the girder. This type of slab construction is referred to in this thesis as an Arch Panel.

A theory has been developed which predicts the ultimate punching shear capacity of a concrete deck slab which behaves as a tied arch. The ultimate load is calculated through an iterative process which has been made available in a program called PUNCH [4]. To ensure adequate confinement each steel tie must have a minimum cross-sectional area and maximum spacing.

2.3 Present Code Criteria

Conventional principles for design of deck slabs for bridges in Canada were based primarily on bending theory until recent years [7], [8]. These principles were still the method of design outlined in the Standard Specifications for Highway Bridges adopted and published by the American Association of State Highway and Transportation Officials (AASHTO) until the LRFD edition of 1994. Only since the Ontario Bridge Design Code of 1979 have the benefits of arching action been formerly accepted as an

alternative to conventional bending theory. This alternative was referred to as the "Empirical Method of Design" and the code merely stipulated a minimum percentage of reinforcing in each horizontal direction, provided the slab parameters fell within certain limits. The latest two Canadian Highway Bridge Design standards also have provisions for the Empirical Method of Design [8], [9]. However, the latest version demonstrates in greater detail the need for confinement at the slab edge.

Also, until very recently, no direct recognition of the unreinforced Arch Panel concept was given in any of the design codes for bridges or buildings. The first appearance of code criteria involving the use of this theory is shown in the Canadian Highway Bridge Design Code, [9] CAN/CSA-S6-00 section 16.7, which was released to the public in the year 2001. The slabs are referred to as FRC Deck Slabs, where the acronym FRC stands for Fibre-Reinforced Concrete.

It is believed that this is the first direction provided to designers in a formally recognized sense for this type of slab design. On a national and international basis, recognition of the fact that transversely confined slabs behave in the manner that they do, has been slow. Design practise is only beginning to acknowledge that tied arch behaviour exists even when internal reinforcing is utilized and confinement is provided.

3.0 Statement of Research

Numerous papers have been written, based on laboratory experimentation, which explain the rationale for the ability of reinforced concrete deck slabs to develop substantially greater ultimate resistance to an applied concentrated load than what is predicted by conventional design based on bending moment resistance. Mufti et al [1] discovered that, with adequate confinement in the plane of a 100mm unreinforced model deck slab of a two-girder bridge, the ultimate resistance to failure by punching under a concentrated load applied perpendicular to the slab was more than twice that of bending resistance when the slab was only partially confined. From this, and other research of this nature, the Unreinforced Concrete Arch Panel (steel free) deck was developed for which the ultimate resistance to point loading relies on the development of arching action in the deck slab. It is now recognized that conventional reinforced concrete slabs were typically overdesigned.

Considerable effort has been taken to investigate the behaviour of cast-in-place and, to a lesser degree, precast arch panel deck slabs when subjected to static, concentrated loading. However, despite the early appearance of typical longitudinal cracks in arch panel deck slabs when in service, only in recent years has fatigue testing been applied to full scale arch panel decks [10, 11, 12, 13]. Furthermore, due to the time and expense of performing full scale fatigue testing, few opportunities have been available to investigate the performance of precast arch panels subjected to fatigue loading. Consequently, limited data has been available to develop a relationship between frequency of loading and crack propagation. In addition, features which are unique to precast deck panels have not been present in much of past experimentation.

It is for the purpose of investigating the behaviour of crack propagation in first generation precast unreinforced concrete arch panel deck slabs due to fatigue that this thesis topic is directed. The findings are anticipated to be beneficial to the further development of concrete slab design theory, bridge code criteria and structural detailing of concrete deck slabs. It is for this reason that the experimental work in the following chapter has been

performed. This takes the form of two (2) experiments: one under laboratory conditions at the University of British Columbia, and the other on an actual logging bridge in the interior of British Columbia. A description of these investigations together with test results are fully detailed in the next Chapter.

Chapter 5 is dedicated to the development of realistic strain spectra in two steel straps on independent deck panels of the Forestry Bridge due to truck loading. Loads are based on the estimated history of truck traffic that crossed the Forestry Bridge since it was first constructed in 1998.

Chapter 6 then presents an exploratory reliability theory that for the first time attempts to assess the reliability of Arch Panel bridge decks based upon a knowledge of the deck material, the loads it is designed to sustain and a knowledge of the rate at which cracks grow under these load patterns. Following this in Chapter 7, an application of the procedure developed in Chapter 6 is presented. The final chapter presents some conclusions and, perhaps more importantly, some suggestions for future research.

4.0 Experimental Methods

4.1 Fatigue and Ultimate Load Testing of Full Scale Precast Concrete Arch Panel Deck Slabs at the University of British Columbia

Two full scale precast arch panel deck slabs were tested for fatigue and ultimate loading at the University of British Columbia. The deck panels were prepared with the same overall dimensions as those of the Forestry Bridge deck panels presented in Section 4.2 of this thesis. The purpose of simulating the actual Forestry Bridge was three-fold.

- By simulating the Forestry Bridge panels, some comparison could be made between results obtained under laboratory conditions relative to results obtained under actual longer term in-service conditions.
- Some appreciation could be obtained for expected behaviour under fatigue loading without waiting years for the results from the field.
- By performing ultimate load testing at the conclusion of the fatigue testing program, an understanding of the remaining strength under ultimate load conditions could be realized.

Latitude was taken with certain details in the design of the panels in the lab in order to investigate the importance of these details with respect to the slab behaviour. One such modification was the amount of fibre reinforcing which was incorporated in the concrete design mix of each of the panels. One panel had the same reinforcing as the Forestry Bridge, the other had a lesser volume fraction of fibres. The second change involved the design compressive strength of the concrete. The concrete used in the panels for the Forestry Bridge consisted of 45 MPa concrete whereas the concrete for the panels for the lab used 35 MPa. A third change involved the number of steel straps which were used in the design of the panels. The Forestry Bridge had three straps per panel. The test panels used in the lab had four steel straps each. Finally, the gap between the Forestry Bridge panels were fully grouted, whereas the gap between the panels in the lab were left ungrouted.

The author's involvement in this experiment was one of assistance in arranging the fabrication of the panels and opinions during the panel design. In addition, periodic witnessing of the testing was undertaken to observe the progression of the cracks during fatigue loading.

4.1.1 Details of Test Panels

Two panels were prepared for the experiment in the laboratory at UBC. Both were fabricated by the same precast fabricator who had constructed the panels for the Forestry Bridge described in Section 4.2. While the panels were dimensioned and constructed to simulate those on the real bridge structure, some modifications to the design were made as described above. Each panel was 4300 mm wide x 3000 mm long and was formed in the shape of a shallow arch. Four 25 mm x 50 mm steel ties spaced evenly along the length of each of the panels were anchored to the panel by three nelson studs at both ends of the straps. The steel conformed to CAN/CSA-G40.21 350A. Concrete for the panels consisted of 35 MPa and was reinforced with fibrillated polypropylene fibres. One panel (Panel 1) had a volume fraction of 0.1% polypropylene, the other (Panel 2) had a volume fraction of 0.4% polypropylene. For ease of forming, concrete was allowed to flow between the top of the strap and the underside of the panel.

The panels were mounted on two steel girders spaced at 3500 mm on centre. Each panel had an edge-stiffening beam at the exterior transverse edge. Grout pockets were strategically located at the perimeter of the panels in order to coincide with clusters of nelson studs welded to the girders. Concrete grout was then cast into the grout pockets which, once set, provided a means of connection between the deck panels and the girders thereby providing composite action. The gap between the two interior transverse edges of the slabs was left ungrouted to conservatively represent failed grout between panels and no additional in-plane stiffening was provided at these locations. A plan and cross section of the panels are shown in Figures 4.1 and 4.2. Photographs of the test panels and loading apparatus are shown in Figures 4.3 to 4.6.

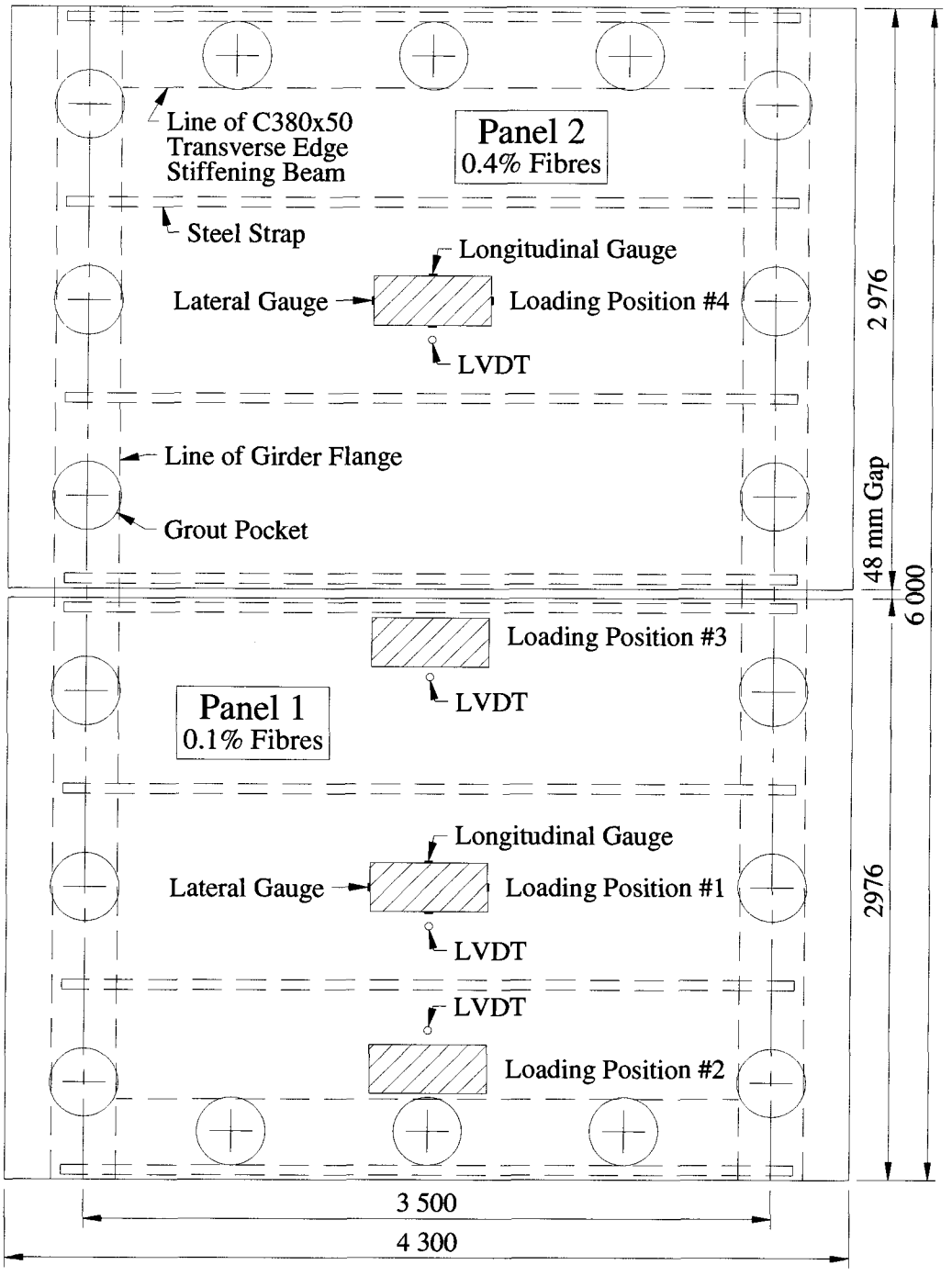

Figure 4.1 - Plan of Test Panels, Showing Location of Load Patches and Instrumentation

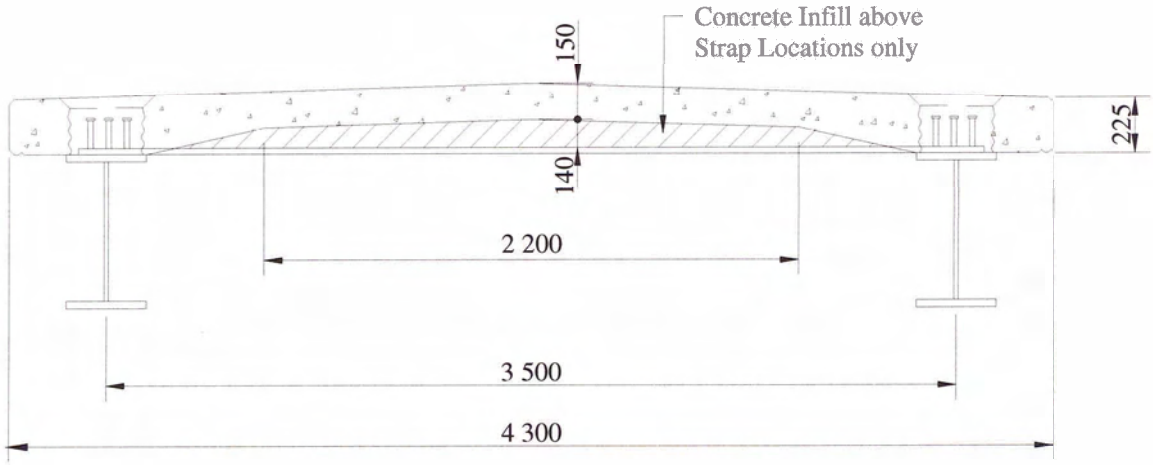

Figure 4.2 - Arch Panel Cross Section

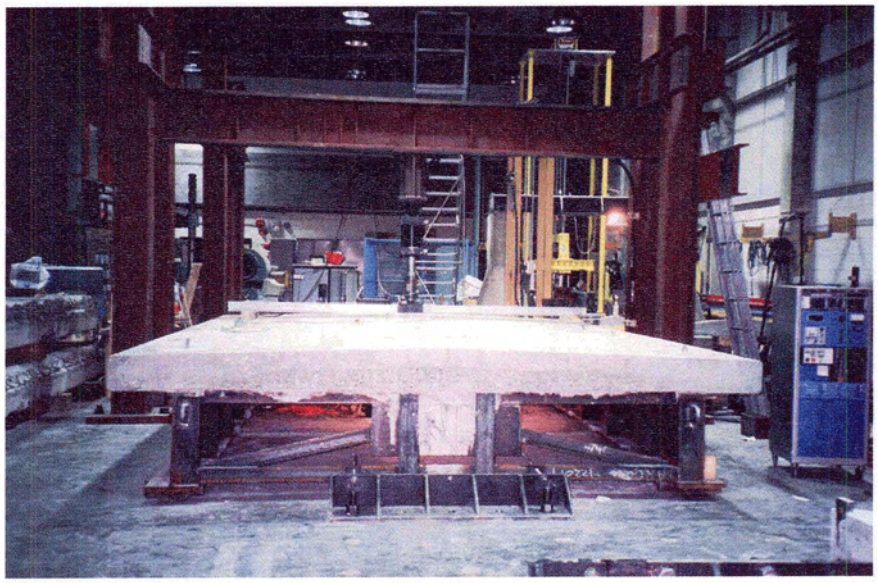

Figure 4.3 - Test Panels and Loading Apparatus

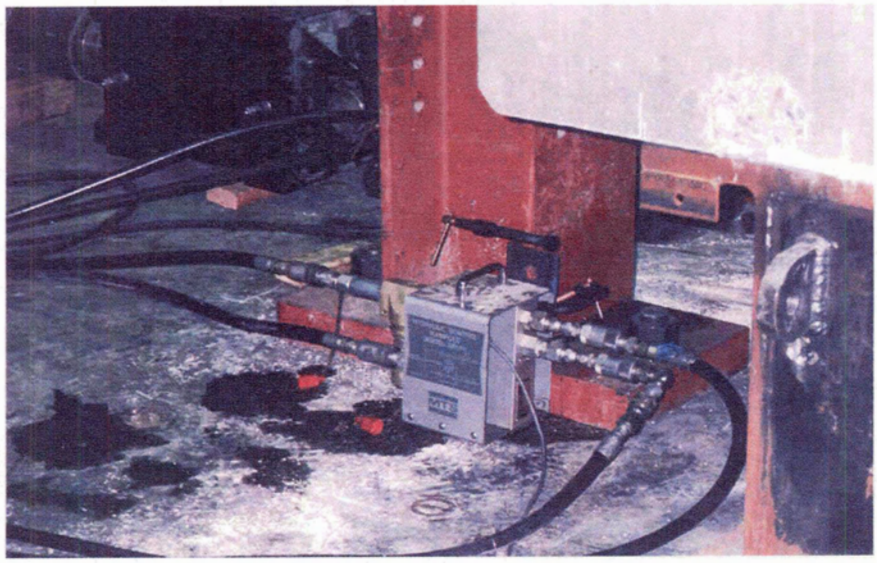

Figure 4.4 - Hydraulic Control Manifold at Base of Steel Column which is Anchored to the Floor Slab

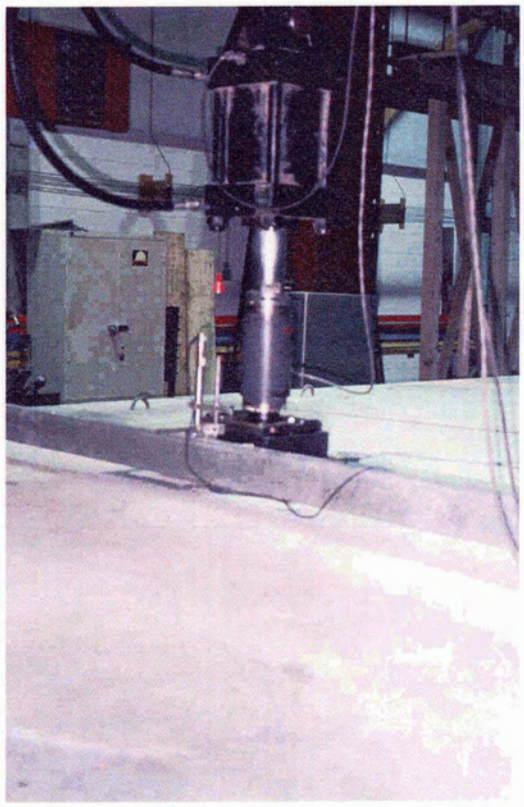

Figure 4.5 - Hydraulic Piston providing Pulsating Load. LVDT Mounted to Straight Edge in Foreground.

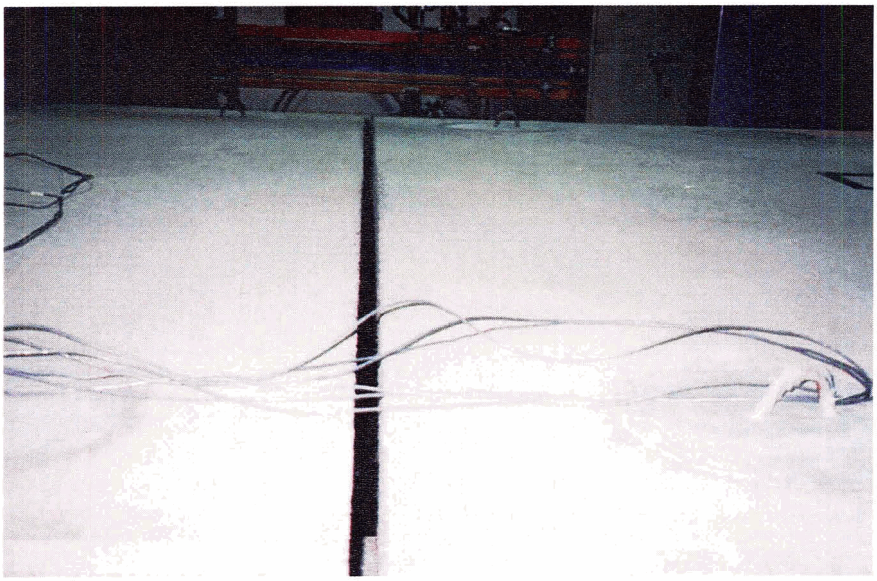

Figure 4.6 - Photograph of Gap between Panels and Grouted Shear Stud Pockets

4.1.2 Panel Loading

Each of the panels was subjected to a central load mounted to a steel frame supported on the floor slab of the laboratory. The load patch in contact with the deck was sized to simulate the contact area of a typical truck wheel (250 mm x 600 mm).

Both panels were first subjected 5 times to a central statically increasing load which peaked at 140 kN. Thereafter, Panel 1 was subjected to hydraulically driven pulsating loads peaking at 140 kN at three different locations: near the centre, near the edge beam and near the free edge transverse joint. The loading sequence and positioning of the loads are as shown in Figure 4.1 and Table 4.1. A total of 500,000 cycles was selected to represent the design requirements for fatigue limit states as outlined in the British Columbia Ministry of Forests "Forest Service Bridge Design and Construction Manual" (FSBDC Manual) [14]. The 140 kN loading is in excess of the maximum wheel load from a single axle of an L-75 off-highway design vehicle for which the bridge structure was designed. A diagram of L-75 axle loading is shown in Figure 4.7 [14]. The wheel load of the L-75 including allowances for eccentric and dynamic loading is approximately 120 kN. Therefore, the applied loading was considered to be

conservative. Fatigue loading on Panel 1 was terminated at 370,000 cycles due to time constraints.

Sequence No.	Load at Patch No.	No. of Cycles	Cumulative No. of Cycles at end of Sequence
1	1	50,000	50,000
2	1	50,000	100,000
3	1	50,000	150,000
4	2	50,000	200,000
5	2	50,000	250,000
6	2	50,000	300,000
7	2	50,000	350,000
8	3	20,000	370,000
9	1	1	1 (ultimate load test)

Table 4.1 - Sequence of Pulsating Load Testing for Panel 1 (loads peaked at 140 kN)

Panel 2 was subjected to a central pulsating 140 kN load as given in Table 4.2. The loading was ceased after 532,000 cycles. Thereafter, both panels were tested to failure under central statically increasing loads.

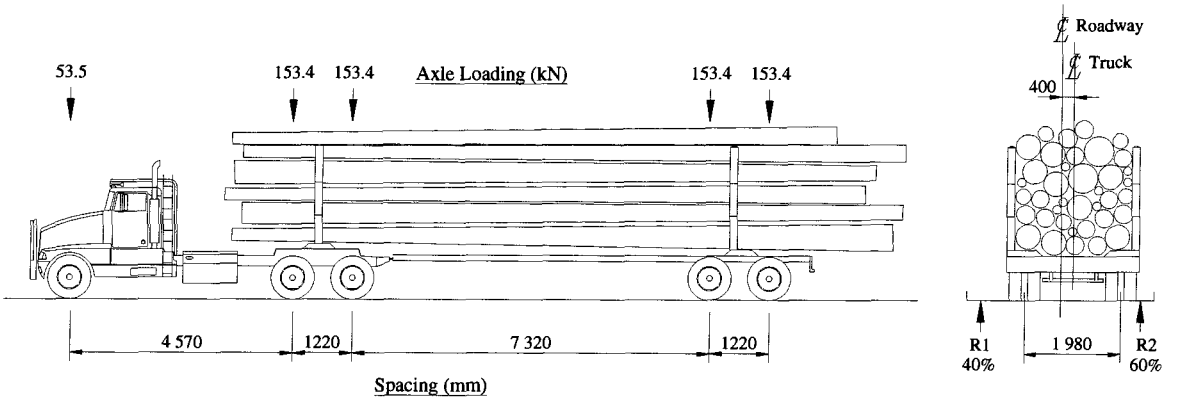

Figure 4.7 - L-75 (Off Highway) Logging Truck Design Load on Forest Road Bridges

Sequence No.	Load at Patch No.	No. of Cycles	Cumulative No. of Cycles at end of Sequence
1	Central	50,000	50,000
2	Central	50,000	100,000
3	Central	50,000	150,000
4	Central	50,000	200,000
5	Central	50,000	250,000
6	Central	50,000	300,000
7	Central	50,000	350,000
8	Central	50,000	400,000
9	Central	50,000	450,000
10	Central	50,000	500,000
11	Central	32,000	532,000
12	Central	1	1 (ultimate load test)

Table 4.2 - Sequence of Pulsating Load Testing for Panel 2 (loads peaked at 140 kN)

4.1.3 Panel Monitoring

A Linear Variable Displacement Transducer (LVDT) and strain gauges were used to monitor the behaviour of the slab during the experiment. The LVDT was used to measure the deflections of the deck slab with respect to the supporting girders. (See Figure 4.5) Strain gauges were located adjacent the central load patches on the top surface of the slab in order to monitor the strains under loading as shown in Figure 4.8.

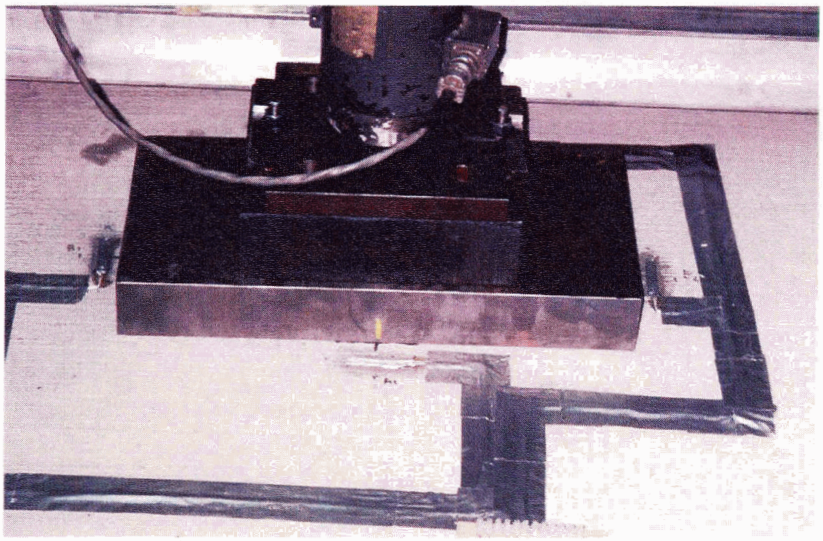

Figure 4.8 - Load Patch and Strain Gauges

The crack pattern and progression of cracks was closely observed and recorded by lab technicians under the direction of Dr. Mufti. Monitoring equipment used is as shown in Figure 4.9 and included an XY plot recorder together with computer monitoring of the deflections. The data acquisition system was designed and assembled by Dr. Newhook. [4]

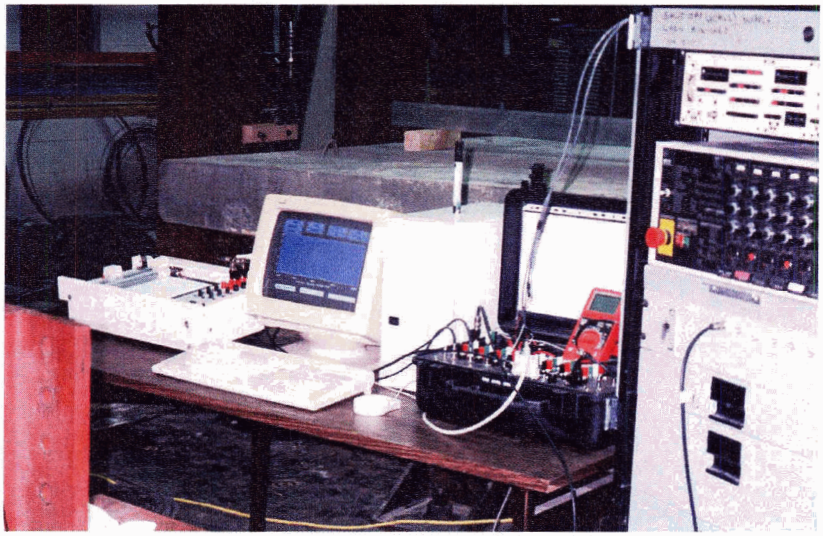

Figure 4.9 - Monitoring Equipment

[4] Private Communication: Vivek Bindiganaville, dated October 22, 2004.

On numerous occasions between February 9, and June 16, 1999, the author witnessed the loading and observed the crack growth characteristics of both slabs. Regular discussions with members of the research team also took place during this time period.

4.1.4 Test Results [15]

4.1.4.1 Fatigue Loading

Figure 4.10 shows the progression of cracks on the bottom of panel 1 as of February 26, 1999, while Figures 4.11 and 4.12 show the progression of cracks on March 19, and May 23, 1999 on the top of Panels 1 and 2, respectively. Figure 4.13 gives the complete pattern of cracking which developed on the two slabs during testing under pulsating loads. The numbers beside each of the cracks indicate the cumulative number of cycles to reach a given location on the particular crack. The top cracks formed directly above the bottom cracks but are shown slightly offset for clarity.

Figure 4.10 - Cracking Pattern on Bottom Surface of Panel 1

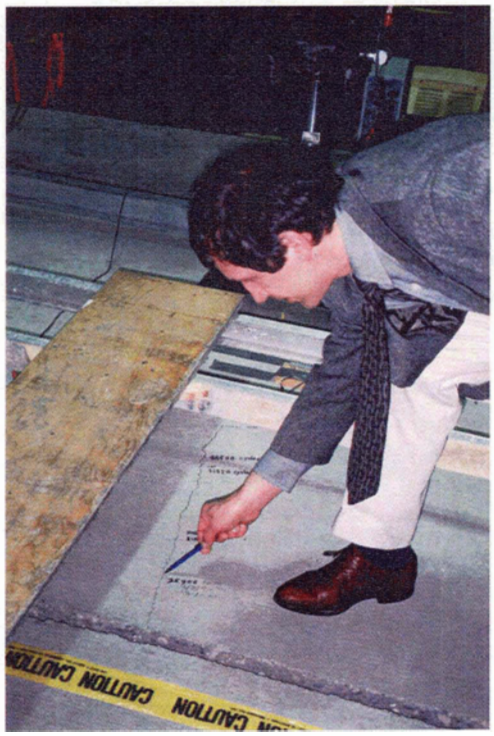

Figure 4.11 - Progression of Cracking on Top Surface of Panel 1

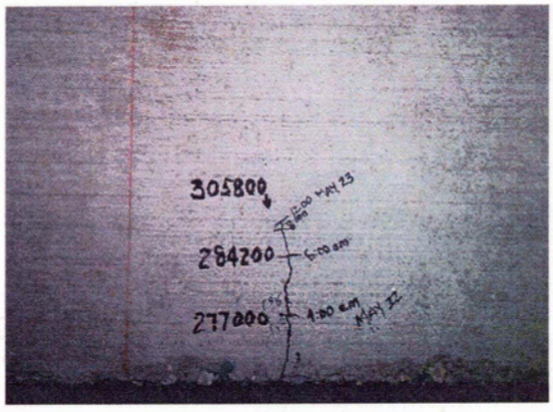

Figure 4.12 - Progression of Cracking on Top Surface of Panel 2

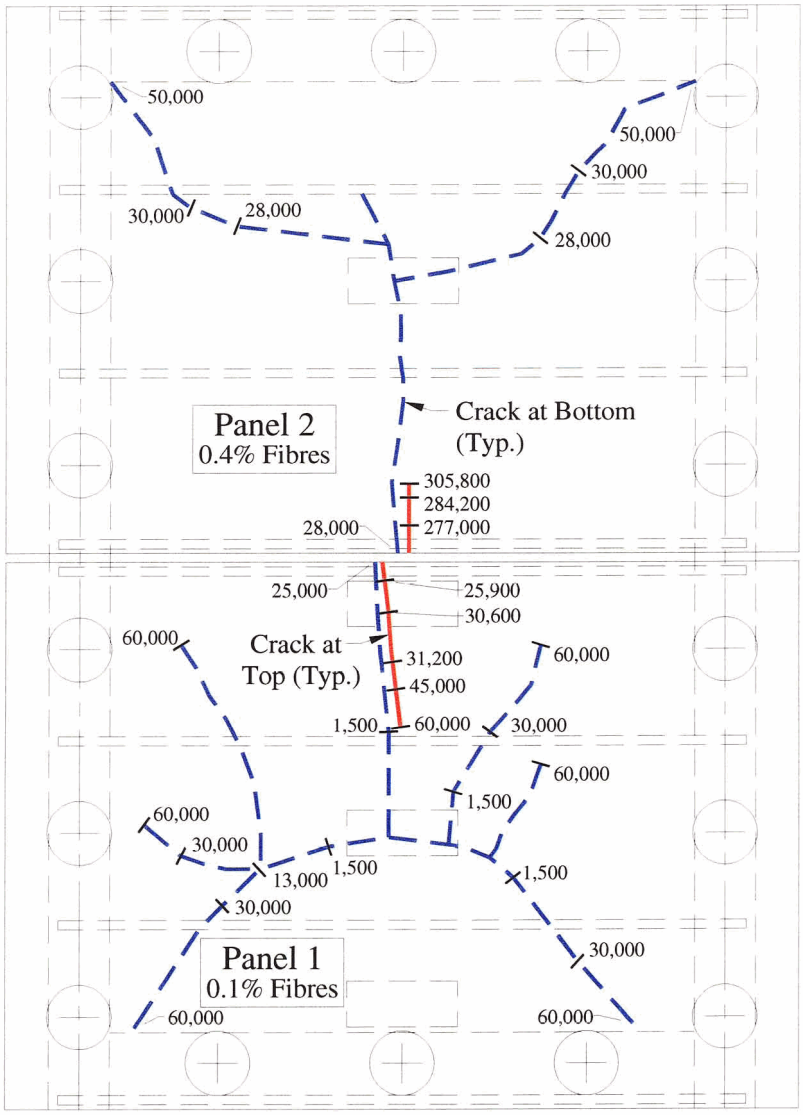

Figure 4.13 - Crack Pattern Developed under Central Pulsating Loads

Key features of the observed results are as follows.

1. Cracks developed after 1500 cycles of the centrally positioned load in panel 1. A similar cracking pattern was not reached in panel 2 until almost 28,000 cycles.
2. Both panels developed a similar Y-shaped crack pattern on the underside, however panel 1 also developed secondary diagonal cracks branching from the main cracks.
3. The complete formation of the Y-shaped crack was 50,000 cycles for panel 1 and 60,000 cycles for panel 2.

4. The bottom surface cracks reached the transverse free edge after approximately the same number of cycles for both panels. The longitudinal cracks reached the edge in 25,000 and 28,000 cycles for panels 1 and 2, respectively.
5. The cracks first progressed from the bottom surface to the top at the transverse free edge on both panels.
6. The number of load cycles required before progression of the crack from the bottom surface to the top at the transverse free edge was far greater for panel 2 than for panel 1. The crack reached the top after only 900 cycles in panel 1 whereas it took 249,000 cycles before the crack progressed to the top surface in panel 2 after the crack had reached the free edge on the bottom surface. This would suggest that the polypropylene fibres play a roll in slowing crack propagation to the top surface.
7. Under the central pulsating load, the crack at the top surface stopped approximately 500 mm short of the loading position in panel 1 and progressed no further between 60,000 and 150,000 cycles. In panel 2, the crack on top progressed no further from the free edge than 500mm between 305,800 and 532,000 cycles.
8. Crack propagation from the bottom surface to the top progressed uninterrupted by the presence of aggregate.

4.1.4.2 Ultimate Static Loading

Due to time constraints in the lab resulting in short notice, the author was unable to witness directly the ultimate static load testing. The failure surfaces were typical of punch failure. The results, outlined in [15], indicate an ultimate failure load of 454 kN for panel 1 and 500 kN for panel 2. Based on wheel loadings, these loadings are more than twice the ultimate design load required for the slab. A photograph of the punch failure is shown in Figure 4.14. It is important to note that Punch Theory predictions are approximately 724 kN for these slabs. (See Appendix A) This comparison emphasizes the significance of a fatigue investigation.

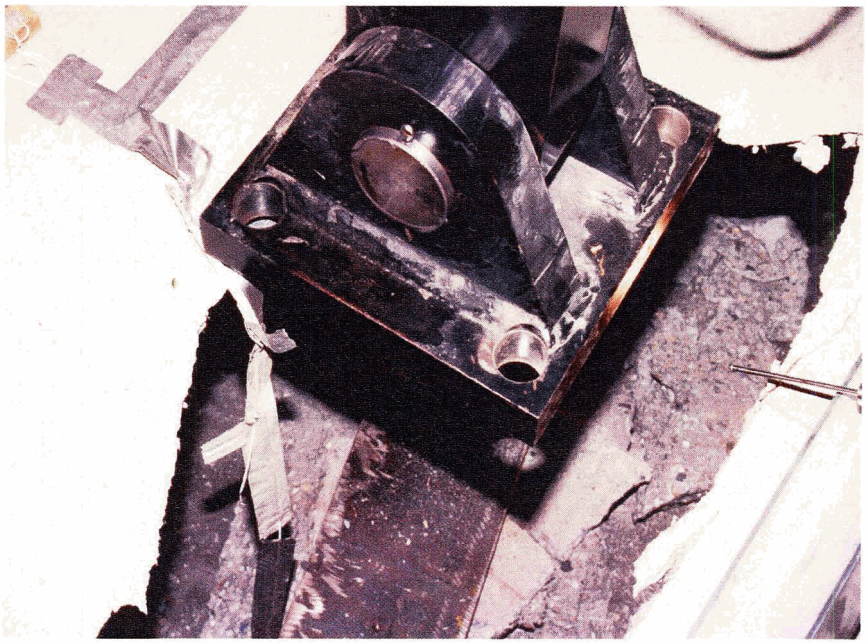

Figure 4.14 - Punch Failure as Viewed from Top of Panel

Comparative load v. deflection curves for panel 1 and longitudinal (compressive) strains recorded from gauges mounted on the slab surface near the load patches of panels 1 and 2, may be found in [15] and are not repeated here as they are outside the scope of this thesis.

4.2 Forestry Bridge Research Project

4.2.1 Concept Development

In recent years, many Forestry Bridge superstructures have been designed using conventionally reinforced precast concrete panels supported by a pair of steel girders. This allows construction to proceed in more remote settings without the need for transporting or site batching concrete. For smaller bridges the panels and girders can be installed with excavators thereby eliminating the need for large cranes. The panels have rectangular or circular voids strategically located over the girders to coincide with a cluster of studs welded to the top flanges of the girders. The voids are then filled with grout providing composite action between the deck slabs and the girders. The width of bridge deck normally varies between 4.27 m and 4.88 m. Figure 4.15 shows combined deck cross sections of the Standard Ministry of Forests Precast Concrete Deck.

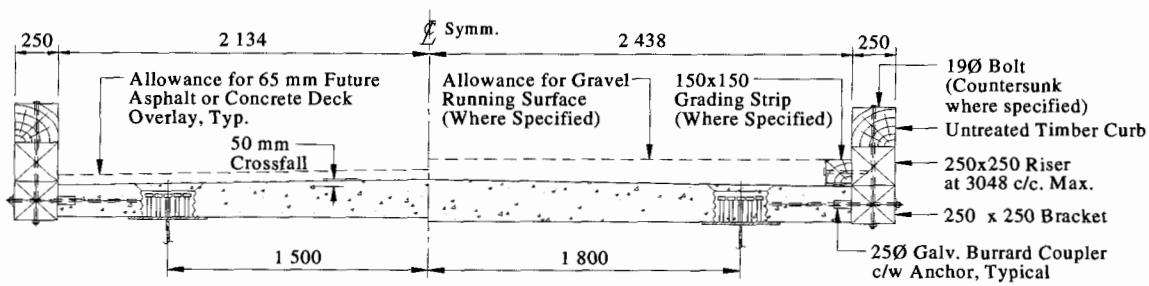

Figure 4.15 - Standard Ministry Precast Concrete Deck Details

In July of 1996, the co-inventors of the Arch Panel Deck concept, Drs. Jaeger, Bakht and Mufti met with the author, to explore the possibility of applying Arch Panel technology to Forestry bridges.

A meeting was arranged between the Engineering Division of the Ministry of Forests, the co-inventors of the Arch Panel concept, and Reid Crowther & Partners Ltd. The purpose of the meeting was to discuss the prospect of arranging a pilot project with which to test the Arch Panel theory. The Ministry of Forests expressed their support of the concept with the understanding that sufficient documentation of theory, backed by test results and in-situ monitoring would be provided to demonstrate that the deck system, when in service on a bridge, would meet and exceed performance expectations for strength, durability and fatigue.

With the support of ISIS Canada Research Network and NSERC, a preliminary deck cross-section was developed over several weeks by the co-inventors of the Arch Panel at Dalhousie University in collaboration with the author. Emphasis was placed on maintaining similar details to those in current use for Forestry Bridge precast deck panels in BC. A certified precast fabricator was invited to participate in the development of the concept. By December of 1996 they had produced two preliminary panels to assess the practicality of production and handling.

In early 1997, final profiles and details of an L-75 deck were developed for production of the first bridge. A full scale precast composite arch panel bridge was constructed in the laboratory of Dalhousie University for testing purposes. The slab was supported on, and grouted to, two steel girders to simulate actual in-situ conditions. A cross-section of the test panel is shown in Figure 4.16. Note that the girders were spaced at 3.5m O.C. in order to reduce the slab overhang. The concrete mix specified a 28 day strength of 45 MPa and a requirement for 0.4% volume fraction of fibrillated polypropylene fibres 40 mm in length.

The slab was tested to failure under a statically-increasing load with a contact area of 250 mm x 500 mm, slightly smaller than that of a single L-75 logging truck dual wheel. The imprint was applied to the centre of the test slab. The deck failed at an ultimate load of 700 kN, almost six times that of an L-75 dual wheel load including allowances for eccentric and dynamic loading. The failure mode was one of punching through the deck

with a failure pattern similar to that shown in Figure 4.17. This is very close to recent Punch Theory prediction of 720 kN. (See Appendix A)

4.2.2 Bridge Site Selection, Design and Construction

In April 1997 approval was received from the Ministry of Forests to construct a pilot Arch Panel bridge on a well- travelled Forestry Service Road. However, it was not until the fall of 1997 that a candidate site was available. The bridge would be located on a road which is well travelled by logging trucks and is also used by the public for access to fishing resorts. Other periodic users include ranchers and mining companies. The conceptual design had been prepared by Forsite Consultants Ltd. for Tolko Industries Ltd.

The location required a single span bridge of 24 m in length to cross a creek. The final design of the bridge was developed by Reid Crowther & Partners Ltd. and the co-inventors of the Arch Panel in cooperation with the Ministry of Forests. A Goetechnical consultant was engaged for recommendations on substructure conditions.

Eight arch panels were fabricated by the same precast fabricator who assisted with the development of the concept. A plan and cross section of the bridge are shown in Figure 4.18. Dimensions of the arch panels were virtually the same as those shown in Figures 4.16 and 4.17. Concrete consisted of a mix design requiring a 28 day compressive strength of 45 MPa and 0.4% fibrillated polypropylene fibres by volume. During fabrication, both the arch panel deck slabs and the steel girders for the bridge were inspected by the Ministry of Transportation plant inspection team. Photographs of the panels being fabricated and the bridge being constructed are shown in Figures 4.19 to 4.23.

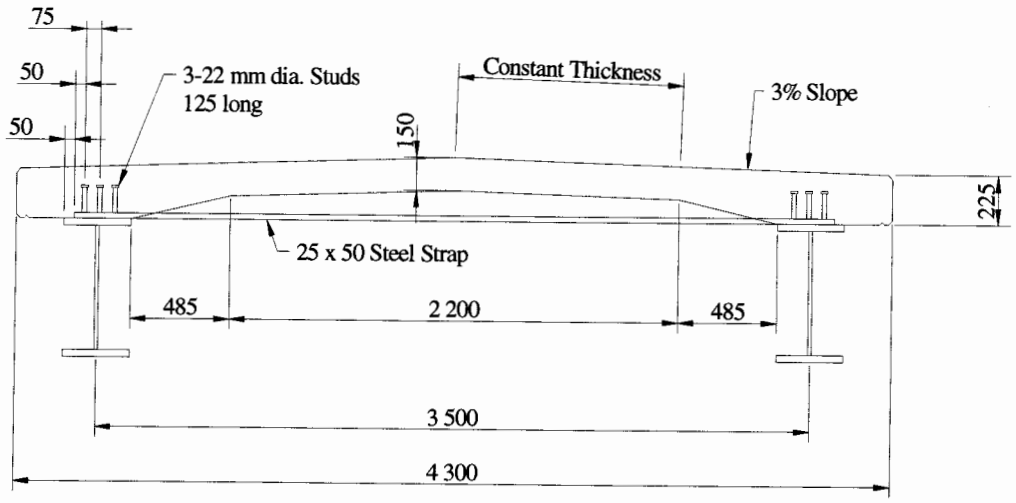

Figure 4.16 - Cross Section of Panel Test Section at Dalhousie University

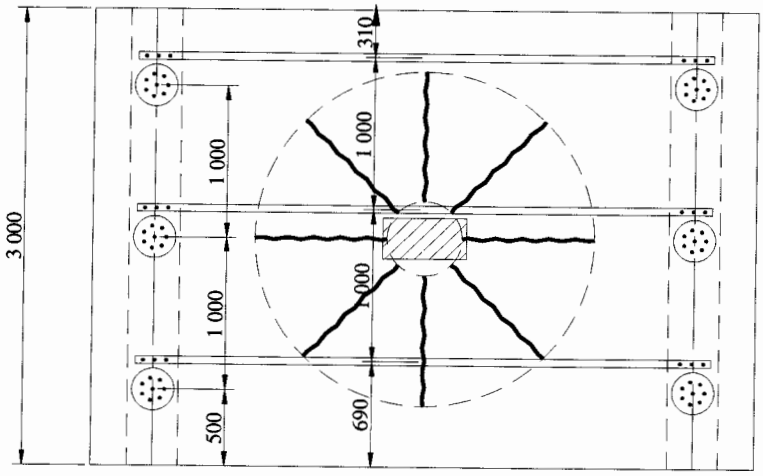

Plan - Interior Panel
Slab Radial Cracking Pattern

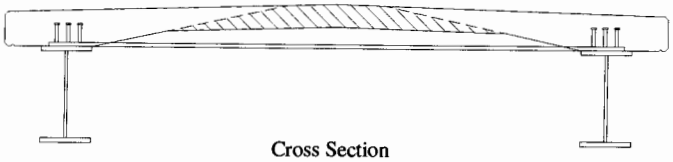

Cross Section
Outline of Punch Cone

Figure 4.17 - Failure Mode of Panel Test Section

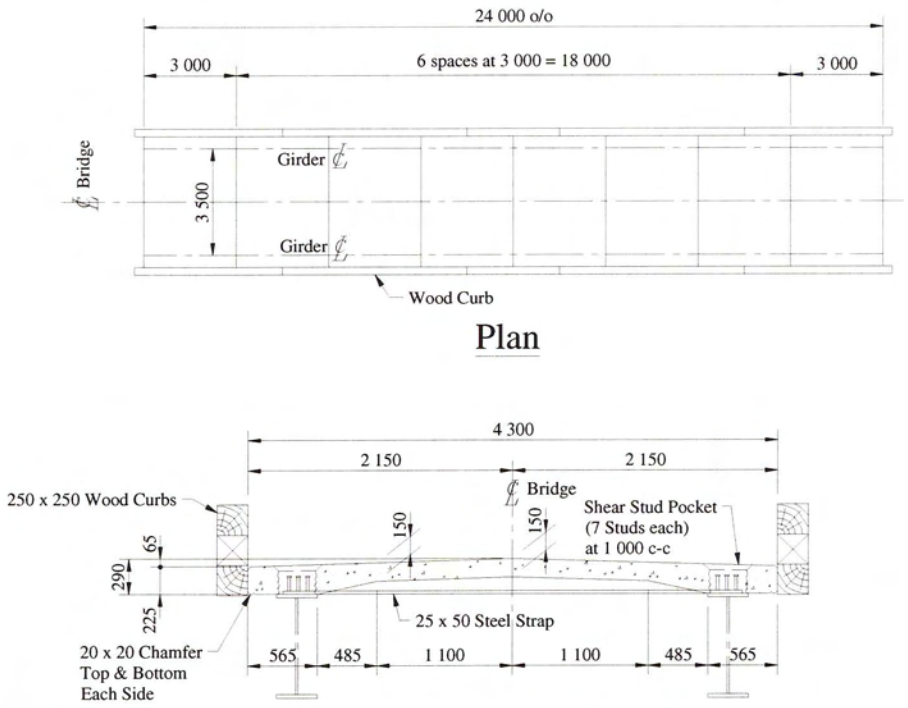

Figure 4.18 - Layout of the Forestry Bridge

Figure 4.19 - Precast Arch Panel Fabrication

Figure 4.20 - Precast Panel Erection

Figure 4.21 - Grout Placement in Grout Pockets and in Joints between Panels

Figure 4.22 - Underside of Deck showing Steel Straps

Figure 4.23 - Underside of Deck showing Steel Channel for Transverse Edge Stiffening

4.2.3 Monitoring Programs

4.2.3.1 April 1, 1998

In April, 1998 an in-situ monitoring program was performed by the author under the direction of Dr. Mufti to assess the behaviour of the bridge under actual truck loading.

The initial objective at this stage was to determine whether the bridge was in fact performing as predicted by design theory; in particular the composite action between the arch panel deck slabs and the steel girders, as well as strains in the straps of the arch panels. The opportunity to perform the monitoring was taken during shut-down of the forest industry due to spring break-up. Arrangements were made with a local trucker to supply a loaded dump truck of known weight. Instrumentation was being provided by Dr. Ventura of UBC with assistance of a graduate student.

Instrumentation:

For purposes of measuring longitudinal strains, four weldable electrical resistance strain gauges were installed on the lower flanges of the girders. Two gauges were installed at the mid-span of the girders and the other two installed at one-third span from the west end of the bridge. An additional two strain gauges were installed on the steel straps of the fifth and sixth panels from the east end of the bridge. For identification, the Panels are numbered from 1 to 8 beginning at the east end of the bridge. Strain gauge 5 is located on the strap nearest the east edge of panel 5. Strain gauge 6 is on the strap in the centre of Panel 6, Figure 4.24.

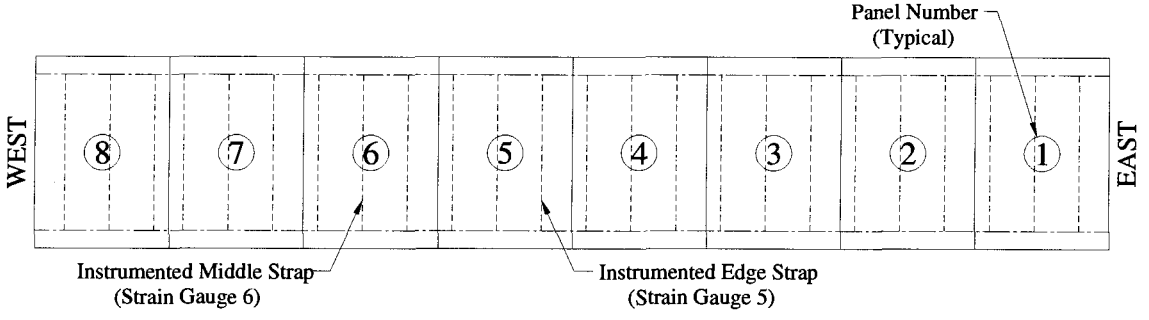

Figure 4.24 - Plan of Panel Layout Showing Locations of Instrumented Steel Straps

A temperature gauge encased in a brass housing was welded to the bridge at mid-span of the upstream girder and an LVDT displacement sensor was positioned to measure vertical displacement of the bottom flange at this location. Further details of the types of sensors and data recorded from the readings can be found in [16].

Test Vehicle:

The test vehicle consisted of a dump truck hauling a trailer carrying an excavator. Weights were discussed with the trucker prior to attending the site. Preliminary calculations were performed in anticipation of simulating L-75 loading. The trucker was requested to have axle loads verified from weigh scales for a half full and a fully loaded box as well as the axle load of the trailer with the excavator. Upon arriving at the site, the scale results were markedly different (lighter) from those expected. Consequently, repositioning of the excavator on the trailer and recalculation was required to estimate simulation of L-75 loading. The weight of the excavator components were later verified with the distributor and calculations were revised to verify the load of the test vehicle. The calculations may be found in Appendix B.

Two different load levels were used in testing the bridge. The first was with the dump truck half full pulling an empty trailer. The second was with the dump truck fully loaded pulling the trailer with the excavator. The vehicle travelled sequentially in three transverse positions: the north or downstream side, the centre and the south or upstream side. These are referred to in the documentation as the left, centre and right sides respectively to reflect the direction in which the test vehicle was travelling with respect to the bridge. In each transverse position, the vehicle was stopped at 22 longitudinal locations in order for readings from the instrumentation to be taken. Longitudinal positions were spaced at 2.0 m intervals except where it was anticipated that maximum moment from the fully loaded truck would occur. At that location an additional reading was taken to provide two 1.0 m intervals. The longitudinal positions were measured with respect to the steering axle of the dump truck.

Figures 4.25 and 4.26 show diagrammatically the transverse and longitudinal positions where readings were taken. Figure 4.27 shows the axle loading of the fully loaded test vehicle carrying the excavator. The maximum moment for the 24 m span calculated for the test vehicle was within 2% of that calculated for the fictitious L-75 truck.

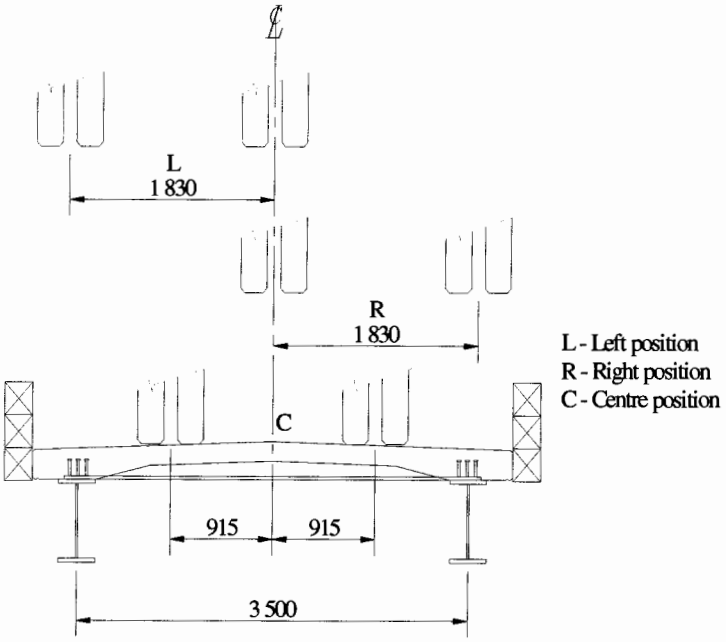

Figure 4.25 - Transverse Positions of the Test Vehicle

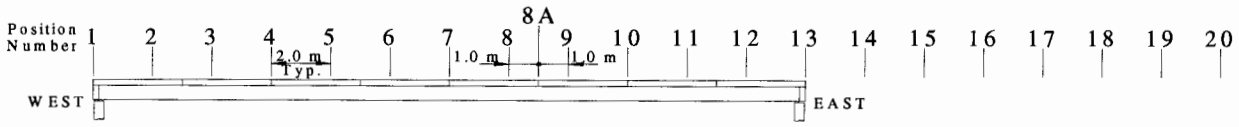

Figure 4.26 - Longitudinal Positions of the Front Axle of the Test Vehicle

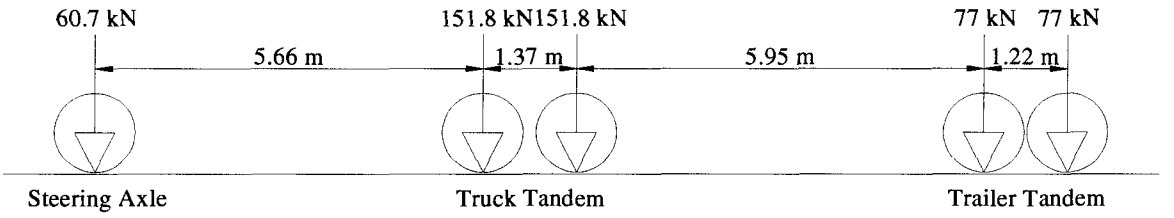

Figure 4.27 - Axle Loadings of Fully Loaded Test Vehicle Carrying Excavator

Dynamic testing was also performed on the bridge using the fully loaded vehicle pulling the trailer carrying the excavator. The vehicle crossed the bridge nine times at approximately 10 km/hr in the centre position. An obstacle consisting of two 2x4's in height (75mm) was placed in the truck's path at the third point of the span in order for the axle to bounce and provide an "impulse" load to the bridge. Dynamic responses were then compared to the static responses from each of the measuring instruments.

Photographs of the testing procedure are shown in Figures 4.28 to 4.31.

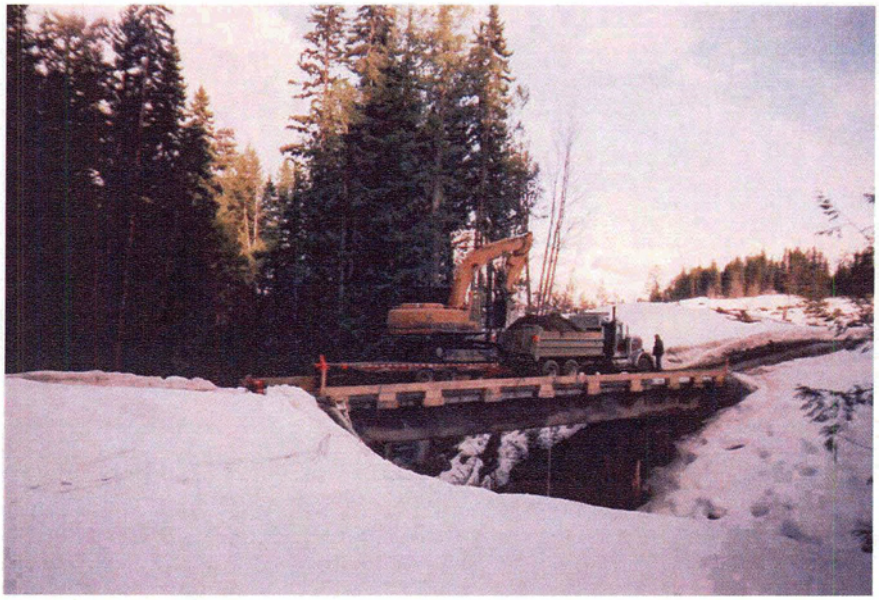

Figure 4.28 - Fully Loaded Test Vehicle on Bridge

Figure 4.29 - Test Vehicle in Left Position (Monitoring Station in Background)

Figure 4.30 - Access Platform beneath Deck

Figure 4.31 - Strain Gauge on Strap 5

Test Results:

Results observed from the testing were as follows [17].

1. The distribution factor for moment in the more heavily loaded girder when the test vehicle was offset from the centre of the bridge was smaller than the factor assumed in the design.
2. The precast arch panel deck slabs act compositely with the girders.

3. The observed maximum strain in the bottom flanges of the girders was approximately 22% smaller than the calculated strain.
4. The axial strains in the straps are little affected by the transverse position of the vehicle. [5]
5. Cross bracing between girders near the slab level provide additional transverse restraint to the deck slab.

Full results from the testing can be found in [16], [17], and [18]. For purposes of this thesis, only results from the fully loaded truck pulling the trailer with the excavator are of interest. Furthermore, what is of significance to the subject matter is the loading v. positioning of the test vehicle relative to the strain recorded from strain gauges 5 and 6 which were located on the straps of arch panels 5 and 6 respectively. This will be discussed in greater detail in the next Chapter.

4.2.3.2 July 15, 1999

In July, 1999 an inspection of the condition of the Forestry Bridge was undertaken by Dr. Mufti and the author. Of relevance was the expected progression of cracking due to fatigue as demonstrated by the experiments at UBC and described in Section 4.1. At this time emphasis was placed on the pattern and length of cracking which had developed under repetitive loading and minimal attention was given to crack width.

Test Method:

The bridge deck was shovelled and swept with hand brooms. Care was taken not to allow debris from the deck to fall into the creek. A water pump was used to wash the deck. Once the deck was cleaned, visual observations of the cracks on both the top and bottom of the deck were taken and the recorded crack width measurements were estimates only. The scaffolding used for installing the instrumentation on the west half of the bridge in the Spring of 1998 was still in place. It was therefore used to access the underside of the bridge deck. However, the deck beneath the east half of the bridge was

[5] This observation is not entirely borne out by the strain gauge results presented in Table 5.1.

less accessible and therefore crack observation was more difficult at this location. Figure 4.32 shows a typical crack on the bottom of the slab and the cleaned deck.

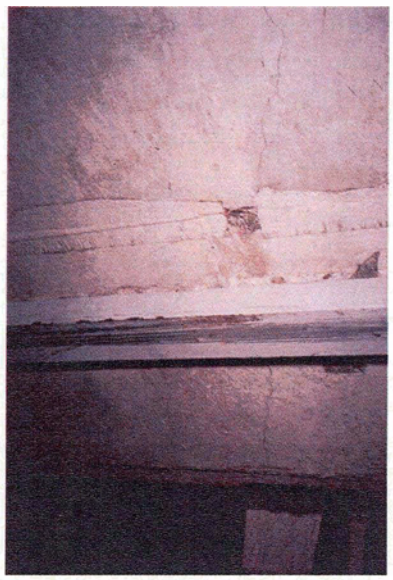

Longitudinal Crack at Underside of Deck
Slab near Transverse Edge Stiffener

Deck Cleaned for Review of Crack Development

Figure 4.32 - Forestry Bridge Field Observations (July 1999)

Test Results:

Figure 4.33 is a copy of a sketch prepared during the field investigation which shows the pattern of cracking that had developed since the bridge was constructed in 1998.

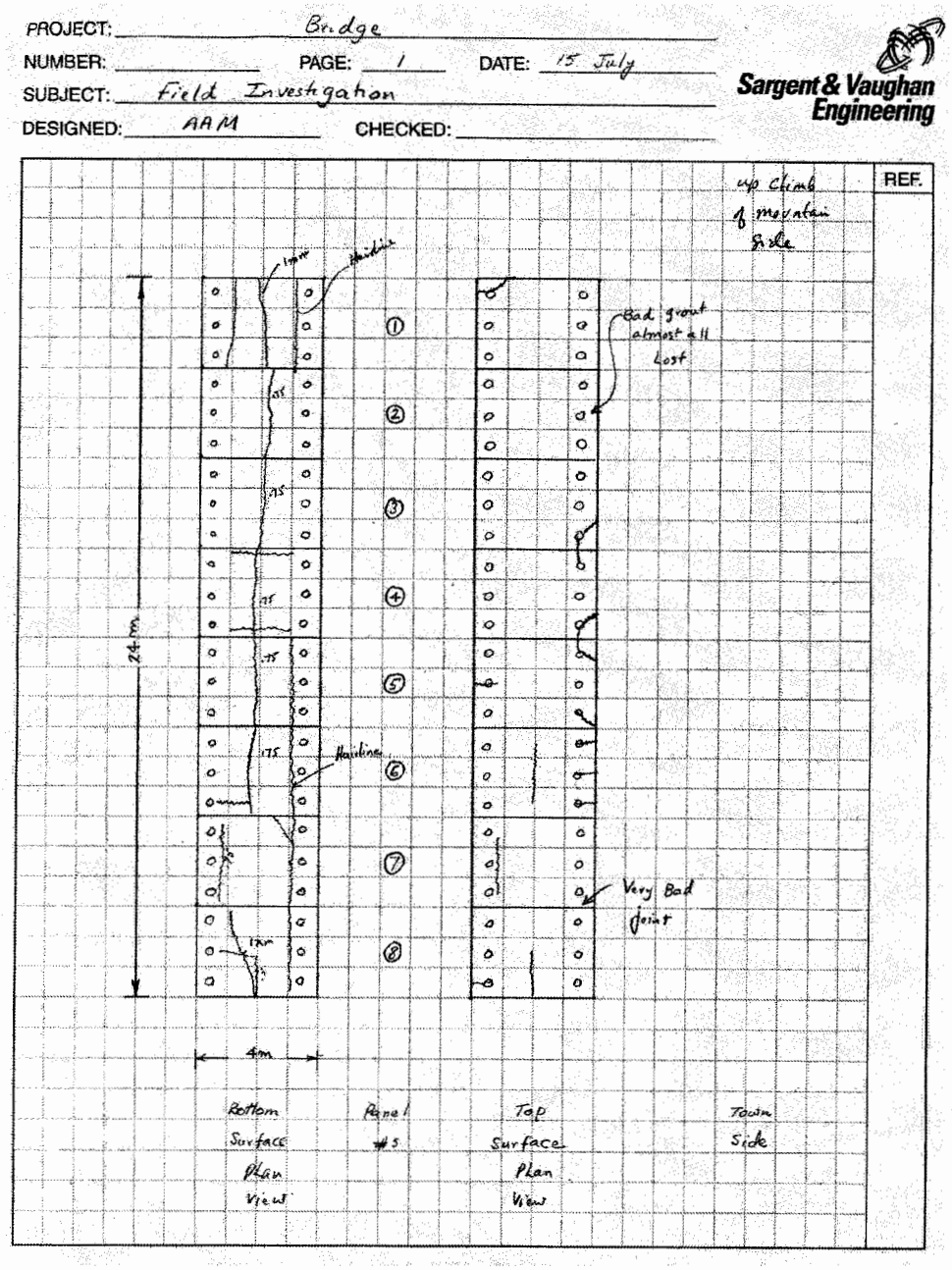

Figure 4.33 - Sketch of Crack Pattern in Forestry Bridge Deck July, 1999

4.2.3.3 October 20, 2003

On October 20, 2003 an inspection of the condition of the Forestry Bridge was undertaken by the author with the assistance of Mr. Dybwad, E.I.T. With a better understanding of the relevance that crack width plays in the progression of fatigue cracking in Arch Panel decks than was known in 1999, much more attention was paid to the measurement of both the length and width of the cracks.

Test Method:

The bridge deck was shovelled and swept with hand brooms. Care was taken not to allow debris from the deck to fall into the creek. A pumper truck was used to wash the deck. Once the deck was cleaned, visual observations of the cracks on both the top and bottom of the deck were taken. Each crack was also measured for length with a hand measuring tape where it did not terminate at the edge of the concrete. The widths of the cracks were measured utilizing a pair of digital calipers viewed under a magnifying glass as shown in Figure 4.34. Access to the exterior slab edges and to the underside of the deck for the east half of the bridge was made available by a bridge testing vehicle or "Snooper Truck" provided by the Ministry of Forests. The original scaffolding used for monitoring in 1999 was still in place and in good condition for access to the underside of the deck for the west half of the bridge. Photographs of the bridge inspection vehicle and typical deck cracks are shown in Figures 4.35 to 4.38.

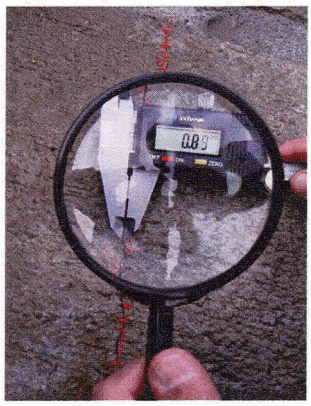

Figure 4.34 - Method of Measurement for Crack Widths, October 2003

Figure 4.35 - Bridge Inspection Vehicle. A Logging Truck Typical of the Road use can be seen on the East Approach to the Bridge

Figure 4.36 - Longitudinal Centre Crack on Top of Panel 8

Figure 4.37 - Longitudinal Centre Crack on Bottom of Panel 5 Strain Gauge 5 can be seen on Steel Strap in Background

Figure 4.38 - Secondary Cracks at Grout Pockets

Results:

The results from the field notes were recorded and mapped onto an autocad drawing. Each crack was given an identification which indicates the deck panel number, whether it was a top or bottom crack, the year it was first recorded (1999 or 2003) and an assigned crack number. Beside each of the cracks, the average crack width was recorded. Drawings showing the crack patterns and crack identification are given in Figure 4.39. In Figure 4.40 the crack widths as measured in October 2003 are shown beside each of the cracks. Included in the figure is a separate drawing showing the top cracks superimposed over the bottom cracks. A comparison between the crack widths recorded in 1999 and 2003 is given in Table 4.3 where all the cracks are recorded.

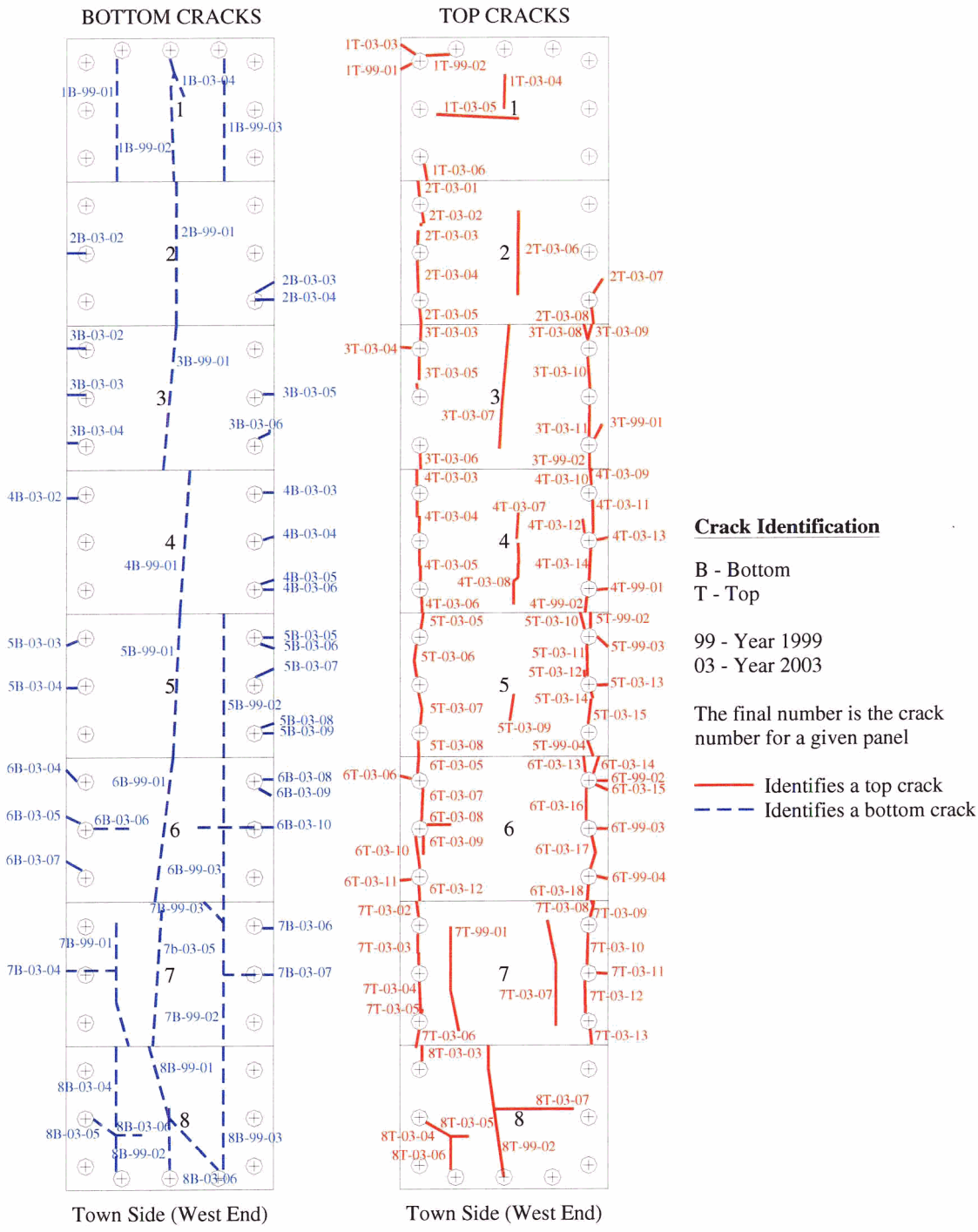

Figure 4.39 - Forestry Bridge Crack Identification Recorded October 20, 2003

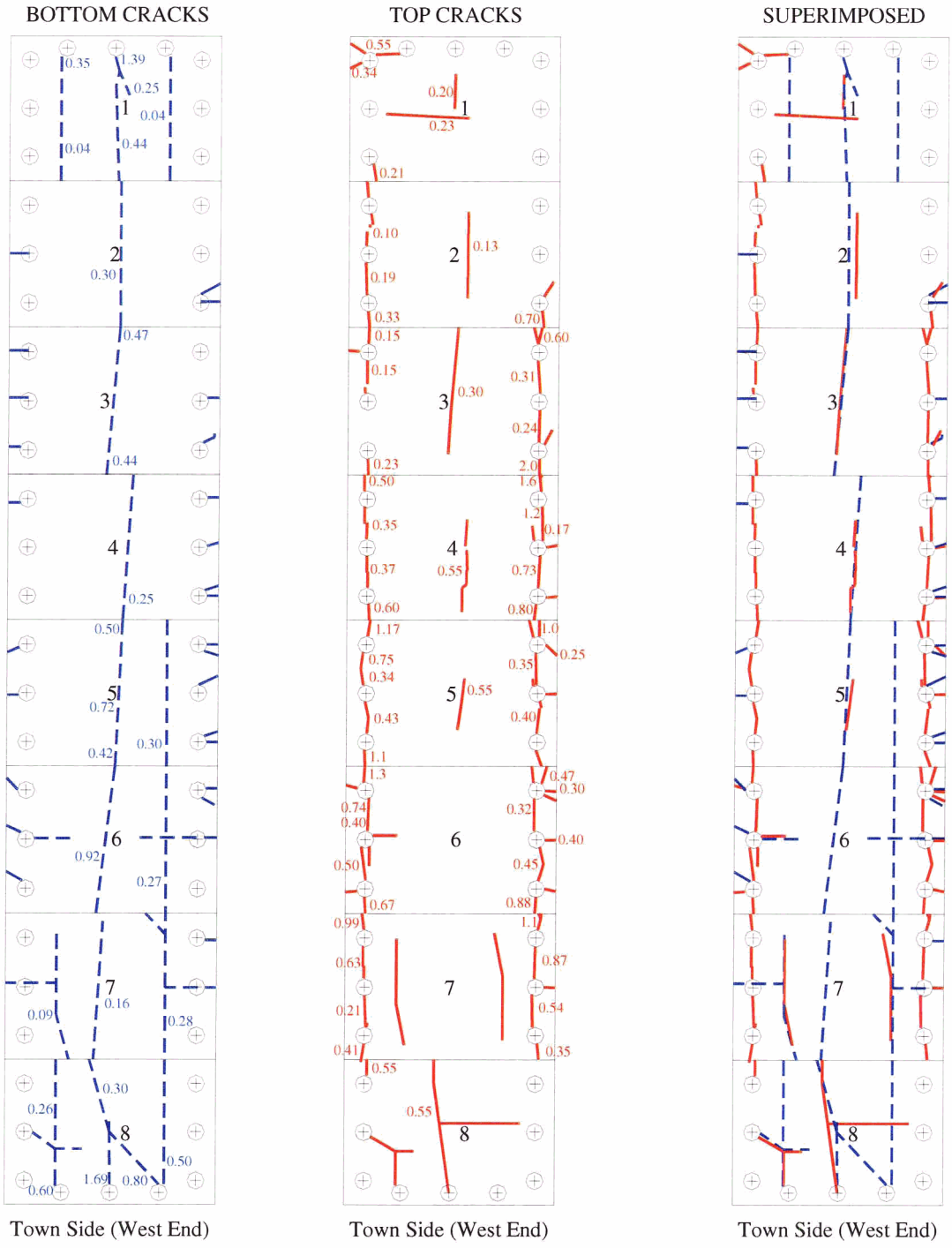

Figure 4.40 - Forestry Bridge Crack Widths Recorded October 20, 2003

Panel	Side	Year	Number	Identification Number	99-Width (mm)	03-Ave Width (mm)
1	B	99	01	1B-99-01	0.10	0.20
1	B	99	02	1B-99-02	1.00	0.90
1	B	99	03	1B-99-03	0.10	0.04
1	B	03	04	1B-03-04		0.25
1	T	99	01	1T-99-01	Hairline	0.34
1	T	99	02	1T-99-02	Hairline	0.55
1	T	03	03	1T-03-03		0.55
1	T	03	04	1T-03-04		0.20
1	T	03	05	1T-03-05		0.23
1	T	03	06	1T-03-06		0.21
2	B	99	01	2B-99-01	0.75	0.30
2	B	03	02	2B-03-02		Hairline
2	B	03	03	2B-03-03		Hairline
2	B	03	04	2B-03-04		Hairline
2	T	03	01	2T-03-01		0.10
2	T	03	02	2T-03-02		0.10
2	T	03	03	2T-03-03		0.10
2	T	03	04	2T-03-04		0.19
2	T	03	05	2T-03-05		0.33
2	T	03	06	2T-03-06		0.13
2	T	03	07	2T-03-07		Hairline
2	T	03	08	2T-03-08		0.70
3	B	99	01	3B-99-01	0.75	0.45
3	B	03	02	3B-03-02		Hairline
3	B	03	03	3B-03-03		Hairline
3	B	03	04	3B-03-04		Hairline
3	B	03	05	3B-03-05		Hairline
3	B	03	06	3B-03-06		Hairline
3	T	99	01	3T-99-01	Hairline	0.24
3	T	99	02	3T-99-02	Hairline	2.00
3	T	03	03	3T-03-03		0.15
3	T	03	04	3T-03-04		Hairline
3	T	03	05	3T-03-05		0.15
3	T	03	06	3T-03-06		0.23
3	T	03	07	3T-03-07		0.30
3	T	03	08	3T-03-08		0.60
3	T	03	09	3T-03-09		Hairline
3	T	03	10	3T-03-10		0.31
3	T	03	11	3T-03-11		0.24
4	B	99	01	4B-99-01	0.75	0.25
4	B	99	02	4B-99-02	Hairline	Hairline

Panel	Side	Year	Number	Identification Number	99-Width (mm)	03-Ave Width (mm)
4	B	99	03	4B-99-03	Hairline	Hairline
4	B	03	04	4B-03-04		Hairline
4	B	03	05	4B-03-05		Hairline
4	B	03	06	4B-03-06		Hairline
4	B	03	07	4B-03-07		Unable to locate
4	B	03	08	4B-03-08		Unable to locate
4	T	99	01	4T-99-01	Hairline	0.15
4	T	99	02	4T-99-02	Hairline	0.80
4	T	99	03	4T-99-03	Hairline	0.80
4	T	03	04	4T-03-04		0.50
4	T	03	05	4T-03-05		0.35
4	T	03	06	4T-03-06		0.37
4	T	03	07	4T-03-07		0.60
4	T	03	08	4T-03-08		0.55
4	T	03	09	4T-03-09		0.55
4	T	03	10	4T-03-10		1.60
4	T	03	11	4T-03-11		1.20
4	T	03	12	4T-03-12		Hairline
4	T	03	13	4T-03-13		0.17
4	T	03	14	4T-03-14		0.73
5	B	99	01	5B-99-01	0.75	0.72
5	B	99	02	5B-99-02	0.10	0.30
5	B	03	03	5B-03-03		Hairline
5	B	03	04	5B-03-04		Hairline
5	B	03	05	5B-03-05		Hairline
5	B	03	06	5B-03-06		Hairline
5	B	03	07	5B-03-07		Hairline
5	B	03	08	5B-03-08		Hairline
5	B	03	09	5B-03-09		Hairline
5	T	99	01	5T-99-01	Hairline	Unable to locate
5	T	99	02	5T-99-02	Hairline	1.0
5	T	99	03	5T-99-03	Hairline	0.25
5	T	99	04	5T-99-04	Hairline	Hairline
5	T	03	05	5T-03-05		1.17
5	T	03	06	5T-03-06		0.55
5	T	03	07	5T-03-07		0.43
5	T	03	08	5T-03-08		1.10
5	T	03	09	5T-03-09		0.55
5	T	03	10	5T-03-10		Hairline
5	T	03	11	5T-03-11		0.35
5	T	03	12	5T-03-12		Hairline
5	T	03	13	5T-03-13		Hairline

Panel	Side	Year	Number	Identification Number	99-Width (mm)	03-Ave Width (mm)
5	T	03	14	5T-03-14		0.40
5	T	03	15	5T-03-15		0.40
6	B	99	01	6B-99-01	0.75	0.92
6	B	99	02	6B-99-02	Hairline	Unable to locate
6	B	99	03	6B-99-03	0.10	0.27
6	B	03	04	6B-03-04		Hairline
6	B	03	05	6B-03-05		Hairline
6	B	03	06	6B-03-06		0.30
6	B	03	07	6B-03-07		Hairline
6	B	03	08	6B-03-08		Hairline
6	B	03	09	6B-03-09		Hairline
6	B	03	10	6B-03-10		Hairline
6	T	99	01	6T-99-01	Hairline	Unable to locate
6	T	99	02	6T-99-02	Hairline	0.30
6	T	99	03	6T-99-03	Hairline	0.40
6	T	99	04	6T-99-04	Hairline	Hairline
6	T	03	05	6T-03-05		1.30
6	T	03	06	6T-03-06		Hairline
6	T	03	07	6T-03-07		0.74
6	T	03	08	6T-03-08		0.40
6	T	03	09	6T-03-09		0.50
6	T	03	10	6T-03-10		0.50
6	T	03	11	6T-03-11		Hairline
6	T	03	12	6T-03-12		0.67
6	T	03	13	6T-03-13		Hairline
6	T	03	14	6T-03-14		0.47
6	T	03	15	6T-03-15		Hairline
6	T	03	16	6T-03-16		0.87
6	T	03	17	6T-03-17		0.45
6	T	03	18	6T-03-18		0.88
7	B	99	01	7B-99-01	0.75	0.09
7	B	99	02	7B-99-02	Hairline	0.28
7	B	99	03	7B-99-03	Hairline	Hairline
7	B	03	04	7B-03-04		0.20
7	B	03	05	7B-03-05		0.16
7	B	03	06	7B-03-06		Hairline
7	B	03	07	7B-03-07		Hairline
7	T	99	01	7T-99-01	Hairline	Hairline
7	T	03	02	7T-03-02		0.99
7	T	03	03	7T-03-03		0.63
7	T	03	04	7T-03-04		0.21
7	T	03	05	7T-03-05		Hairline

Panel	Side	Year	Number	Identification Number	99-Width (mm)	03-Ave Width (mm)
7	T	03	06	7T-03-06		0.41
7	T	03	07	7T-03-07		Hairline
7	T	03	08	7T-03-08		Hairline
7	T	03	09	7T-03-09		1.10
7	T	03	10	7T-03-10		0.87
7	T	03	11	7T-03-11		Hairline
7	T	03	12	7T-03-12		0.54
7	T	03	13	7T-03-13		0.35
8	B	99	01	8B-99-01	1.00	0.50
8	B	99	02	8B-99-02	Hairline	1.69
8	B	99	03	8B-99-03	Hairline	0.30
8	B	03	04	8B-03-04		0.30
8	B	03	05	8B-03-05		0.26
8	B	03	06	8B-03-06		Hairline
8	T	99	01	8T-99-01	Hairline	Unable to locate
8	T	99	02	8T-99-02	Hairline	0.55
8	T	03	03	8T-03-03		0.55
8	T	03	04	8T-03-04		Hairline
8	T	03	05	8T-03-05		Hairline
8	T	03	06	8T-03-06		Hairline
8	T	03	07	8T-03-07		Hairline

Abbreviations:

B-Bottom
T-Top
99-1999
03-2003

Table 4.3 - Record of Forestry Bridge Arch Panel Crack Width Measurements July 1999 and October 2003

Of interest is the development of numerous secondary cracks in the vicinity of the grout pockets which formed on the slab between the years 1999 and 2003. Although not the focus of this thesis, it is worth noting that this type of cracking was not evident in the fatigue test performed at UBC. It was also noticed that cracks had progressed from the bottom to the top surface of the slab in the middle of the slab, away from the grouted joint. This reinforces the conclusion proposed by Mufti et al, that it was the compressive field around the stationary pulsating load in the experiment at UBC which prevented the top surface cracks from travelling through the load patch [15]. Furthermore, what has been demonstrated is that the cracks do not require a free edge to initiate progression from the bottom to the top surface.

5.0 Development of Truck Loading Strain Spectra

5.1 Assessment of Data and Development of Test Vehicle Loading Spectra

The data recorded from the load testing of the bridge described in Section 4.2.3.1 was used to develop a load spectrum response for each of the two panels on the bridge which had strain gauges attached to the steel straps beneath the panels. The strains are shown in Table 5.1 for each of the left, centre and right positions of the test vehicle [16].

Position	Distance (m)	Left		Centre		Right	
		Channel 5 (με)	Channel 6 (με)	Channel 5 (με)	Channel 6 (με)	Channel 5 (με)	Channel 6 (με)
0	0	2	2			-6	-7
1	2	2	6	7	6	-4	-2
2	4	2	8	1	6	-2	0
3	6	4	17	7	24	0	15
4	8	7	28	11	32	2	22
5	10	10	43	16	51	9	41
6	12	20	95	21	105	16	91
7	14	29	123	32	139	28	124
8	16	55	79	66	93	53	83
8A	17	76	52	93	63	80	50
9	18	75	51	89	65	76	50
10	20	47	68	55	86	42	65
11	22	28	59	37	71	29	61
12	24	38	22	50	31	38	20
13	26	32	9	45	13	31	6
14	28	12	2	22	7	14	-1
15	30	4	0	7	2	5	1
16	32	1	1	3	2	1	0
17	34	1	0	4	4	-1	-4
18	36	1	1	1	4	0	0
19	38	1	0	2	1	-1	0
20	40	0	0	0	0	0	0

Table 5.1 - Recorded Strains from Static Testing of Fully Loaded Test Vehicle

It became evident in reviewing the results that wheel loads which were remote from the given panel whose steel strap was being monitored, contributed to the strain in the strap. For example, as the steering axle of the test vehicle began to cross the bridge at Panel 8, or as the rear axle of the trailer was exiting the bridge on Panel 2, and to a minor degree Panel 1, strains were being recorded in the straps in Panels 5 and 6.

In developing the spectrum, it was noticed that strains in the straps with the test vehicle in the centre position on the bridge were typically higher than when the vehicle was closer to either curb. For the peak strain conditions on the strap, the difference between the strain from the centre loading and the least of either left or right transverse position loading was 22% for gauge 5 and 13% for gauge 6. However, the premise is that during normal operation of the bridge, there is an equal chance of the vehicle being in any one of the three transverse positions. Therefore the mean of the 3 strains was taken for each of the longitudinal positions of the test vehicle on the bridge. The differences between the strains from the centre loading positions and the means are 12% and 8% for gauges 5 and 6 respectively for the peak strain conditions. For the least of the left or right transverse positions, the differences between peak mean values for strain are -9% and -5% for gauges 5 and 6 respectively. The mean strains are shown in Table 5.2. Plots of the mean strain relative to the truck position for each of the two strain gauges are shown in Figures 5.1 and 5.2.

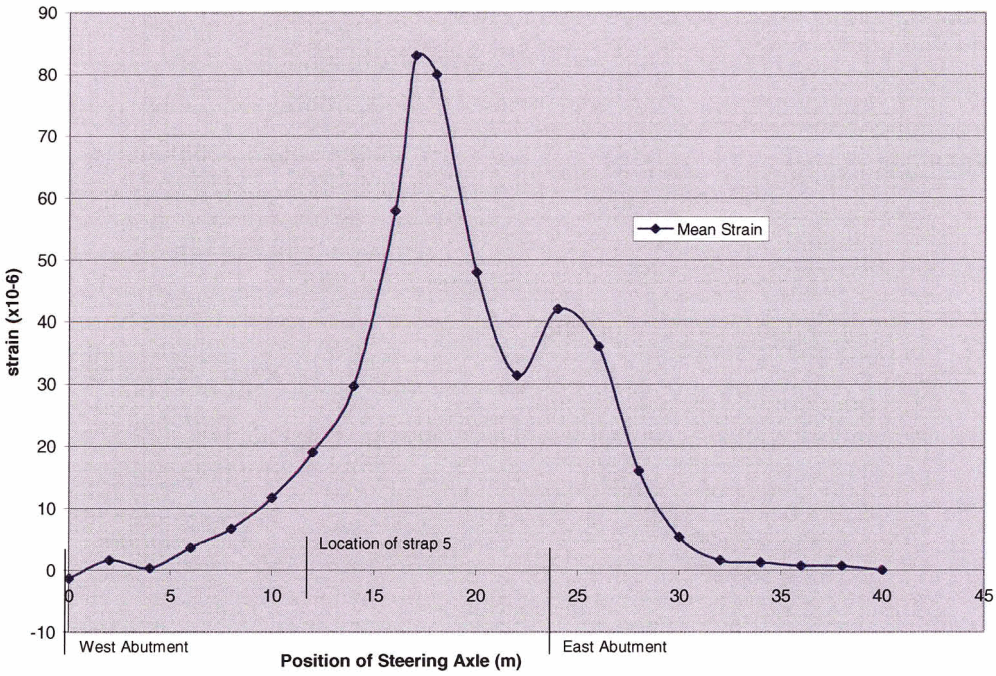

Figure 5.1 - Forestry Bridge Test Vehicle-Spectrum for Strain in Arch Panel Strap Strain Gauge 5

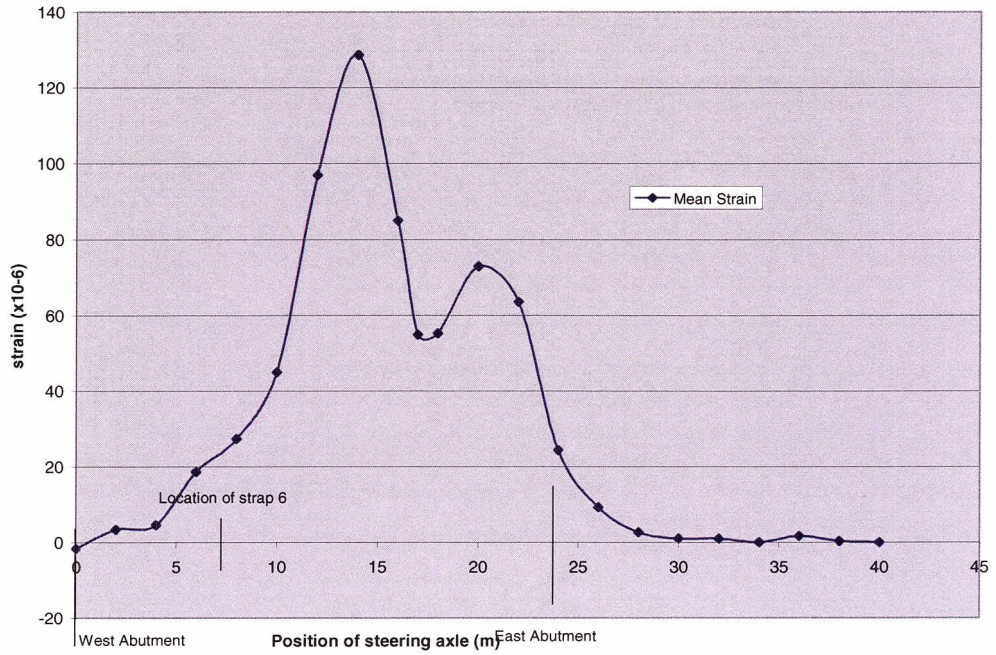

Figure 5.2 - Forestry Bridge Test Vehicle-Spectrum for Strain in Arch Panel Strap Strain Gauge 6

Position	Distance (m)	Gauge 5 Mean Strain (με)	Gauge 6 Mean Strain (με)
0	0	-1	-2
1	2	2	3
2	4	0	5
3	6	4	19
4	8	7	27
5	10	12	45
6	12	19	97
7	14	30	129
8	16	58	85
8A	17	83	55
9	18	80	55
10	20	48	73
11	22	31	64
12	24	42	24
13	26	36	9
14	28	16	3
15	30	5	1
16	32	2	1
17	34	1	0
18	36	1	2
19	38	1	0
20	40	0	0

Table 5.2 - Mean Strains for Strains for Strain Gauges 5 and 6 due to Passage of Test Vehicle

5.2 Development of Theoretical Test Vehicle Loading Strain Spectra

In order to develop truck loading v strain spectra which could be applied to other types of vehicles, influence coefficients due to the test vehicle crossing the bridge were developed. This was done by means of "marching" the test vehicle across the bridge and observing the influence of each axle on the mean values of strain obtained as described in Section 5.1. Independent strain values were identified for the isolated steering axle and trailer axle loads as the truck entered and exited the bridge. These values were then pro-rated linearly for the other two axles which either followed or preceded them. In the case of the tandem axle, each axle was treated independently since it was found that by

separating the two axles, the influence on the resulting spectrum was significant. The method was one of trial and error as it was felt that greater accuracy in developing formulae to describe the influence from each of the axles was not warranted. Influence coefficients for strain in the straps at each of the two strap locations are presented in Figure 5.3.

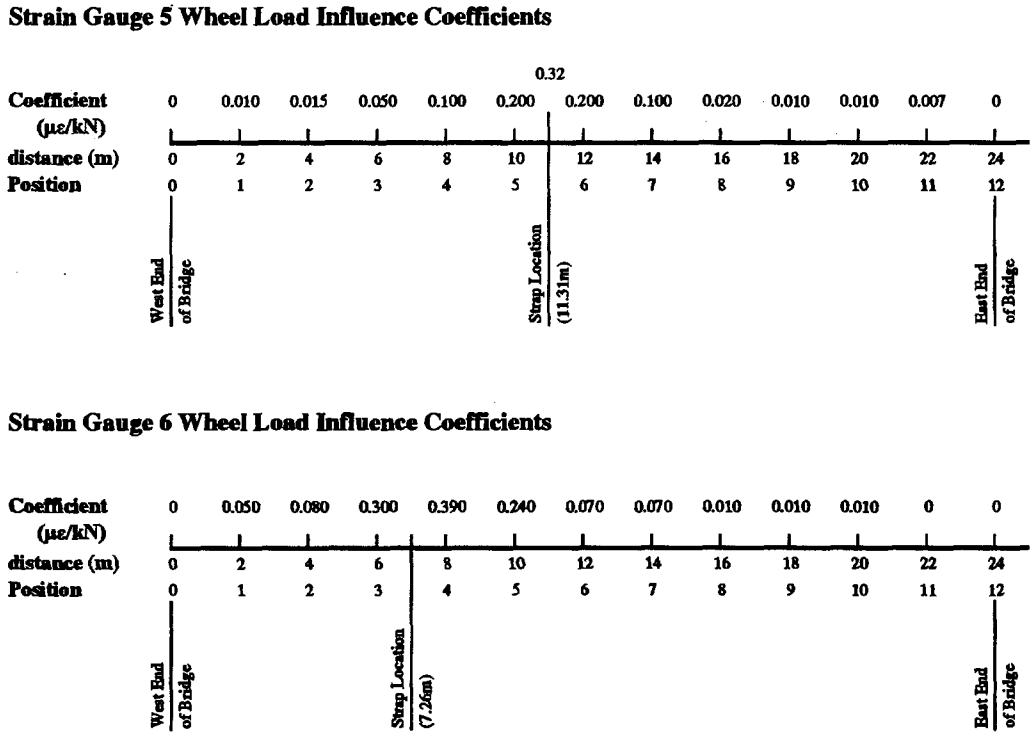

Figure 5.3 - Estimated Influence Coefficients for Strain in Gauges 5 and 6

The resulting theoretical contributions to strain at each of the test vehicle positions were then estimated based on the influence coefficients. These are shown in Tables 5.3 and 5.4 for strain gauges 5 and 6. The theoretical strains in the straps developed in this way are shown alongside the mean strains obtained from the real test vehicle in Tables 5.5 and 5.6. The results, which are a reasonably accurate representation of the real truck spectrum, were plotted on the graph of the mean strain v truck loading obtained in Section 5.1 and are shown in Figures 5.4 and 5.5.

Axle Position	Distance (m)	154 kN Tandem axle		303.6kN Tandem Axle		60.7kN Single Axle Load	Total Strain in Strap (με)
		77kN Axle Load	77kN Axle Load	151.8kN Axle Load	151.8kN Axle Load		
0	0	0	0	0	0	0	**0**
1	2	0	0	0	0	0.010	**1**
2	4	0	0	0	0	0.015	**1**
3	6	0	0	0	0.007	0.050	**4**
4	8	0	0	0.007	0.010	0.100	**9**
5	10	0	0	0.012	0.015	0.200	**16**
6	12	0	0	0.012	0.050	0.200	**22**
7	14	0	0.005	0.075	0.100	0.100	**33**
8	16	0.010	0.012	0.120	0.250	0.020	**59**
8A	17	0.012	0.015	0.200	0.320	0.015	**82**
9	18	0.015	0.030	0.300	0.200	0.010	**80**
10	20	0.050	0.075	0.150	0.100	0.010	**48**
11	22	0.100	0.130	0.060	0.018	0.007	**30**
12	24	0.200	0.320	0.015	0.010	0	**44**
13	26	0.210	0.160	0.010	0.010	0	**32**
14	28	0.100	0.060	0.009	0.007	0	**15**
15	30	0.020	0.015	0.005	0	0	**3**
16	32	0.010	0.010	0	0	0	**2**
17	34	0.010	0.008	0	0	0	**1**
18	36	0.007	0.005	0	0	0	**1**
19	38	0	0	0	0	0	**0**
20	40	0	0	0	0	0	**0**

Table 5.3 - Contribution of Independent Axles from Test Vehicle to Strain in Strap at Strain Gauge 5

Axle Position	Distance (m)	154 kN Tandem axle		303.6kN Tandem Axle		60.7kN Single Axle Load	Total Strain in Strap (με)
		77kN Axle Load	77kN Axle Load	151.8kN Axle Load	151.8kN Axle Load		
0	0	0	0	0	0	0	**0**
1	2	0	0	0	0	0.05	**3**
2	4	0	0	0	0	0.08	**5**
3	6	0	0	0	0.01	0.3	**20**
4	8	0	0	0.02	0.05	0.39	**34**
5	10	0	0	0.07	0.12	0.24	**43**
6	12	0	0	0.25	0.35	0.07	**95**
7	14	0	0.03	0.39	0.39	0.07	**125**
8	16	0.05	0.07	0.3	0.2	0.01	**86**
8A	17	0.06	0.08	0.24	0.1	0.01	**63**
9	18	0.08	0.2	0.15	0.07	0.01	**56**
10	20	0.3	0.39	0.07	0.06	0.01	**73**
11	22	0.39	0.32	0.05	0.01	0	**64**
12	24	0.24	0.1	0.01	0.01	0	**29**
13	26	0.07	0.07	0.01	0	0	**12**
14	28	0.07	0.03	0	0	0	**8**
15	30	0.01	0.01	0	0	0	**2**
16	32	0.01	0.01	0	0	0	**2**
17	34	0.01	0	0	0	0	**1**
18	36	0.01	0	0	0	0	**1**
19	38	0	0	0	0	0	**0**
20	40	0	0	0	0	0	**0**

Table 5.4 - Contribution of Independent Axles from Test Vehicle to Strain in Strap at Strain Gauge 6

Position	Distance (m)	Theoretical Strain (με)	Measured Mean Strain (με)
0	0	0	-1
1	2	1	2
2	4	1	0
3	6	4	4
4	8	9	7
5	10	16	12
6	12	22	19
7	14	33	30
8	16	59	58
8A	17	82	83
9	18	80	80
10	20	48	48
11	22	30	31
12	24	44	42
13	26	32	36
14	28	15	16
15	30	3	5
16	32	2	2
17	34	1	1
18	36	1	1
19	38	0	1
20	40	0	0

Table 5.5 - Comparison of Theoretical v Measured Mean Strain in Strain Gauge 5

Position	Distance (m)	Theoretical Strain (με)	Measured Mean Strain (με)
0	0	0	-2
1	2	3	3
2	4	5	5
3	6	20	19
4	8	34	27
5	10	43	45
6	12	95	97
7	14	125	129
8	16	86	85
8A	17	63	55
9	18	56	55
10	20	73	73
11	22	64	64
12	24	29	24
13	26	12	9
14	28	8	3
15	30	2	1
16	32	2	1
17	34	1	0
18	36	1	2
19	38	0	0
20	40	0	0

Table 5.6 - Comparison of Theoretical v Measured Mean Strain in Strain Gauge 6

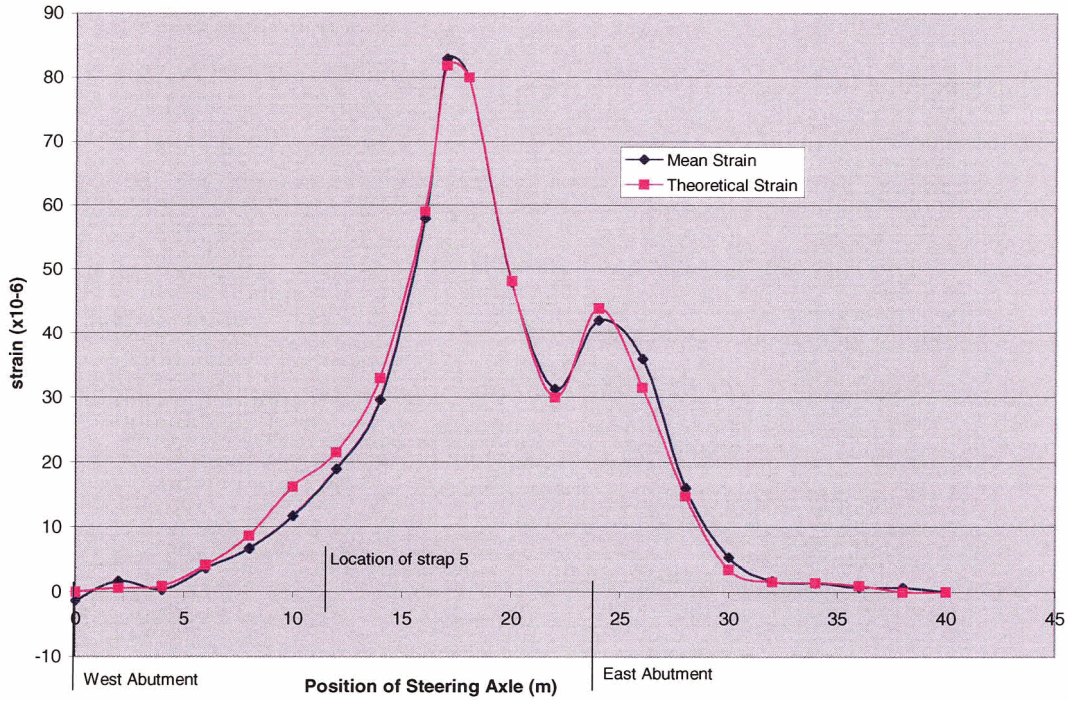

Figure 5.4 - Forestry Bridge Test Vehicle-Spectra for Strain in Arch Panel Strap Strain Gauge 5

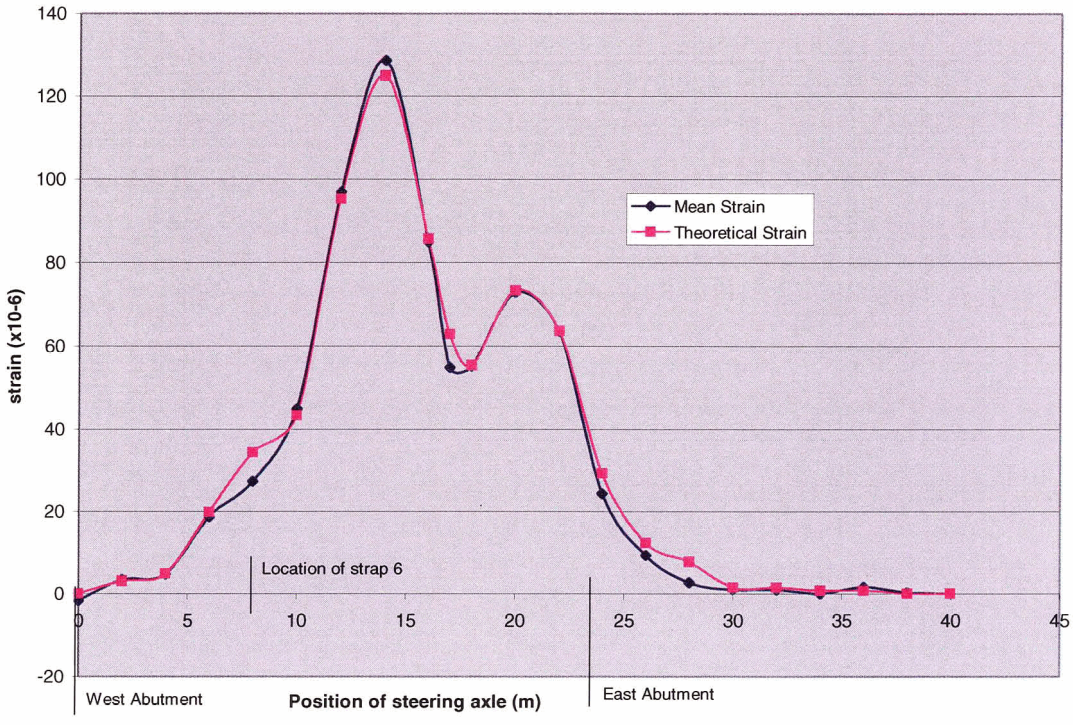

Figure 5.5 - Forestry Bridge Test Vehicle and Theoretical-Spectra for Strain in Arch Panel Strap Strain Gauge 6

5.3 Development of FERIC Truck Loading Spectra

In order to evaluate the behaviour of the unreinforced concrete panels under fatigue loading it was necessary to obtain an estimate of the actual truck loading to which the panels were subjected. Through the cooperation of the Ministry of Forests Regional Bridge Engineer, data was obtained from the primary users in the Forest Industry [6]. These included Weyerhauser Canada, Tolko Industries and BC Timber Sales. All three submitted an estimate of the number of loaded logging trucks and lowbed vehicles which crossed the bridge during the 5 year period from when the bridge was constructed in 1998 through until the fall of 2003. It should be noted that all loaded vehicles had gross vehicle weights of less than the L-75 design vehicle as it was necessary for them to travel on the Ministry of Transportation highway system as part of their normal route.

Since the types of trucks varied, a realistic approximation was made of the logging truck configurations based on information provided by the three main users. Representative vehicles were selected from the April 1998 publication of "Popular B.C. Vehicle Configurations for Hauling Full Length Logs" as published by the Forest Engineering Research Institute of Canada (FERIC) [19]. Table 1 from the publication is shown in Figure 5.6. For ease of reference in this thesis, the vehicles have been numbered from 1 to 11. The specific FERIC vehicles selected as representative of the actual trucks which crossed the Forestry Bridge are configurations 1, 2, 4, 7 and 8. Contact was also made directly with FERIC [7] to obtain the axle spacing and distribution of axle loads for the FERIC truck configurations. For the lowbed axle configuration and distribution of axle loads, contact was made with a truck transport company which services the area in which the Forestry Bridge is located [8]. The axle loadings and configurations for the FERIC vehicles and a typical lowbed are shown in Figure 5.7. The estimated truck traffic which crossed the bridge during the five year period from 1998 to 2003 is shown in Table 5.7.

---

[6] Private communications: Gary McClelland, Regional Bridge Engineer, BC Ministry of Forests, dated November 6, 7, 12, 2003; January 27, 2004; March 4, 23, 2004; April 30, 2004.
[7] Private communication: Eric Anlin, FERIC, dated July 22, 2004.
[8] Private communication: Darlen Transport, Kamloops, dated July 19, 2004.

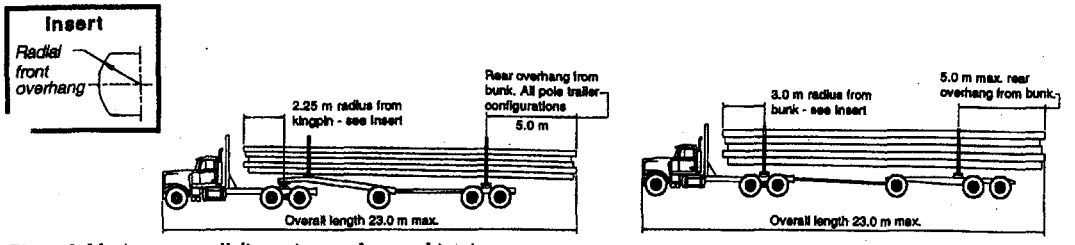

Figure 2. Maximum overall dimensions, other combinations.

Table 1. Typical B.C. Vehicle Configurations.

	Configuration	Max. GVW [a] (kg)	Max.load [a]/ axle group [b] (kg)	Typical tare / max. net capacity (kg)	GVW [a] with popular 11-in. steer [d] tires (kg)	Axles (no.)	Articulation points (no.)
1	Tandem log truck / tandem pole trailer	43 100	Steer: 9 100 Drive: 17 000 Trailer: 17 000	13 875 / 29 225	40 147	5	1
2	Tandem log truck / tridem pole trailer	50 100	Steer: 9 100 Drive: 17 000 Trailer: 24 000	15 700 / 34 400	47 147	6	1
3	Tridem log truck / tandem pole trailer	47 500	Steer: 6 500 [c] Drive: 24 000 Trailer: 17 000	16 960 / 30 540	47 500	6	1
4	Tridem log truck / tridem pole trailer	54 500	Steer: 6 500 [c] Drive: 24 000 Trailer: 24 000	18 780 / 35 720	54 500	7	1
5	Tandem log truck / quadaxle trailer	60 100	Steer: 9 100 Drive: 17 000 Tandem: 17 000 each	17 000 / 43 100	57 147	7	2
6	Tandem log truck / triaxle trailer	52 200	Steer: 9 100 Drive: 17 000 Single: 9 100 Tandem: 17 000	15 700 / 36 500	49 247	6	2
7	Truck tractor / jeep / tandem pole trailer [e]	52 200	Steer: 9 100 Drive: 17 000 Jeep: 9 100 Trailer: 17 000	16 700 / 35 500	49 247	6	2
8	Dog logger [e]	52 200	Steer: 9 100 Drive: 17 000 Tandem: 17 000 Dog: 9 100	16 500 / 35 700	49 247	6	2
9	Truck tractor / tandem jeep / tandem trailer [e]	60 100	Steer: 9 100 Drive: 17 000 Jeep: 17 000 Trailer: 17 000	19 400 / 40 700	57 147	7	2
10	Truck tractor / jeep / dog logger [e]	61 300	Steer: 9 100 Drive 17 000 Jeep: 9 100 Tandem: 17 000 Dog: 9 100	19 400 / 41 900	58 347	7	3
11	Truck tractor / jeep / triaxle trailer	61 300	Steer: 9 100 Drive: 17 000 Jeep: 9 100 Single: 9 100 Tandem: 17 000	18 600 / 42 700	58 347	7	3

[a] Weights do not include allowances, see notes for specification. [b] Restrictions apply to axle group and steering axle loading, see text for clarification. [c] Legal steering axle load can be increased to 9100 kg for configurations equipped with a self loader. [d] Steer axle load reduced to 6147 kg with 11" tires on all combinations, except to 6500 kg with 315 mm tires on tridem log trucks. All other axles at maximum allowable loads. [e] Tridem pole trailer not to be used in combination with jeeps or dogloggers.

Figure 5.6 - FERIC Logging Truck Vehicle Configuration for BC

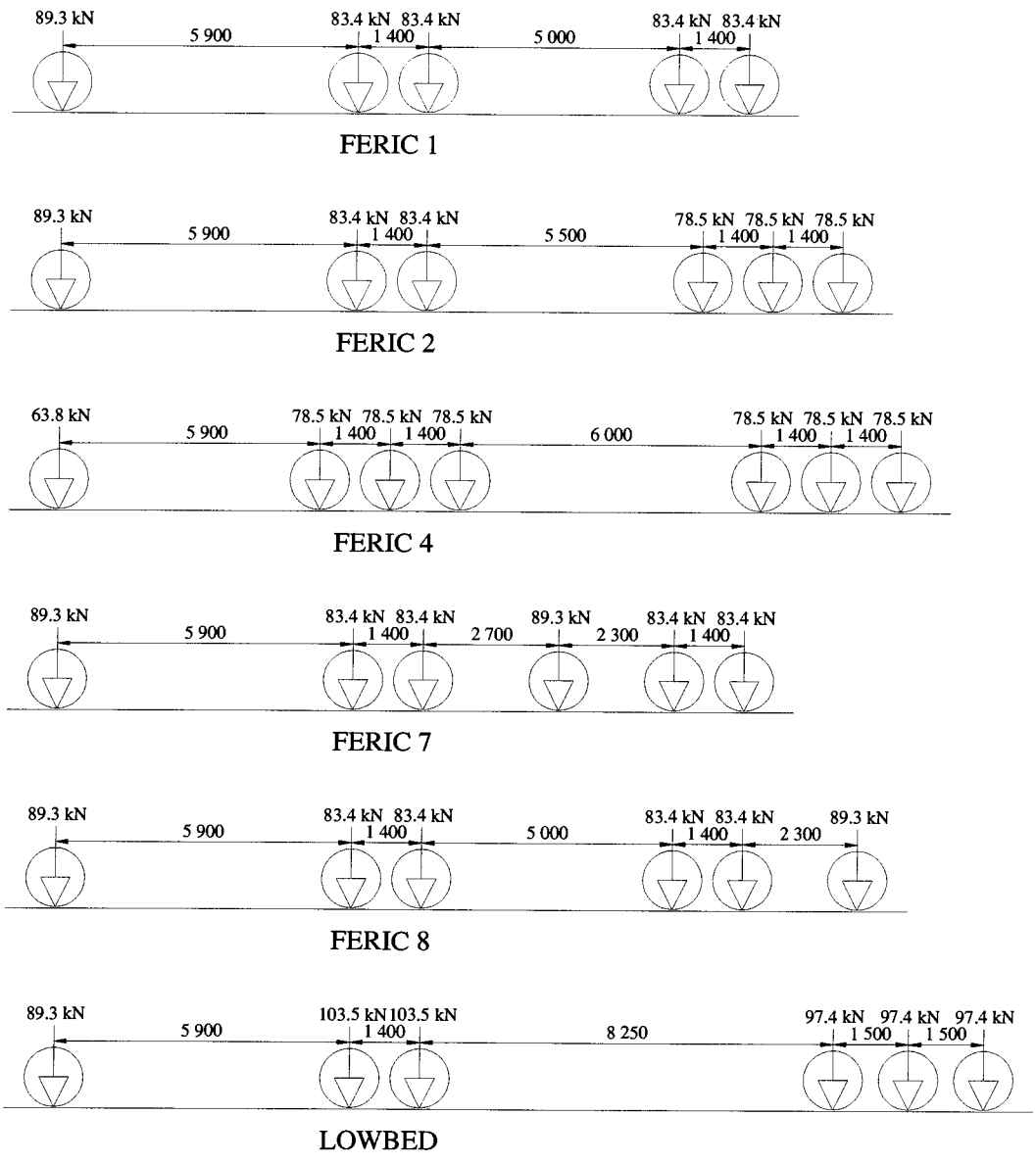

Figure 5.7 - Typical Vehicle Configurations

Company	Year	Vehicle						Totals
		FERIC 1	FERIC2	FERIC4	FERIC7	FERIC8	Lowbed	
BCTS	1998				250	250	30	**530**
	1999						10	**10**
	2000				625	625	35	**1285**
	2001						10	**10**
	2002				125	125	15	**265**
	2003				80	80	10	**170**
	Total	**0**	**0**	**0**	**1080**	**1080**	**110**	**2270**
Tolko	1998							**0**
	1999							**0**
	2000	64	602	602			11	**1279**
	2001						6	**6**
	2002							**0**
	2003	12	111	112			8	**243**
	Total	**76**	**713**	**714**	**0**	**0**	**25**	**1528**
Weyerhauser	1998							**0**
	1999							**0**
	2000							**0**
	2001		265	265			12	**542**
	2002		265	265			12	**542**
	2003		265	265			12	**542**
	Total	**0**	**795**	**795**	**0**	**0**	**36**	**1626**

Table 5.7 - Loading History for Forestry Bridge 1998 to 2003

Load spectra for the lowbeds and FERIC logging trucks were developed using the coefficients from the theoretical test vehicle loading strain spectra as described in Section 5.2 for channels 5 and 6. The trucks were "marched" across the bridge in the direction in which they would have travelled when loaded and the contributions from each of the axle loads at any given position were summed to provide a point on the graph of strain v the longitudinal position of the steering axle relative to the bridge. The theoretical contributions to strain from the axles of each of the vehicles are given in Tables 5.8 and 5.9 for channels 5 and 6 respectively. The graphs resulting from these coefficients are shown in Figures 5.8 and 5.9. These graphs are representative of the load spectrums applicable for each of the vehicles for both channels. Note that all loaded FERIC vehicles were considered to be travelling from the east towards the west end of the bridge. Lowbeds were considered to travel loaded in both directions of travel since the

equipment they were hauling required transportation both into and out of the logging area.

FERIC 1	Vehicle Axle Load (kN)							Total Strain in Strap (με)
Location of	1st Axle	2nd Axle	3rd Axle	4th Axle	5th Axle	6th Axle	7th Axle	
Steering Axle (m)	89.3	83.4	83.4	83.4	83.4	-	-	
24	0							0
22	0.007							1
20	0.010	0						1
18	0.010	0.001						1
17	0.015	0.005	0					2
16	0.020	0.007	0.003					3
14	0.100	0.010	0.008					10
12	0.200	0.010	0.010	0				20
10	0.200	0.020	0.013	0.006	0.002			21
8	0.100	0.100	0.045	0.100	0.007			30
6	0.050	0.200	0.130	0.010	0.010			34
4	0.015	0.200	0.230	0.019	0.011			40
2	0.010	0.100	0.150	0.090	0.030			32
0	0	0.050	0.085	0.180	0.110			35
-2		0.015	0.035	0.220	0.210			40
-4		0.010	0.013	0.110	0.180			26
-6		0	0.008	0.060	0.090			13
-8			0	0.020	0.045			5
-10				0.011	0.014			2
-12				0.002	0.009			1
-14				0	0			0
-16								
-18								
-20								

FERIC 2	Vehicle Axle Load (kN)							Total Strain in Strap (με)
Location of	1st Axle	2nd Axle	3rd Axle	4th Axle	5th Axle	6th Axle	7th Axle	
Steering Axle (m)	89.3	83.4	83.4	78.5	78.5	78.5	-	
24	0							0
22	0.007							1
20	0.010	0						1
18	0.010	0.001						1
17	0.015	0.005	0					2
16	0.020	0.007	0.003					3
14	0.100	0.010	0.008					10
12	0.200	0.010	0.010	0				20
10	0.200	0.020	0.013	0.005	0	0		21
8	0.100	0.100	0.045	0.009	0.006	0.001		22
6	0.050	0.200	0.130	0.010	0.010	0.007		34
4	0.015	0.200	0.230	0.016	0.010	0.020		41
2	0.010	0.100	0.150	0.065	0.018	0.011		29
0	0	0.050	0.085	0.160	0.080	0.030		32
-2		0.015	0.035	0.240	0.180	0.110		46
-4		0.010	0.013	0.120	0.220	0.210		45
-6		0	0.008	0.070	0.110	0.180		29
-8			0	0.025	0.060	0.090		14
-10				0.012	0.020	0.045		6
-12				0.006	0.011	0.014		2
-14				0	0.002	0.009		1
-16					0	0		0
-18								
-20								

FERIC 4	Vehicle Axle Load (kN)							Total Strain in Strap (με)
Location of	1st Axle	2nd Axle	3rd Axle	4th Axle	5th Axle	6th Axle	7th Axle	
Steering Axle (m)	63.8	78.5	78.5	78.5	78.5	78.5	78.5	
24	0							0
22	0.007							0
20	0.010	0						1
18	0.010	0.004	0					1
17	0.015	0.007	0.002					2
16	0.020	0.009	0.005	0				2
14	0.100	0.010	0.009	0.007				8
12	0.200	0.014	0.010	0.010				15
10	0.200	0.050	0.017	0.010	0	0		19
8	0.100	0.140	0.070	0.020	0.007	0.002	0	25
6	0.050	0.240	0.170	0.100	0.010	0.008	0.005	45
4	0.015	0.150	0.240	0.200	0.010	0.010	0.009	50
2	0.010	0.080	0.120	0.200	0.020	0.012	0.010	35
0	0	0.035	0.065	0.100	0.100	0.035	0.015	27
-2		0.013	0.025	0.050	0.200	0.120	0.060	37
-4		0.008	0.011	0.015	0.200	0.230	0.150	48
-6		0	0.005	0.010	0.100	0.160	0.250	41
-8			0	0	0.050	0.090	0.130	21
-10					0.015	0.040	0.075	10
-12					0.010	0.013	0.030	4
-14					0	0.008	0.012	2
-16						0	0.007	1
-18							0	0
-20								

FERIC 7	Vehicle Axle Load (kN)							Total Strain in Strap (με)
Location of	1st Axle	2nd Axle	3rd Axle	4th Axle	5th Axle	6th Axle	7th Axle	
Steering Axle (m)	89.3	83.4	83.4	89.3	83.4	83.4	-	
24	0							0
22	0.007							1
20	0.010	0						1
18	0.010	0.001						1
17	0.015	0.005	0					2
16	0.020	0.007	0.003					3
14	0.100	0.010	0.008	0				10
12	0.200	0.010	0.010	0.007	0	0		20
10	0.200	0.020	0.013	0.010	0.006	0.002		22
8	0.100	0.100	0.045	0.010	0.010	0.007		23
6	0.050	0.200	0.130	0.020	0.010	0.010		35
4	0.015	0.200	0.230	0.100	0.019	0.011		49
2	0.010	0.100	0.150	0.200	0.090	0.030		50
0	0	0.050	0.085	0.200	0.180	0.110		53
-2		0.015	0.035	0.100	0.220	0.210		49
-4		0.010	0.013	0.050	0.110	0.180		31
-6		0	0.008	0.015	0.060	0.090		15
-8			0	0.010	0.020	0.045		6
-10				0	0.011	0.014		2
-12					0.002	0.009		1
-14					0	0		0
-16								
-18								
-20								

FERIC 8	Vehicle Axle Load (kN)							Total Strain in Strap (με)
Location of	1st Axle	2nd Axle	3rd Axle	4th Axle	5th Axle	6th Axle	7th Axle	
Steering Axle (m)	89.3	83.4	83.4	83.4	83.4	89.4	-	
24	0							0
22	0.007							1
20	0.010	0						1
18	0.010	0.001						1
17	0.015	0.005	0					2
16	0.020	0.007	0.003					3
14	0.100	0.010	0.008					10
12	0.200	0.010	0.010	0	0			20
10	0.200	0.020	0.013	0.006	0.002			21
8	0.100	0.100	0.045	0.100	0.007	0		30
6	0.050	0.200	0.130	0.010	0.010	0.007		34
4	0.015	0.200	0.230	0.019	0.011	0.010		41
2	0.010	0.100	0.150	0.090	0.030	0.010		33
0	0	0.050	0.085	0.180	0.110	0.020		37
-2		0.015	0.035	0.220	0.210	0.100		49
-4		0.010	0.013	0.110	0.180	0.200		44
-6		0	0.008	0.060	0.090	0.200		31
-8			0	0.020	0.045	0.100		14
-10				0.011	0.014	0.050		7
-12				0.002	0.009	0.015		2
-14				0	0	0.010		1
-16						0		0
-18								
-20								

Low Bed Out	Vehicle Axle Load (kN)							Total Strain in Strap (με)
Location of	1st Axle	2nd Axle	3rd Axle	4th Axle	5th Axle	6th Axle	7th Axle	
Steering Axle (m)	89.3	103.5	103.5	97.4	97.4	97.4	-	
24	0							0
22	0.007							1
20	0.010							1
18	0.010							1
17	0.015	0						1
16	0.020	0.005	0					2
14	0.100	0.009	0.007					11
12	0.200	0.010	0.010					20
10	0.200	0.015	0.010					20
8	0.100	0.060	0.020	0				17
6	0.050	0.150	0.100	0.006	0	0		31
4	0.015	0.250	0.200	0.010	0.007	0.003		50
2	0.010	0.130	0.200	0.010	0.010	0.008		38
0	0	0.075	0.100	0.017	0.010	0.010		22
-2		0.030	0.050	0.090	0.020	0.013		20
-4		0.012	0.015	0.180	0.100	0.045		34
-6		0.007	0.010	0.220	0.200	0.130		55
-8		0	0	0.120	0.200	0.230		54
-10				0.060	0.100	0.160		31
-12				0.020	0.050	0.090		16
-14				0.011	0.015	0.040		6
-16				0.003	0.010	0.013		3
-18				0	0	0.009		1
-20						0		0

Low Bed In	Vehicle Axle Load (kN)							Total Strain in Strap (με)
Location of	1st Axle	2nd Axle	3rd Axle	4th Axle	5th Axle	6th Axle	7th Axle	
Steering Axle (m)	89.3	103.5	103.5	97.4	97.4	97.4	-	
0	0							0
2	0.010							1
4	0.015							1
6	0.050	0						4
7	0.100	0.007	0					10
8	0.200	0.012	0.010					20
10	0.200	0.030	0.015					23
12	0.100	0.075	0.050					22
14	0.020	0.130	0.100	0				26
16	0.015	0.200	0.130	0.005				36
18	0.010	0.250	0.200	0.009	0	0		48
20	0.010	0.150	0.200	0.014	0.010	0.003		40
22	0.007	0.060	0.100	0.040	0.015	0.011		24
24	0	0.015	0.020	0.090	0.050	0.025		20
26		0.010	0.010	0.180	0.100	0.065		36
28		0.009	0.010	0.230	0.200	0.120		56
30		0.005	0.007	0.130	0.200	0.230		56
32		0	0	0.040	0.100	0.180		31
34				0.013	0.020	0.080		11
36				0.010	0.010	0.017		4
38				0.008	0.010	0.010		3
40				0.003	0.007	0.010		2
42				0	0	0.006		1
44						0		0

Table 5.8 - Contribution of Independent Axles to Strain in Strap at Strain Gauge 5

FERIC 1	Vehicle Axle Load (kN)							Total Strain in Strap (με)
Location of	1st Axle	2nd Axle	3rd Axle	4th Axle	5th Axle	6th Axle	7th Axle	
Steering Axle (m)	89.3	83.4	83.4	83.4	83.4	-	-	
24	0							0
22	0.000							0
20	0.010							1
18	0.010							1
17	0.010	0.000						1
16	0.010	0.000	0.000					1
14	0.070	0.010	0.003					7
12	0.070	0.010	0.010					8
10	0.240	0.010	0.010	0.000				23
8	0.390	0.070	0.020	0.008	0.000			43
6	0.300	0.070	0.070	0.010	0.010			40
4	0.080	0.240	0.100	0.010	0.010			37
2	0.050	0.390	0.270	0.060	0.010			65
0	0	0.300	0.390	0.070	0.070			69
-2		0.080	0.230	0.210	0.070			49
-4		0.050	0.070	0.370	0.240			61
-6		0	0.040	0.320	0.390			63
-8			0	0.120	0.300			35
-10				0.050	0.080			11
-12				0.010	0.050			5
-14				0	0			0
-16								
-18								
-20								

FERIC 2	Vehicle Axle Load (kN)							Total Strain in Strap (με)
Location of	1st Axle	2nd Axle	3rd Axle	4th Axle	5th Axle	6th Axle	7th Axle	
Steering Axle (m)	89.3	83.4	83.4	78.5	78.5	78.5	-	
24	0							0
22	0							0
20	0.010							1
18	0.010							1
17	0.010							1
16	0.010	0	0					1
14	0.070	0.010	0.003					7
12	0.070	0.010	0.010					8
10	0.240	0.010	0.010	0				23
8	0.390	0.070	0.020	0.006	0	0		43
6	0.300	0.070	0.070	0.010	0.008	0.001		40
4	0.080	0.240	0.100	0.010	0.010	0.010		38
2	0.050	0.390	0.270	0.040	0.010	0.010		64
0	0	0.300	0.390	0.070	0.060	0.010		69
-2		0.080	0.230	0.150	0.070	0.070		49
-4		0.050	0.070	0.320	0.320	0.080		67
-6		0	0.040	0.370	0.370	0.260		82
-8			0	0.180	0.320	0.390		70
-10				0.060	0.110	0.280		35
-12				0.030	0.050	0.070		12
-14				0	0.010	0.040		4
-16					0	0		0
-18								
-20								

FERIC 4	Vehicle Axle Load (kN)							Total Strain in Strap (με)
Location of	1st Axle	2nd Axle	3rd Axle	4th Axle	5th Axle	6th Axle	7th Axle	
Steering Axle (m)	63.8	78.5	78.5	78.5	78.5	78.5	78.5	
24	0							0
22	0							0
20	0.010							1
18	0.010							1
17	0.010	0						1
16	0.010	0.004	0					1
14	0.070	0.010	0.006	0				6
12	0.070	0.010	0.010	0.010				7
10	0.240	0.030	0.010	0.010				19
8	0.390	0.070	0.050	0.010	0	0		35
6	0.300	0.100	0.070	0.070	0.010	0.003	0	39
4	0.080	0.280	0.160	0.070	0.010	0.010	0.005	47
2	0.050	0.390	0.350	0.240	0.010	0.010	0.010	82
0	0	0.220	0.350	0.390	0.070	0.030	0.010	84
-2		0.060	0.150	0.300	0.070	0.070	0.040	54
-4		0.030	0.060	0.080	0.240	0.090	0.070	45
-6		0	0.020	0.050	0.390	0.280	0.140	69
-8			0	0	0.300	0.390	0.320	79
-10					0.080	0.240	0.370	54
-12					0.050	0.070	0.180	24
-14					0	0.040	0.060	8
-16						0	0.030	2
-18							0	0
-20								

FERIC 7	Vehicle Axle Load (kN)							Total Strain in Strap (με)
Location of	1st Axle	2nd Axle	3rd Axle	4th Axle	5th Axle	6th Axle	7th Axle	
Steering Axle (m)	89.3	83.4	83.4	89.3	83.4	83.4	-	
24	0							0
22	0							0
20	0.010							1
18	0.010							1
17	0.010							1
16	0.010	0	0					1
14	0.070	0.010	0.003					7
12	0.070	0.010	0.010	0				8
10	0.240	0.010	0.010	0.010	0			24
8	0.390	0.070	0.020	0.010	0.008	0		44
6	0.300	0.070	0.070	0.010	0.010	0.010		41
4	0.080	0.240	0.100	0.070	0.010	0.010		43
2	0.050	0.390	0.270	0.070	0.060	0.010		72
0	0	0.300	0.390	0.220	0.070	0.070		89
-2		0.080	0.230	0.380	0.210	0.070		83
-4		0.050	0.070	0.320	0.370	0.240		89
-6		0	0.040	0.100	0.320	0.390		71
-8			0	0.050	0.120	0.300		39
-10				0	0.050	0.080		11
-12					0.010	0.050		5
-14					0	0		0
-16								
-18								
-20								

FERIC 8	Vehicle Axle Load (kN)							Total Strain in Strap (με)
Location of	1st Axle	2nd Axle	3rd Axle	4th Axle	5th Axle	6th Axle	7th Axle	
Steering Axle (m)	89.3	83.4	83.4	83.4	83.4	89.4	-	
24	0							0
22	0							0
20	0.010							1
18	0.010							1
17	0.010							1
16	0.010	0	0					1
14	0.070	0.010	0.003					7
12	0.070	0.010	0.010					8
10	0.240	0.010	0.010	0				23
8	0.390	0.070	0.020	0.008	0			43
6	0.300	0.070	0.070	0.010	0.010	0		40
4	0.080	0.240	0.100	0.010	0.010	0.009		38
2	0.050	0.390	0.270	0.060	0.010	0.010		66
0	0	0.300	0.390	0.070	0.070	0.010		70
-2		0.080	0.230	0.210	0.070	0.060		55
-4		0.050	0.070	0.370	0.240	0.070		67
-6		0	0.040	0.320	0.390	0.210		81
-8			0	0.120	0.300	0.370		68
-10				0.050	0.080	0.320		39
-12				0.010	0.040	0.110		14
-14				0	0	0.050		4
-16						0		0
-18								
-20								
Low Bed Out	Vehicle Axle Load (kN)							Total Strain in Strap (με)
Location of	1st Axle	2nd Axle	3rd Axle	4th Axle	5th Axle	6th Axle	7th Axle	
Steering Axle (m)	89.3	103.5	103.5	97.4	97.4	97.4	-	
24	0							0
22	0							0
20	0.010							1
18	0.010							1
17	0.010							1
16	0.010	0						1
14	0.070	0.006	0					7
12	0.070	0.010	0.009					8
10	0.240	0.010	0.010					24
8	0.390	0.050	0.010					41
6	0.300	0.070	0.060	0				40
4	0.080	0.160	0.070	0.009	0	0		32
2	0.050	0.350	0.210	0.010	0.010	0.004		65
0	0	0.370	0.370	0.010	0.010	0.010		80
-2		0.170	0.320	0.050	0.010	0.010		58
-4		0.060	0.120	0.070	0.070	0.030		35
-6		0.020	0.050	0.200	0.070	0.070		40
-8		0	0.010	0.350	0.240	0.100		68
-10			0	0.340	0.390	0.270		97
-12				0.120	0.300	0.390		79
-14				0.050	0.080	0.230		35
-16				0.010	0.050	0.070		13
-18				0	0	0.040		4
-20						0		0

Low Bed In	Vehicle Axle Load (kN)							Total Strain in Strap (με)
Location of	1st Axle	2nd Axle	3rd Axle	4th Axle	5th Axle	6th Axle	7th Axle	
Steering Axle (m)	89.3	103.5	103.5	97.4	97.4	97.4	-	
0	0							0
2	0.050							4
4	0.080							7
6	0.300	0						27
7	0.390	0.040	0					39
8	0.240	0.070	0.040					33
10	0.070	0.220	0.070					36
12	0.070	0.390	0.280					76
14	0.010	0.280	0.390	0				70
16	0.010	0.210	0.330	0.020				59
18	0.010	0.100	0.260	0.040	0	0		42
20	0.010	0.070	0.090	0.070	0.050	0.020		31
22	0	0.030	0.070	0.370	0.080	0.050		59
24		0.010	0.020	0.390	0.300	0.140		84
26		0.010	0.010	0.270	0.390	0.360		101
28		0.005	0.010	0.100	0.240	0.350		69
30		0	0	0.070	0.070	0.180		31
32				0.020	0.070	0.070		16
34				0.010	0.010	0.060		8
36				0.010	0.010	0.010		3
38				0.003	0.010	0.010		2
40				0	0	0.007		1
42						0		0
44								

Table 5.9 - Contribution of Independent Axles to Strain in Strap at Strain Gauge 6

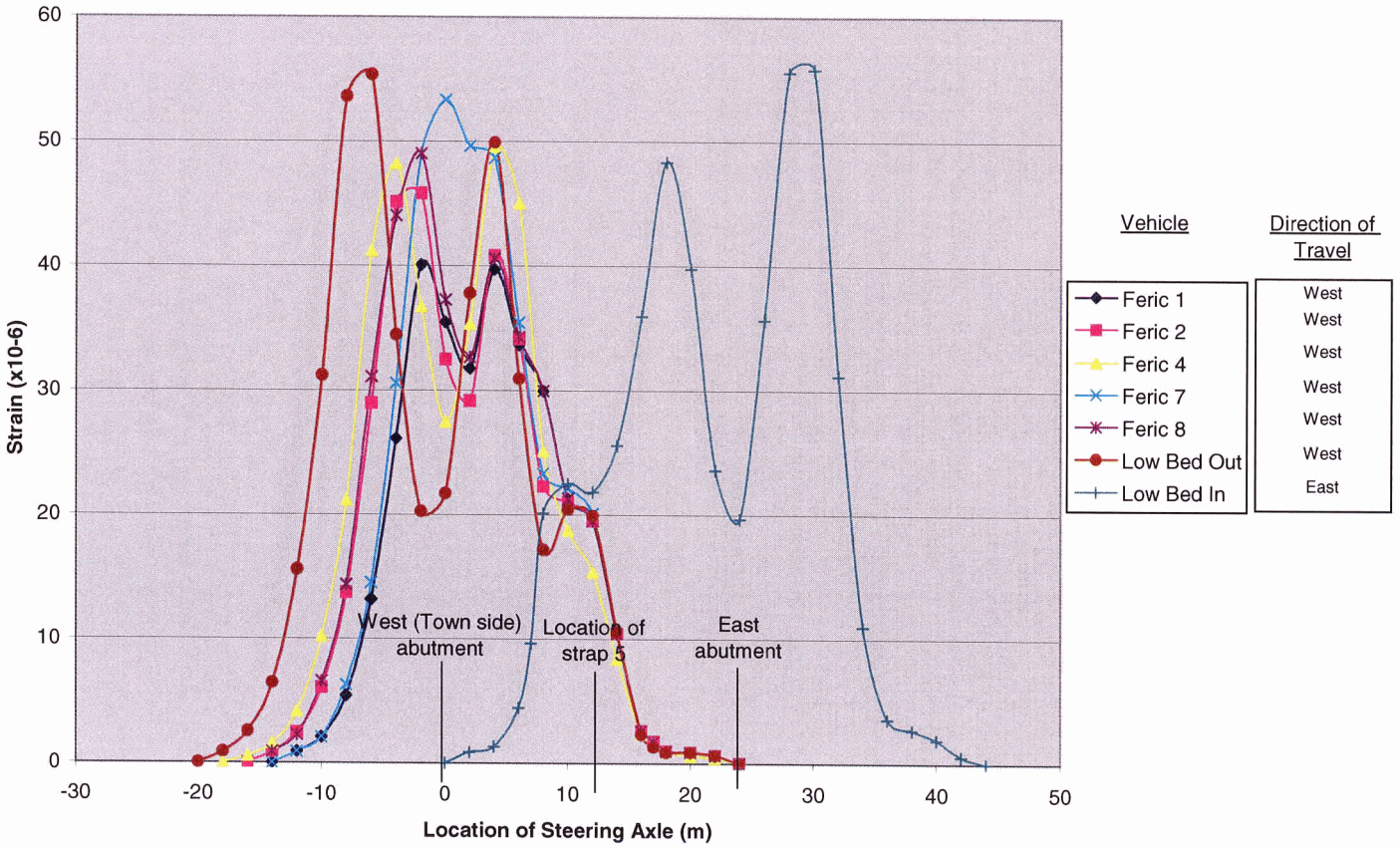

Figure 5.8 - Strain v Position of FERIC Vehicles and Low Beds on Forestry Bridge Strain Gauge 5

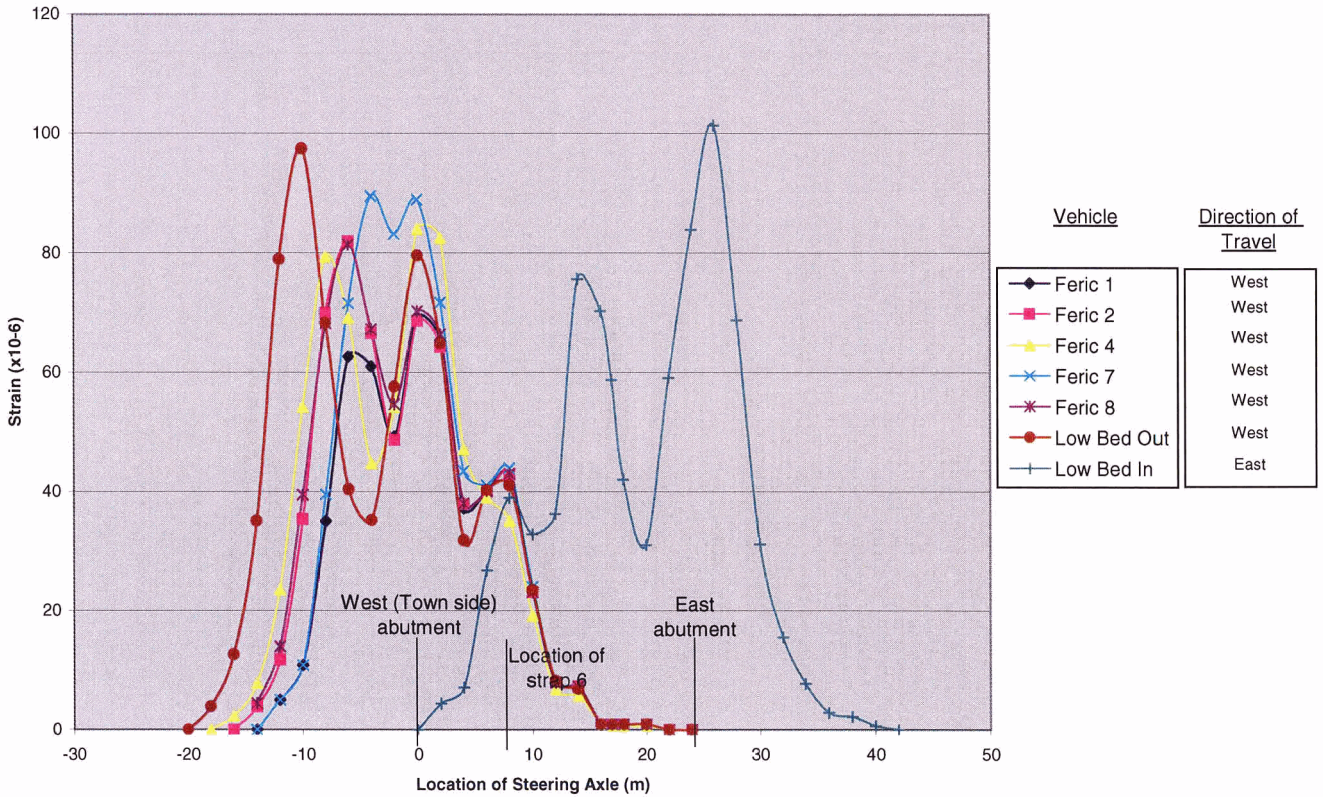

Figure 5.9 - Strain v Position of FERIC Vehicles and Low Beds on Forestry Bridge Strain Gauge 6

The spectra in Figures 5.8 and 5.9 pertaining to Forestry Bridges are presented here for the first time. As can be seen, a considerable amount of effort has been expended on their derivation. It is the opinion of this author that similar amounts of effort should be expended on other civil engineering structures in order to eventually assess their reliabilities. Good progress in this direction has indeed been made under the auspices of ISIS Canada. Finally, the reliability analysis presented in the following chapters would not have been possible without the derivation of the spectra presented in these two figures.

6.0 Theoretical Developments Pertaining to Establishing a Reliability Measure for Precast Unreinforced Concrete Arch Panel Bridges

The objective of this Chapter is to establish the theory behind a method of assessing the reliability of Arch Panel bridge decks, in particular, and concrete bridge decks, in general. The formulation developed here may be viewed as an indication of future approaches to assessing the reliability of bridge structures in general.

The approach is a novel modification and interpretation of Yang's [20] lognormal stochastic process procedure of assessing the reliability of aircraft structures. References [20 - 25] may be reviewed for more information.

6.1 On the Development of a Procedure of Assessing the Reliability of Bridge Decks

Following, in particular, the fracture mechanics approach of Provan and Farhangdoost [25, 23], the reliability assessment procedure is developed as follows.

1. A ***Crack's Mouth Opening Displacement (CMOD)***, given the symbol δ, is chosen as the fundamental observable in this approach. While it is possible to monitor the time variation of the CMOD while a bridge is in operation, δ in this case refers to the CMOD of cracks when a bridge is unloaded. The conceptual model is illustrated in Figure 6.1.

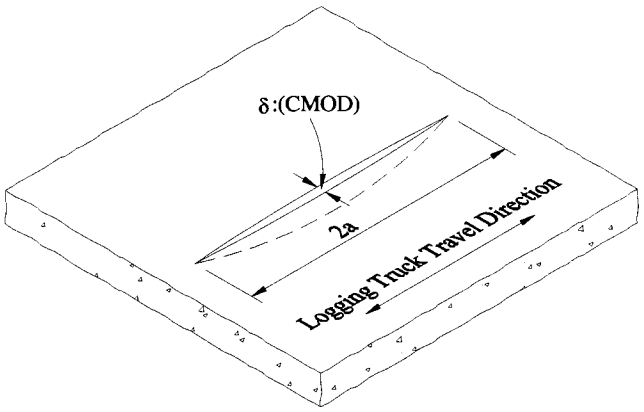

Figure 6.1 - Model of Crack Mouth Opening Displacement

2. Following an approach modified from that first suggested by Yang et al [20], it is hypothesized that δ obeys the law:

$$\frac{d\delta}{dn} = X(n)\ C\ \Delta k^m \quad , \tag{6.1}$$

where:

- δ = Crack Mouth Opening Displacement (CMOD)
- n = Index identifying each fully loaded truck axle set crossing
- $X(n)$ = a non-negative, stationary lognormal random process
- C = the bridge's concrete material coefficient
- m = the bridge's concrete material exponent
- Δk = a stress intensity factor range.

While δ represents the CMOD and C and m are material coefficients pertaining to the concrete under review, the Δk and $X(n)$ require further discussion.

3. The stress intensity factor range is hypothesized as depending only on the actual loading pattern and the current CMOD, i.e.:

$$\Delta k = \Delta k(\delta, \Delta\sigma) \quad , \tag{6.2}$$

where:

- $\Delta\sigma$ = the nominal stress range experienced by a bridge deck in the vicinity of a crack as a result of a single 'standard' axle set loading profile, discussed in the previous Chapter, and a detailed stress analysis of the deck structure.

From a detailed analysis of bridge deck cracks, a specific form for Δk could eventually be established. In this analysis, however, it is assumed that cracks penetrate the entire deck and that a "Through Thickness Crack", commonly discussed in the context of the fracture mechanics of solids [23], is an appropriate approximation. In this case, Δk may be written as:

$$\Delta k = \sqrt{\pi a}\ \Delta\sigma \ , \tag{6.3}$$

where, as illustrated in Figure 6.1, a represents ½ the length of a crack.

It appears a justifiable approximation for δ to depend linearly on a, i.e., $a = D\,\delta$. Incorporating this approximation and eqns (6.3) and (6.1), the rate at which bridge deck cracks grow becomes:

$$\frac{d\delta}{dn} = X(n)\left[C\ \pi^{m/2}\ D^{m/2}\right]\left[\sqrt{\delta}\ \Delta\sigma\right]^m = X(n)\ C'\left[\sqrt{\delta}\ \Delta\sigma\right]^m \ , \tag{6.4}$$

$$C' = C\ \pi^{m/2}\ D^{m/2} \ .$$

4. As mentioned, the primary objective is to be in a position to assess the reliability of a bridge deck on the basis of detailed crack CMOD information gained initially from inspections. It is therefore necessary to carry out at least two inspections from which the basic unknowns of eqn (6.4) may be estimated.

Let τ represent the number of 'standard' axle sets that have crossed the bridge between the first inspection, I1, and the second, I2. The CMOD of a specific crack, *i*, at inspection I1, identified as δ_1^i, will have expanded to δ_2^i under the action of these τ axle sets. Rearranging eqn(6.4) prior to integration, it follows that:

$$\int_{\delta_1^i}^{\delta_2^i} \frac{d\delta^i}{\delta^{i(m/2)}} = X(n)\, C_i'\, \Delta\sigma^m\, \tau\ , \tag{6.5}$$

resulting in:

$$\left[\delta_2^{i[(2-m)/2]} - \delta_1^{i[(2-m)/2]}\right] = \frac{(2-m)}{2} X(n)\, C_i'\, \Delta\sigma^m\, \tau\ . \tag{6.6}$$

5. Realizing that the stationary random process, $X(n)$, plays no role in analyzing the growth of a single crack, *i* in this case, eqn (6.6) may be used to determine its parameters C_i' and *m*. From a review of data pertaining to the crack growth in metals [23], a representative value for a concrete's exponent may be taken as $m = 3$. With this choice, eqn (6.6) becomes:

$$C_i' = \frac{2}{\Delta\sigma^3\, \tau}\left(\frac{1}{\sqrt{\delta_1^i}} - \frac{1}{\sqrt{\delta_2^i}}\right)\ . \tag{6.7}$$

Hence, for the crack identified here by *i*, C_i' may be determined explicitly.

6. Realistically in any bridge deck that is subject to cracking there are bound to be numerous cracks of various sizes. Identifying the cracks by $i = 1,...,\eta$, and their corresponding CMODs by δ^i, then a complete set of $C_i's$ may be found from an

implementation of eqn (6.7) for each crack. Subsequently, an average value of these $C_i's$ may be determined.

7. The inherent scatter in the growth of concrete bridge deck cracks is, as a consequence of the above, described by a non-negative, stationary, lognormal random process $X(n)$. Taking the log of eqn (6.4) results in:

$$\Psi(n) = Z(n) + C_c + 3\Gamma(n) \quad , \tag{6.8}$$

where:

$$\begin{aligned} Z(n) &= \log\left(X(n)\right) \quad , \\ \Psi(n) &= \log\left(\frac{d\delta}{dn}\right) \quad , \\ \mathrm{C_c} &= aver\left(\log C_i'\right) \quad \text{and} \\ \Gamma(n) &= \log\left(\Delta\sigma\sqrt{\delta(n)}\right) \quad . \end{aligned} \tag{6.9}$$

Hence, eqn (6.8) represents a straight line with a dispersion about its mean described by the now stationary, normal random process $Z(n)$.

Since the mean of $X(n)$ is unity, the mean of $Z(n)$ is zero. Hence, $Z(n)$ is completely described by its auto correlation function at any two time intervals:

$$R_{zz}(n_1, n_2) = \frac{1}{\eta}\sum_{i=1}^{\eta}\left(Z^i(n_1)Z^i(n_2)\right) \quad . \tag{6.10}$$

Furthermore, the random process being stationary dictates that $R_{zz}(n_1, n_2)$ depends only on the number of fully loaded standard axle set crossings the bridge deck has experienced during the designated time interval, specifically

$\tau = (n_2 - n_1)$ axle sets. Commonly, this stationary auto correlation function is assumed to be an exponentially decaying function of τ [20], i.e.:

$$R_{zz}(\tau) = \tilde{\sigma}^2 \exp\left(-\xi|\tau|\right) \quad , \tag{6.11}$$

where:

- $\tilde{\sigma}^2 = \frac{1}{\eta}\sum_{i=1}^{\eta}\left(Z^i(0)Z^i(0)\right) = R_{zz}(0)$ is the process' variance, and
- ξ is the correlation parameter of the process.

8. Finally, with a knowledge of $R_{zz}(\tau)$, established by an implementation of eqn (6.10) for a specific τ, and the variance $\tilde{\sigma}^2$, ξ may be determined by considering the log of both sides of eqn (6.11), i.e.:

$$\xi = \frac{\left[\log(\tilde{\sigma}^2) - \log(R_{zz}(\tau))\right]}{|\tau|} \quad . \tag{6.12}$$

9. To recap, for bridge decks being subjected to 'standard' logging truck traffic, the precise measurement of the CMOD of bridge deck cracks at two distinct inspections I1 and I2, results in being able to establish the basic parameters of this analysis, namely; $C_c = aver\left(\log C_i'\right)$, $\tilde{\sigma}^2$ and ξ. From these parameters and provided bridge decks are subjected to the same loading profile, the distribution of crack mouth opening displacements, δ, at any stage in the life of the bridge deck may be estimated.

10. Finally, incorporating the concept of the critical 'knuckle' CMOD, namely δ_K as discussed in section 7.1.3, as being the maximum allowable crack dimension prior to when the crack should be repaired, the number of 'standard' axle sets passing

over a specific Arch Panel span in order to maintain a specific reliability, R^*, may be determined.

A full illustration of the procedure developed in this Chapter is presented in the following, which details its application to data retrieved from the previously discussed Forestry bridge.

7.0 Reliability Assessment of a First Generation Arch Panel Bridge

The objective of this Chapter is to present an application as to how a knowledge of:

1. the types and number of loaded logging truck axle sets traversing the bridge – see Section 5.3;
2. their 'standard' signature or load spectrum – see Section 5.3;
3. the characteristic material properties of the unreinforced concrete used in the construction of the 1st generation Arch Panel logging bridge – see Section 5.4.2.2;
4. the critical knuckle dimension of this specific type of the concrete; and
5. the crack mouth opening displacement of a significant number of cracks measured at two different inspections,

may be used to assess the potential reliability of the bridge itself. It is important to repeat the observation that this is an illustration of this exploratory procedure and is in no way to be misconstrued as being a definitive assessment of the specific bridge's actual reliability. All conjectures are exploratory at this point and more detailed research must be undertaken before an approach based upon the methods being developed in this thesis may be accepted. These points are returned to in the last Chapter on suggestions for future research.

7.1 Listing of the Required First Generation Arch Panel Bridge Input Parameters

7.1.1 The Types and Number of Loaded Logging Truck Axle Sets Traversing the Arch Panel Bridge Between July 1999 and November 2003; namely τ.

Extracting information that was previously developed and presented in Chapter 5 and listed in Table 5.7, the total number of each type of truck travelling over the Arch Panel bridge between July 1999 and November 2003, representing 52 months, is presented in Table 7.1. In this table, the number of FERIC 8 trucks has been added to the number of

FERIC 2 trucks since the signature patterns of both these truck types are, from Figures 5.8 and 5.9, essentially the same. The numbers listed were deduced from the information presented in Table 5.7 using the summation:

$$\frac{5}{12}(1999\text{ trucks})+(2000\text{ trucks})+(2001\text{ trucks})+(2002\text{ trucks})+\frac{11}{12}(2003\text{ trucks})\ .(7.1)$$

	FERIC 1	FERIC 2 & 8	FERIC 4	FERIC 7	LOWBEDS
No. of Each Type of Truck Using Bridge in 52 Months	75	2299	1478	823	132
Channel 5; High Strain	40	48	50	53	55
Channel 5; Low Strain	40	40	48	49	48
Channel 6: High Strain	70	82	85	88	99
Channel 6: Low Strain	63	70	80	88	79
High Axle Set Strain	55	65	65	70	76
Low Axle Set Strain	52	55	64	70	65
High Axle Set Stress Range (MPa)	1.7	2.01	2.01	2.16	2.35
Low Axle Set Stress Range (MPa)	1.61	1.7	2.00	2.16	2.01

Table 7.1 - Stress Ranges Associated with the Axle Sets of Loaded Logging Trucks Crossing the Arch Panel Span during a 52 Month Period.

7.1.2 Peak Strains and Stresses Associated with Each Truck Type Axle Set

From a careful review of the information presented in Figures 5.8 and 5.9 of Chapter 5, it is observed that each truck type as it passed over the span registered two peak strains, plus a third significantly smaller value.

In this analysis, each peak strain is associated with either a tandem axle set or a tridem axle set of both the FERIC and lowbed trucks. The third is associated with the front axle of the cab. All the logging truck loading signature information presented in Chapter 5 is retrieved here and presented in Table 7.1.

The fracture toughness of the concrete is based on a fraction of the calculated split-cylinder strength as estimated from the 28 day compressive strength (f'c) of 45 MPa [26], [27]. A value of 0.35 $\sqrt{f'c}$ was chosen to represent the direct tensile strength of the slab concrete. Therefore using 2.35 MPa as the fracture toughness of concrete to represent the maximum peak stress range, and prorating the rest, the last 2 rows of this Table converts the peak strains to the stress ranges being experienced by every location in the Arch Panel deck span.

	2.35 MPa	2.16 MPa	2.01 MPa	2.00 MPa	1.70 MPa
No. of Axle Sets at Each Stress Level	132	1646	3909	1478	2449
Total No. of All Axle Sets Using Bridge in 52 Months		=	**9614**		
Average Stress Range (MPa)		=	**2.04**		
No of Axle Sets at Each Stress Level per Month	3	32	75	28	47
No. of All Axle Sets Traversing Bridge per Month		=	**185**		

Table 7.2 - Compilation of the Axle Sets and Stress Ranges being Experienced by the Arch Panel Bridge Span over Each Month and during the 52 Month CMOD Measuring Interval.

7.1.3 The Critical Knuckle Size δ_K of the Arch Panel Concrete

At the University of Manitoba, recent testing to failure under a 50t pulsating load of a single arch panel deck slab with edge beams indicated a marked increase in the rate of change of observed crack width after a specific number of load cycles. A plot of the crack width v. number of load cycles is shown in Figure 7.1. [9] The location on the graph where the crack width begins to increase rapidly under further cyclic loading is referred to in this thesis as the "Knuckle Point"; the crack width, or CMOD, at this location is the critical knuckle size, δ_k.

[9] Private Communication: Amjad Memon, Ph.D. Candidate, University of Manitoba, July 26 and 30, November 2, 2004.

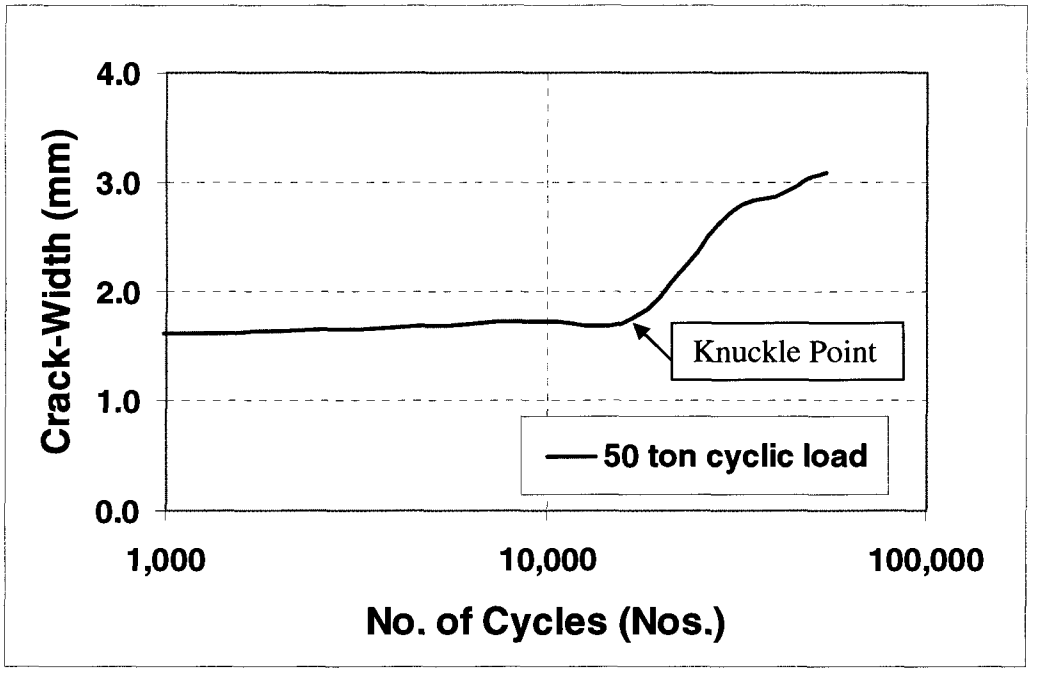

Figure 7.1 - Crack Width v No. of Load Cycles for Arch Panel Deck Subject to 50t Pulsating Load

A representative value for this dimension after considerable discussion with Profs Mufti and Provan is taken as [28] [10] [11]:

$$\delta_K = 3.6mm \ . \tag{7.2}$$

7.1.4 The Identification of Cracks and their Dimensions in 1999 and 2003

Table 7.3 presents all the information and calculations based upon the previous chapters findings concerning the observable longitudinal cracks in the Arch Panel bridge deck. Of the 79 cracks measured in Chapter 5, only 23 are longitudinal and located essentially in the centre of the span. Furthermore, any crack that obviously penetrated the deck in 2003 was counted as a single crack. As mentioned previously, no confidence is placed on the

[10] Private Communication: Dr. Aftab Mufti, P.Eng., dated July 26, 2004.
[11] Private Communication: Amjad Memon, P.H.D. Candidate University of Manitoba, dated July 26, 2004.

1999 numbers since the measuring procedures at that time were not well established. A far more reliable listing of the November 2003 measured CMODs is, however, presented.

7.1.5 Generation of the Basic Parameters, namely; $C_c = aver(\log C_i')$, $\tilde{\sigma}^2$ and ξ

Using the equations presented in Chapter 6, the basic parameters required for an illustration of the procedure are used and their values are also presented in Table 7.3., the important numbers required for the last step in the reliability assessment process are:

$$C_C = 5.02045E-22 \ ,$$

$$\tilde{\sigma}^2 = 7.4825E-08 \ , \text{ and}$$

$$\xi = 1.21052\text{E-}05 \ . \qquad (7.3)$$

Assessment of Type 1 ArchPanel bridge CMODs													
N2003 =	9614												
Pa =	2.04E+06												
Crack #	CMOD	1+CMOD	Ln	sqrt	1/	CMOD	1+CMOD	Ln	Z0*ZN2003	sqrt	1/	1/sqrt	C'
i	1999	- mean	CMOD	CMOD	sqrt	2003	- mean	CMOD		CMOD	sqrt	1999 -	
	(m)	1999	1999	1999	1999	(m)	2003	2003		2003	2003	2003	
1B-99-01	0.0001	0.9998496	-0.00015045	0.01	100	0.0002	0.999803478	-0.000197	2.9569E-08	0.014142136	70.7106781	29.2893219	7.17703E-22
1B-99-02	0.0008	1.0005496	0.00054941	0.028284271	35.3553391	0.0009	1.000503478	0.0005034	2.7655E-07	0.03	33.3333333	2.02200573	4.9547E-23
1B-99-03	0.0001	0.9998496	-0.00015045	0.01	100	0.0004	1.000003478	3.478E-06	5.2329E-10	0.02	50	50	1.2252E-21
1B-03-04	0.00012	0.9998696	-0.00013044	0.010954451	91.2870929	0.0003	0.999853478	-0.000147	1.9114E-08	0.015811388	63.2455532	28.0415397	6.87127E-22
1T-03-04	0.00011	0.9998596	-0.00014044	0.010488088	95.3462589	0.0002	0.999803478	-0.000197	2.7603E-08	0.014142136	70.7106781	24.6355808	6.03668E-22
1T-03-05	0.0001	0.9998496	-0.00015045	0.01	100	0.0002	0.999833478	-0.000167	2.5055E-08	0.015165751	65.9380473	34.0619527	8.34651E-22
2B-99-01	0.00015	0.9998996	-0.00010044	0.012247449	81.6496581	0.0003	0.999903478	-9.65E-05	9.6951E-09	0.017320508	57.7350269	23.9146312	5.86002E-22
3B-99-01	0.0003	1.0000496	4.9564E-05	0.017320508	57.7350269	0.0005	1.000053478	5.348E-05	2.6505E-09	0.021213203	47.1404521	10.5945748	2.59609E-22
4B-99-01	0.00017	0.9999196	-8.0438E-05	0.013038405	76.6964989	0.0003	0.999853478	-0.000147	1.1787E-08	0.015811388	63.2455532	13.4509457	3.29601E-22
5B-99-01	0.0007	1.0004496	0.00044946	0.026457513	37.7964473	0.0007	1.000323478	0.0003234	1.4537E-07	0.026832816	37.2677996	0.52864768	1.29539E-23
5B-99-02	0.0001	0.9998496	-0.00015045	0.01	100	0.0003	0.999903478	-9.65E-05	1.4522E-08	0.017320508	57.7350269	42.2649731	1.03566E-21
5T-03-09	0.0002	0.9999496	-5.0436E-05	0.014142136	70.7106781	0.0006	1.000153478	0.0001535	7.7402E-09	0.023452079	42.6401433	28.0705348	6.87838E-22
6B-99-01	0.00075	1.0004996	0.00049944	0.027386128	36.5148372	0.0009	1.000523478	0.0005233	2.6138E-07	0.030331502	32.9690237	3.5458135	8.68863E-23
6B-99-03	0.0001	0.9998496	-0.00015045	0.01	100	0.0003	0.999873478	-0.000127	1.9036E-08	0.016431677	60.8580619	39.1419381	9.5913E-22
7B-99-01	0.00005	0.9997996	-0.00020045	0.007071068	141.421356	9E-05	0.999693478	-0.000307	6.1453E-08	0.009486833	105.409255	36.0121009	8.82437E-22
7B-99-02	0.00014	0.9998896	-0.00011044	0.01183216	84.5154255	0.0003	0.999883478	-0.000117	1.287E-08	0.016733201	59.7614305	24.753995	6.0657E-22
7B-03-05	0.0001	0.9998496	-0.00015045	0.01	100	0.0002	0.999763478	-0.000237	3.5588E-08	0.012649111	79.0569415	20.9430585	5.13187E-22
8B-99-01	0.001	1.0007496	0.00074928	0.031622777	31.6227766	0.0015	1.001103478	0.0011029	8.2636E-07	0.038729833	25.819889	5.80288763	1.42193E-22
8B-99-03	0.0001	0.9998496	-0.00015045	0.01	100	0.0001	0.999703478	-0.000297	4.4617E-08	0.01	100	0	0
8B-03-04	0.00012	0.9998696	-0.00013044	0.010954451	91.2870929	0.0003	0.999903478	-9.65E-05	1.2591E-08	0.017320508	57.7350269	33.552066	8.22157E-22
8B-03-06	0.0001	0.9998496	-0.00015045	0.01	100	0.0001	0.999703478	-0.000297	4.4617E-08	0.01	100	0	0
8T-99-02	0.00025	0.9999996	-4.3478E-07	0.015811388	63.2455532	0.0006	1.000153478	0.0001535	6.6725E-11	0.023452079	42.6401433	20.6054099	5.04913E-22
8T-03-06	0.0001	0.9998496	-0.00015045	0.01	100	0.0001	0.999703478	-0.000297	4.4617E-08	0.01	100	0	0
Mean =	0.0002504	1	-3.5791E-08			0.0004	1	-5.47E-08			Mean of C' =		5.02045E-22
Variance =	7.486E-08	7.486E-08	7.4825E-08			1E-07	1.14496E-07	1.144E-07					
				Rzz(N2003)	=				8.406E-08				
								Xi =	1.21052E-05				

Table 7.3 - An EXCEL Spreadsheet Where $C_c = aver(\log C_i')$, $\tilde{\sigma}^2$ and ξ are Deduced from Data Obtained from the First Generation Arch Panel Bridge

7.2 The Illustrative Reliability of the Arch Panel Bridge

Using the MATLAB program presented in Appendix C, the growth of 23 cracks under the conditions listed above are shown in Figure 7.2.

Choosing a minimum allowable reliability of 0.98, which represents 1 crack in 50 exceeding the knuckle dimension of $\delta_K = 3.6mm$, a possible reliability estimate and indication of when the Forestry bridge should be inspected is shown in Figure 7.3. From this figure, it is conjectured that the bridge should be inspected after 15,600 loaded logging truck axle sets have traversed the span. At the indicated annual traffic discussed in Chapter 5, and presented in Figure 7.3 this inspection should take place after approximately seven years.

This number illustrates in a graphic manner the power of the approach being suggested in this thesis of ensuring the safety of arch panel bridge decks in the future. The process also demonstrates one means of utilizing data collected from the monitoring of existing structures in order to estimate reliability and to assist in the establishment of parameters for future design.

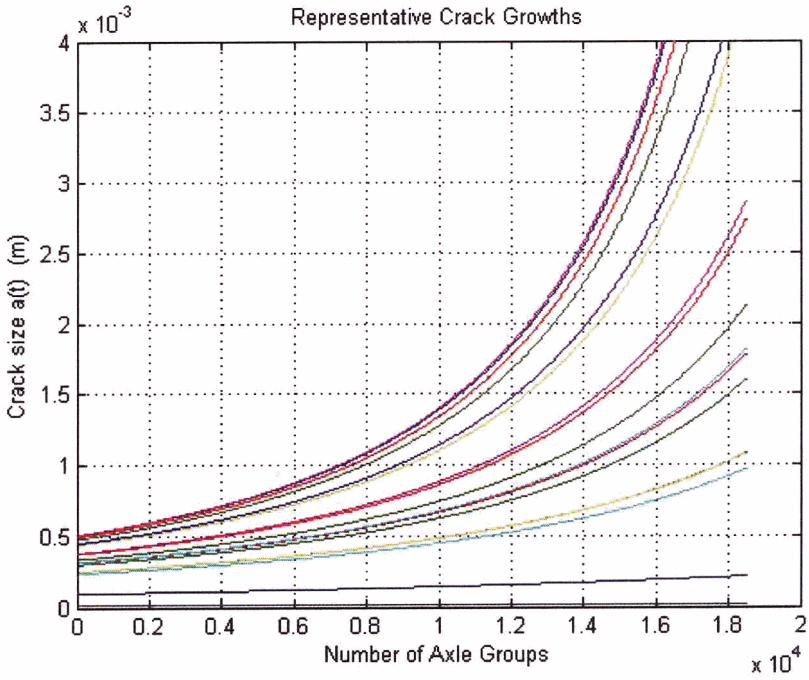

Figure 7.2 - A Representation of the Growth in the CMOD δ of $i = 1,\cdots,23$ Cracks

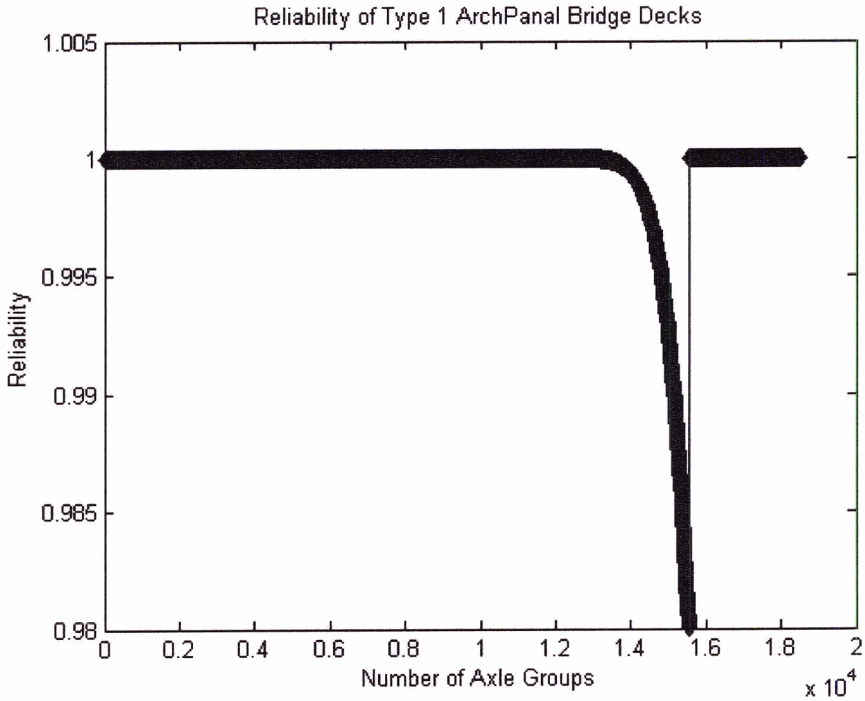

Figure 7.3 - For a Reliability of 0.98, an Inspection Should Take Place after Approximately 7 Years of Operation

8.0 Conclusions and Recommendations for Future Research

This thesis has illustrated a process that has the potential of revolutionizing the methods currently available for assuring the reliability of many structures due to fatigue, in particular, bridges. The importance of taking fatigue into consideration is highlighted by the observation that while the punching shear capacity of the Dalhousie slab indicated a value of 720 kN, a value close to that predicted by Punch Theory (see Appendix A), the corresponding capacity of the UBC slab, having been subjected to 370,000 and 532,000 cycles of fatigue loading, gave values of 454 kN and 500 kN, respectively.

While it is acknowledged that the current illustrated steps are in an embryonic state, the procedure highlighted does have a considerable amount of validity. To recap, the reliability assessment and the scheduling of inspection/repair intervals depends on an adherence to modifications of the following steps that have been applied in an exploratory manner to a first generation Arch Panel forestry bridge.

1. As a precursor to any estimation of reliability, the mechanical properties of the material itself must be documented. As is well understood and while there is a wide variety in properties, as much information as possible concerning the material and the nature of its reinforcement must be ascertained and understood. For example, the concrete used in the construction of the first generation unreinforced concrete Arch Panel forestry bridge has an estimated tensile strength of 2.35 MPa.

2. One of the prime objectives illustrated in this investigation is to fully determine the loading patterns a proposed structure is expected to sustain. For example, this information may be gathered and documented by a real-time monitoring of the strains, and thereby the stresses, a similar structure is sustaining. From this information and after a considerable amount of consultation, a standard load spectrum, similar to the aircraft manufacturers' FALSTAFF, TWIST and MINI-TWIST spectra, may be developed for this class of structure. Once such a

spectrum has been accepted by industry, it may be used in the design of subsequent structures being developed for similar uses.

In Chapter 5 a possible procedure leading to the establishment of real-time spectra applicable to an Arch Panel forestry bridge deck used almost exclusively by the logging industry has been presented. While it is acknowledged that the spectra developed for this purpose and presented in Figures 5.8 and 5.9 are of a very preliminary nature they ideally illustrate the type of information that can be extracted from a careful monitoring of bridge structures. These preliminary Arch Panel Forestry bridge loading spectra are presented here for the first time.

3. Advantage should be taken, where possible, of monitoring systems in the behaviour of real civil engineering structures. What has been illustrated in Chapter 5 is the influence on strains due to loading from axles remote from the test location. This illustrates that simulated single axle loading as typically performed in laboratory experiments, although of benefit in demonstrating the progression of cracks, may be unconservative for representing truck loading.

4. Either from the real-time civionic monitoring of a bridge itself or from a detailed investigation of the truck type, the number and frequency with which the axle set loading spectra occur must be determined. This information is of importance in establishing a suitable inspection/repair interval. Also, if the truck crossing pattern changes over time, then this new information should be incorporated into a recalculation of the inspection/repair interval. For the forestry bridge being studied in this investigation the number of truck axle sets crossing the span per month was established as 185. Without an estimation of this number, the inspection interval suggested in Chapter 7 could not have been established.

5. Definitions of what constitutes *damage* in the context of civil engineering structures must be further developed. In this investigation, the Crack Mouth Opening Displacement (CMOD) and its associated critical knuckle CMOD have

been chosen as suitable parameters for monitoring damage. Other measures, such as crack length as in the UBC lab experiment, or depth could equally well have been selected.

6. Having decided on a *damage* measure, it must be monitored in a consistent and timely manner. While the CMOD of 79 cracks were successfully and precisely measured in 2003, the same cannot be said about the corresponding 1999 field study. One of the failings of this current investigation is that three reliable CMOD measurement regimes were not available to the author. With three good listings it would have been possible to establish an estimate of the Arch Panel CMOD's growth parameter: m. In this illustration and based upon a review of the crack growth characteristics of metals, an interim value of $m = 3$ was selected. It is highly unlikely, however, that this value actually applies to the unreinforced concrete in question. If the reliability assessment procedure illustrated in this thesis were to become an acceptable industry standard, then much future research effort must be expended in determining m for all types of unreinforced and reinforced concretes.

7. Some reliability assessment procedure based upon a damage accumulation algorithm should now be invoked. The initial theory behind one such method is presented for the first time in Chapter 6. Again it is re-emphasized that the method suggested in this thesis is of an embryonic nature and much work will be required to develop the lognormal stochastic process to a stage where researchers and practicing Civil Engineers will be comfortable using the suggested procedure. Nevertheless, the procedure developed here has considerable potential. Also, it is to be noted that the procedure depends on all of the above information being available. If one is missing, an estimate of a structure's reliability cannot be made.

8. In the previous Chapter, an application of the suggested procedure is presented. All of the required parameters have been incorporated into this assessment of the

reliability of a first generation Arch Panel forestry bridge deck. While it is acknowledged that actual numbers involved do not represent an actual reliability assessment of the deck, the benefits of approaching the determination of structural reliability in this way has been dramatically illustrated.

9. Future research involving the establishment of the reliability of bridge structures should involve modifications of the techniques highlighted in this thesis. Specifically for concrete bridge decks governed by CMOD; the material characteristics, including an idea of a concrete's knuckle CMOD dimension; the loads, nature and frequency of the vehicular traffic traversing a bridge structure; and a fully developed reliability estimation procedure should be the objectives of future researchers in this area. Fortunately, various aspects of this research are already being promoted by the ISIS National Centre of Excellence, which to date has documented the importance of adopting a civionics approach.

References:

[1] Mufti, A.A., Jaegar, L.G., Bakht, B., and Wegner, L.D., "Experimental Investigation of FRC slabs Without Internal Steel Reinforcement", Canadian Journal of Civil Engineering, 1993, 20 (3), pp. 398-406.

[2] Petroski, H., "Design Paradigms", Press Syndicate of the University of Cambridge, 1994.

[3] Newhook, J.P., and Mufti, A.A., "Steel-Free Concrete Bridge Deck-The Salmon River Project: Experimental Verification", Proceedings Annual Conference of the CSCE held in Edmonton, 1996.

[4] Newhook, J., Mufti, A.A., "Punch Program User and Theoretical Manuals", Nova Scotia CAD/CAM Centre, Technical University of Nova Scotia, 1996.

[5] Bakht, B, "Revisiting Arching in Deck Slabs", Canadian Journal of Civil Engineering, 23 (4), pp. 973-981, 1996.

[6] Bakht, B. and Mufti, A.A., "Arching in Deck Slabs", Journal of Institution of Engineers (India), Vol. 77, pp. 123-128, 1996.

[7] National Standard of Canada, "Design of Highway Bridges – CAN3-S6-M78" Canadian Standards Association, August , 1978.

[8] National Standard of Canada, "Design of Highway Bridges – CAN/CSA-S6-88" Canadian Standards Association, June 1988.

[9] National Standard of Canada, "Canadian Highway Bridge Design Code – CAN/CSA-S6-00" CSA International, December 2000.

[10] Selvadurai, A.P.S., and Bakht, B., "Simulation of Rolling Wheel Loads on an FRC Deck Slab", Proceedings 2nd University Industry Workshop on FRC held in Toronto, pp. 273-287, 1996.

[11] Bakht, B., and Selvadurai, A.P.S., "Performance of Steel-Free Deck Slabs Under Simulated Wheel Loads", Second International Conference on Advanced Composite Materials in Bridges and Structures held in Montreal, pp. 767-776, 1996.

[12] Mufti, A.A., Bakht, B., Tadros, G., Newhook, J, Butt, S., "Structural Health Monitoring of Innovative Bridge Decks", Presentation at SPIE's 6th Annual International Symposium on NDE for Health Monitoring and Diagnostics, Newport Beach, California, March 4-8, 2001.

[13] Matsui, S., Tokai, D., Higashiyama, H., and Mizukoshi, M., "Fatigue Durability of Fiber Reinforced Concrete Decks Under Running Wheel Load", Proceedings of the Third International Conference on Concrete Under Severe Conditions, CONSEC'01, Vancouver, British Columbia, Volume 1, pp. 982-991, June 18-20, 2001.

[14] Ministry of Forests, "Forest Service Bridge Design and Construction Manual", Resource Tenures and Engineering Branch, July 30, 1999.

[15] Mufti, A.A., Banthia, N., Bakht, B., "Fatigue Testing of Precast Arch Panels", Proceedings of the Third International Conference on Concrete Under Severe Conditions, CONSEC'01, Vancouver, British Columbia, Volume 1, pp. 1032-1041, June 18-20, 2001.

[16] Cook, S, Ventura, C.E., Jackson, S., Black, C., "Static and Dynamic Strain Measurements of the Lindquist Bridge", University of British Columbia, 1998.

[17] Sargent, D.D., Ventura, C.E., Mufti, A.A., Bakht, B., "Testing of Steel-Free Bridge Decks", Concrete International, Vol. 21, pp. 55-61, August 1999.

[18] Sargent, D.D., Mufti, A.A., Bakht, B., "Design, Construction and Field Testing of Steel-Free Arch Panel Bridge Deck for Forestry Bridges", Proceedings of the 1999 Canadian Society for Civil Engineering Annual Conference, Vol I, pp. 95-104, 1999.

[19] Webb, C.R., "Popular B.C. Vehicle Configurations for Hauling Full Length Logs: Maximum Weights and Dimensions Guide, Effective October 1997", Forest Engineering Research Institute of Canada, 1998.

[20] Yang, J.N., et al., "Statistical Modeling of Fatigue-Crack Growth in a Nickel-base Super-alloy, Engng. Fracture Mechanics", Vol. 18, pp. 257 – 270, 1983.

[21] Yang, J.N., Manning, S.D., Rudd, J.L. and Hsi, W.H., "Stochastic Fatigue Crack Propagation", Proc. of 26th AIAA/ASME/ASCE/AHS Structures, Structural Dynamics and Materials Conf., Orlando, AIAA Paper No. 85 - 0666, pp. 225 - 233 (Apr. 1985); also appeared in J. of Aircraft, AIAA, Sept.1985.

[22] Yang, J.N., Hsi, W.H. and Manning, S.D., Stochastic Crack Growth Models for Application to Aircraft Structures, in: "Probabilistic Fracture Mechanics and Reliability", J.W. Provan (ed.), Martinus Nijhoff, pp. 213 - 267, 1987.

[23] Farhangdoost, K. and Provan, J.W., A Stochastic Systems Approach to Fatigue Reliability - An Application to Ti-6A1-4V, in: "Engineering Fracture Mechanics - Special Issue on Reliability of Structural Components Under Fatigue", G.I. Schueller, Guest Ed., Vol. 53, No. 5, 1996.

[24] Farhangdoost, K. and Provan, J.W., On Fatigue Reliability Assessment, "Fatigue '93, Proceedings of the Fifth International Conference on Fatigue and Fatigue Thresholds", J.-P. Baïlon and J.I. Dickson, (Eds.), Vol. 2, pp. 707 - 712, Engineering Materials Advisory Services, U.K., 1993.

[25] Provan, J.W. and Farhangdoost, K., A New Stochastic Systems Approach to Structural Integrity, in: "FAA/NASA International Symposium on Advanced Structural Integrity Methods for Airframe Durability and Damage Tolerance", Hampton, VA, USA, May 4 - 6, 1994.

[26] Pillai, S.U., Kirk, D.W., "Reinforced Concrete Design-Second Edition", McGraw-Hill Ryerson Limited, 1988.

[27] Winter, G., A.H Nilson, "Design of Concrete Structures-Ninth Edition", McGraw-Hill Book Company, 1979.

[28] Memon, A.H., Mufti, A.A., "Fatigue Behaviour of Concrete Bridge Deck Slabs Reinforced with FRP and Steel Straps", Proceedings of the 5th Structural Specialty Conference of the Canadian Society for Civil Engineering, Saskatchewan, pp. ST-229-1 – ST-229-10, June 2-5, 2004.

Appendix A - Punch Theory Printouts

UBC Experiment:

PUNCH.RES

UNITS METRIC KN, MM, SECOND
Clear Span Between Girders= 3500.00
Diameter of Equivalent Circle for Load= 541.000
Maximum Compressive Stress of Concrete= 35.0000
Elastic Axial Stiffness of Strap= 158.000
Strap to Load Spacing= 0.000000
Depth Of Slab= 236.000
Beta to Define Rectangular Stress Block= 0.883000
Concrete Constant used for confinement= 10.0000
Area of Load Patch= 150000.
Yield strain= 0.200000E-02

DELTA	ALPHA	P	STRN
0.00	0.00	0.	0.00000
0.67	15.70	25.	0.00005
1.35	15.38	49.	0.00010
2.02	15.10	73.	0.00015
2.70	14.84	96.	0.00020
3.37	14.60	118.	0.00025
4.05	14.38	140.	0.00030
4.72	14.18	162.	0.00035
5.39	13.99	183.	0.00039
6.07	13.81	204.	0.00044
6.74	13.65	224.	0.00049
7.42	13.49	244.	0.00053
8.09	13.35	264.	0.00058
8.77	13.21	283.	0.00062
9.44	13.08	302.	0.00067
10.11	12.96	321.	0.00071
10.79	12.84	339.	0.00076
11.46	12.73	357.	0.00080
12.14	12.62	375.	0.00085
12.81	12.52	392.	0.00089
13.49	12.42	410.	0.00093
14.16	12.33	426.	0.00098
14.83	12.24	443.	0.00102
15.51	12.16	459.	0.00106
16.18	12.08	476.	0.00110
16.86	12.00	491.	0.00114
17.53	11.92	507.	0.00119
18.21	11.85	522.	0.00123
18.88	11.78	538.	0.00127
19.55	11.71	552.	0.00131
20.23	11.65	567.	0.00135
20.90	11.58	582.	0.00139
21.58	11.52	596.	0.00143
22.25	11.46	610.	0.00147
22.93	11.40	624.	0.00151
23.60	11.35	637.	0.00155
24.27	11.29	651.	0.00159
24.95	11.24	664.	0.00163
25.62	11.19	677.	0.00167
26.30	11.14	690.	0.00171
26.97	11.09	702.	0.00175
27.65	11.04	714.	0.00179
28.19	11.00	724.	0.00182

******* Punch Load-Strain in concrete=.002 *******

Dalhousie Experiment:

PUNCH.RES

UNITS METRIC KN, MM, SECOND
Clear Span Between Girders= 3500.00
Diameter of Equivalent Circle for Load= 477.000
Maximum Compressive Stress of Concrete= 45.0000
Elastic Axial Stiffness of Strap= 158.000
Strap to Load Spacing= 0.000000
Depth Of Slab= 238.000
Beta to Define Rectangular Stress Block= 0.858000
Concrete Constant used for confinement= 10.0000
Area of Load Patch= 125000.
Yield strain= 0.200000E-02

DELTA	ALPHA	P	STRN
0.00	0.00	0.	0.00000
0.68	15.49	25.	0.00005
1.36	15.20	49.	0.00010
2.04	14.94	73.	0.00016
2.72	14.71	97.	0.00021
3.40	14.49	119.	0.00026
4.08	14.28	142.	0.00030
4.76	14.09	164.	0.00035
5.44	13.92	185.	0.00040
6.12	13.75	206.	0.00045
6.80	13.60	227.	0.00050
7.48	13.45	248.	0.00054
8.16	13.32	268.	0.00059
8.84	13.19	287.	0.00064
9.52	13.06	307.	0.00068
10.20	12.95	326.	0.00073
10.88	12.84	345.	0.00078
11.56	12.73	363.	0.00082
12.24	12.63	382.	0.00087
12.92	12.53	400.	0.00091
13.60	12.44	417.	0.00096
14.28	12.36	435.	0.00100
14.96	12.27	452.	0.00104
15.64	12.19	469.	0.00109
16.32	12.11	486.	0.00113
17.00	12.04	502.	0.00117
17.68	11.96	518.	0.00122
18.36	11.90	534.	0.00126
19.04	11.83	550.	0.00130
19.72	11.76	566.	0.00134
20.40	11.70	581.	0.00139
21.08	11.64	596.	0.00143
21.76	11.58	611.	0.00147
22.44	11.52	626.	0.00151
23.12	11.47	640.	0.00155
23.80	11.42	654.	0.00160
24.48	11.36	668.	0.00164
25.16	11.31	682.	0.00168
25.84	11.26	696.	0.00172
26.52	11.22	709.	0.00176
27.10	11.18	720.	0.00179

******* Punch Load-Strain in concrete=.002 *******

Appendix B - Test Vehicle Load Calculations

DATE Apr 01/98 PROJECT No. 3594 - 2

PREPARED BY: DBS PAGE No. 1 of 6

LINDQUIST CK. BRIDGE MONITORING

ON-SITE WEIGHT DETERMINATION W/ TRUCKER

33 cubic ft/cy fill } estimates
2800 #/cy gravel } by Dbd

STEERING AXLE	DRIVER TANDEM	TRAILER TANDEM	
	21' (6.34m)	23'-9" (7.24m)	
4070 kg (8975 lb) (39.9 kN)	12,280 kg (27082 lb.) (120 kN)		EMPTY TRUCK
		4552 kg (10,040 lb) (44.66 kN)	EMPTY TRAILER WHEN HOOKED TO TRUCK
7482 kg (16500 lb) (73.4 kN)	22671 kg (50,000 lb) (222.4 kN)		TRUCK WITH GRAVEL (FULL LOAD)
7482 lb (16500 lb) (73.4 kN)	26742 kg (58976 lb) (262.3 kN)	18,601 kg (41,024 lb) (182.5 kN)	TRUCK WITH GRAVEL (FULL LOAD) WITH HOE ON TRAILER HOOKED TO TRUCK

73.4 (39.9) / 33.5 gravel × 33/28 = 39.5 / 39.9 TRUCK / 79.4

222.4 (120.1) / 102.4 gravel × 33/28 = 120.7 kN TRUCK / 120.9 / 39.9 yoke / 279.9

262.3 − 222.4 =

DATE MAY/98 PROJECT No. 35794 · 2
PREPARED BY: DJS PAGE No. 2 of 6

Lindquist Bridge Monitoring

Determining wt. & wt. distribution for Truck, fully loaded with gravel, and with trailer attached, carrying a Case 9020B Excavator, whose bucket is forward over the tailgate of the truck box.

Check on trailer load:

wt. of empty trailer:
- over wheels = 4552 kg.
- over yolk:

Truck w/ gravel & hoe = 26742
Truck w/ gravel = <22671>
wt. of hoe & trailer Σ 4071 kg

But wt. of hoe & trailer on trailer tandem = 18601 kg.
DDT. wt. of empty trailer over tandem <4552 kg>
wt. of excavator on rear tandem = Σ 14049 kg
Total wt. of excavator = 16044 kg (from Case brochure)
operator = <270 kg>
15974 kg

∴ wt. of excavator over yolk = 15974 - 14049 kg.
= 1925 kg.

∴ wt. of trailer over yolk = 4017 - 1925 = 2092 kg

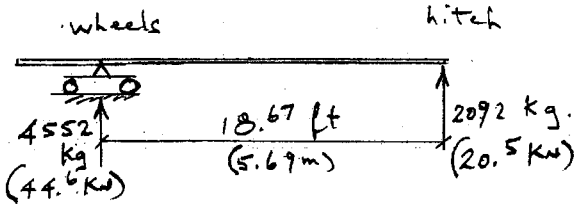

FORM 29A 05-96

DATE MAY/98 PROJECT No. 35794 - 2

PREPARED BY: DS PAGE No. 3 of 6

LINDQUIST Bridge Monitoring

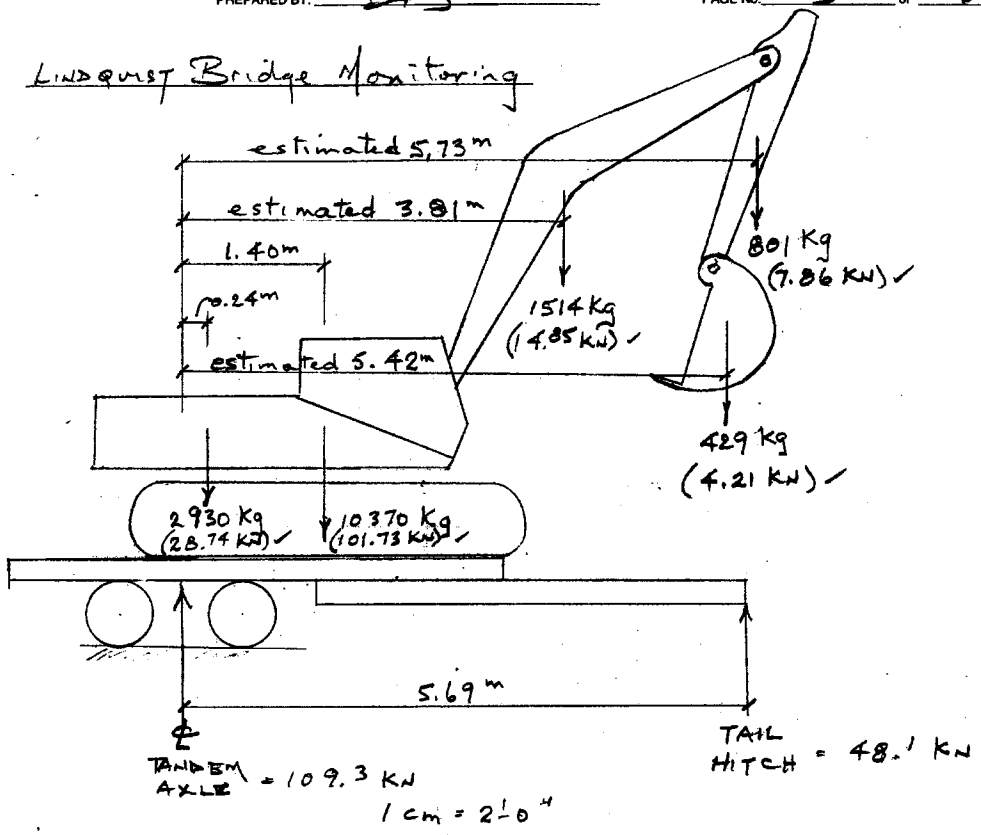

16044 (157.4 KN)

<1514>	BOOM	p. 16 of Manufacturer's Brochure
<801>	ARM	p. 9
<2930>	COUNTERWEIGHT	p. 9
<429>	BUCKET	p. 18, 19
10370 Kg		p. 19

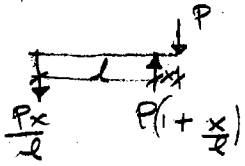

$$R_{TAIL\ HITCH} = \frac{28.74(6.24) + 101.73(1.4) + 14.85(3.81) + 4.21(5.42) + 7.86\left(1 + \frac{0.24}{5.69}\right)}{5.69}$$

$$= \frac{6.9 + 142.4 + 56.6 + 22.8 + 7.92}{5.69}$$

$$= 48.1\ KN$$

$$R_{TANDEM} = 157.4 - 48.1 = 109.3\ KN$$

DATE 1 MAY/98 PROJECT No. 35794 - 2

PREPARED BY: DDS PAGE No. 4 of 6

LINDQUIST CK. BRIDGE MONITORING

DISTRIBUTION OF TAIL HITCH LOAD TO GRAVEL TRUCK

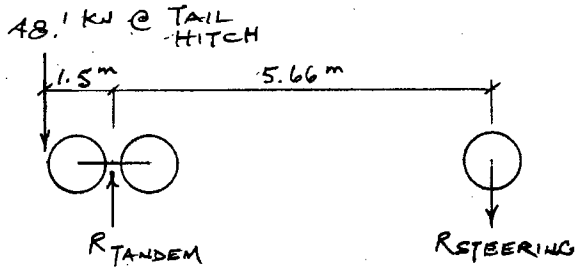

$$R_{TANDEM} = 48.1\left(1 + \frac{1.5}{5.66}\right) = 60.8 \text{ KN}$$

$$R_{STEERING} = 48.1\left(\frac{1.5}{5.66}\right) = -12.7$$

$$\Sigma \quad 48.1 \text{ KN} \quad \text{checks}$$

DATE MAY/98 PROJECT No. 35794 · 2
PREPARED BY: DDS PAGE No. 5 of 6

LINDQUIST CK. BRIDGE MONITORING

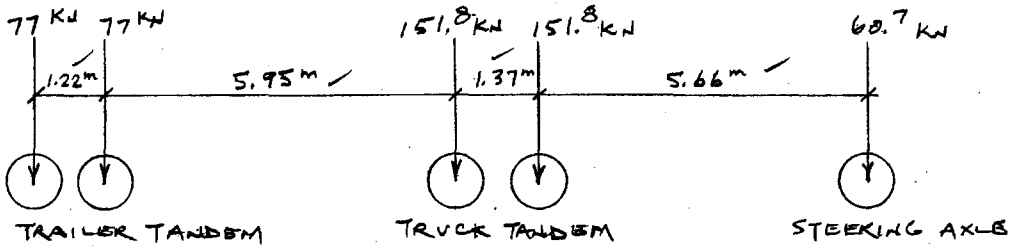

109.3	EXCAVATOR	222.4	TRUCK w/ GRAVEL	73.4 KN	
44.6	TRAILER	60.8	EXCAVATOR	-12.7	
Σ 153.9 KN		20.5	TRAILER	Σ 60.7 KN	
		Σ 303.7 KN			

check: 153.9 + 303.7 + 60.7 = 518.3 KN from above } checks ✓
vs : 182.5 + 262.3 + 73.4 = 518.2 KN from scales

$$C.G. = \frac{151.8(5.66+7.03) + 77(12.98+14.2)}{518.3} = 7.75\,m \text{ from steering axle}$$

$\frac{0.72+23.1}{2}$ =

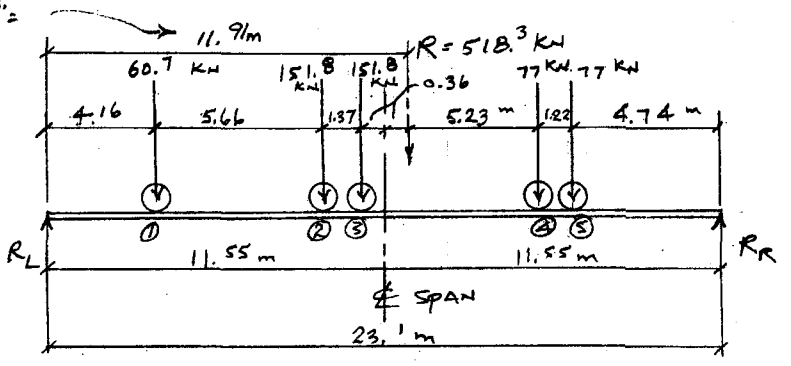

$$R_L = \frac{518.3(11.19)}{23.1} = 251.1\ KN$$

M_{max} @ axle ③ = 11.19(251.1) − 7.03(60.7) − 1.37(151.8)

= 2810 − 427 − 208 = 2175 KN·m @ 11.19 m from left end of span

checks with PC Bridge Moment = 2173.8 KN·m @ 12.0 m from end of span (or 11.0 m from opposite end)

FORM 2SA 05-96

DATE MAY/98 PROJECT No. 35794 - 2

PREPARED BY: DDS PAGE No. 6 of 6

LINDQUIST CK. BRIDGE MONITORING

Distribution Factor

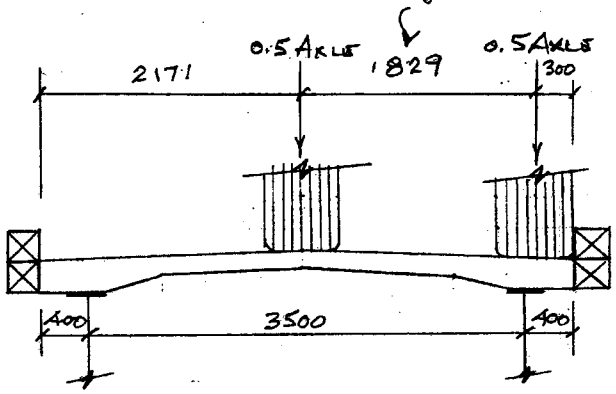

$R_L = \left(\frac{1.729}{3.5} - \frac{0.1}{3.5}\right) 0.5\,\text{AXLE}$

$= 0.233\ \text{AXLE}$

$R_R = \left(\frac{1.771}{3.5} + \frac{3.6}{3.5}\right) 0.5\,\text{AXLE}$

$= 0.767\ \text{AXLE}$

$M_L = 0.767(2175) = 1668\ \text{KN.m}$

FROM DESIGN NOTES:

L75 $M_L = 0.671(2449) = 1643\ \text{KN.m}$ ← D.F.

— COMPARABLE

Bridge Analysis by PCBRIDGE™ v2.00 05-20-1998 10:22

File (Project) Name : NEWFILE.DAT

1 Span Bridge took less than 1 minute(s) to analyze.

Span Number : 1
Span Length : 23.0
Relative EI : 1.00
Dead Load : 0.00

5 Concentrated Loads (Loads INCLUDE distribution factor of 1.00)

<spacing>|load|<spacing>|load| ...

< 0.0>| 60.70| < 5.5>|151.80| < 1.5>|151.80| < 5.5>| 77.00| < 1.5>| 77.00|

User Def Vehicle is MOVING

Bridge Dist	@ Veh Loc	MAX Reaction
0.0	-5.5L	395.8
23.0	28.5	395.8

Bridge Dist	Span No	Span Dist	@ Veh Loc	MAX +Moment	@ Veh Loc	MAX -Moment	@ Veh Loc	MAX Shear	@ Veh Loc	Deflect Coeff
0.0	1	0.0	9.5L	0.0	4.5L	-0.0	-5.0L	385.9	14.0L	-0.0
0.5	1	0.5	-5.0L	192.9	0.0	0.0	-4.5L	375.9	3.0L	-325.7
1.0	1	1.0	-4.5L	375.9	0.0	0.0	-4.0L	366.0	3.0L	-650.0
1.5	1	1.5	-4.0L	548.9	0.0	0.0	-3.5L	356.0	3.0L	-971.1
2.0	1	2.0	-3.5L	712.0	0.0	0.0	-3.0L	346.1	3.0L	-1287.8
2.5	1	2.5	-3.0L	865.2	0.0	0.0	-2.5L	336.1	3.0L	-1598.3
3.0	1	3.0	-2.5L	1008.4	0.0	0.0	-2.0L	326.2	3.0L	-1901.3
3.5	1	3.5	-2.0L	1141.6	0.0	0.0	-1.5L	316.2	3.0L	-2195.2
4.0	1	4.0	-1.5L	1264.9	0.0	0.0	-1.0L	306.3	3.0L	-2478.8
4.5	1	4.5	-1.0L	1378.3	0.0	0.0	-0.5L	296.3	3.0L	-2750.9
5.0	1	5.0	-0.5L	1481.7	0.0	0.0	0.0L	286.4	3.0L	-3010.3
5.5	1	5.5	0.0L	1575.1	0.0	0.0	0.5L	275.1	3.0L	-3255.9
6.0	1	6.0	0.5L	1681.0	0.0	0.0	1.0L	263.8	3.0L	-3486.4
6.5	1	6.5	1.0L	1775.7	0.0	0.0	1.5L	252.6	3.0L	-3700.6
7.0	1	7.0	1.5L	1859.1	0.0	0.0	2.0L	241.3	3.5L	-3897.6

NOTE:SHEAR values are calculated just to the
LEFT of Bridge or Span Dist(ance) for vehicles facing right and
RIGHT of Bridge or Span Dist(ance) for vehicles facing left.

NEWFILE.DAT Bridge Analysis by PCBRIDGE tm v2.00 05-20-1998 10:22

Bridge Dist	Span No	Span Dist	@ Veh Loc	MAX +Moment	@ Veh Loc	MAX -Moment	@ Veh Loc	MAX Shear	@ Veh Loc	Deflect Coeff
7.5	1	7.5	2.0L	1931.2	0.0	0.0	2.5L	230.0	3.5L	-4078.2
8.0	1	8.0	2.5L	1992.1	0.0	0.0	3.0L	218.8	3.5L	-4239.7
8.5	1	8.5	3.0L	2041.7	0.0	0.0	3.5L	207.5	3.5L	-4380.8
9.0	1	9.0	3.5L	2080.0	0.0	0.0	4.0L	196.2	3.5L	-4500.4
9.5	1	9.5	2.5L	2109.5	0.0	0.0	4.5L	185.0	3.5L	-4597.5
10.0	1	10.0	3.0L	2142.2	0.0	0.0	5.0L	173.7	3.5L	-4671.7
10.5	1	10.5	3.5L	2163.6	0.0	0.0	5.5L	162.4	4.0L	-4726.1
11.0	1	11.0	4.0L	2173.8	0.0	0.0	6.0L	151.2	4.0L	-4757.8
11.5	1	11.5	4.5L	2172.7	23.0L	0.0	6.5L	139.9	4.0L	-4766.1
12.0	1	12.0	19.0	2173.8	23.0L	0.0	17.0	151.2	19.0	-4757.8
12.5	1	12.5	19.5	2163.6	23.0L	0.0	17.5	162.4	19.0	-4726.1
13.0	1	13.0	20.0	2142.2	23.0L	0.0	18.0	173.7	19.5	-4671.7
13.5	1	13.5	20.5	2109.5	23.0L	0.0	18.5	185.0	19.5	-4597.5
14.0	1	14.0	19.5	2080.0	23.0L	0.0	19.0	196.2	19.5	-4500.4
14.5	1	14.5	20.0	2041.7	23.0L	0.0	19.5	207.5	19.5	-4380.8
15.0	1	15.0	20.5	1992.1	23.0L	0.0	20.0	218.8	19.5	-4239.7
15.5	1	15.5	21.0	1931.2	23.0L	0.0	20.5	230.0	19.5	-4078.2
16.0	1	16.0	21.5	1859.1	23.0L	0.0	21.0	241.3	19.5	-3897.6
16.5	1	16.5	22.0	1775.7	23.0L	0.0	21.5	252.6	20.0	-3700.6
17.0	1	17.0	22.5	1681.0	23.0L	0.0	22.0	263.8	20.0	-3486.4
17.5	1	17.5	23.0	1575.1	23.0L	0.0	22.5	275.1	20.0	-3255.9
18.0	1	18.0	23.5	1481.7	23.0L	0.0	23.0	286.4	20.0	-3010.3
18.5	1	18.5	24.0	1378.3	23.0L	0.0	23.5	296.3	20.0	-2750.9
19.0	1	19.0	24.5	1264.9	23.0L	0.0	24.0	306.3	20.0	-2478.8
19.5	1	19.5	25.0	1141.6	23.0L	0.0	24.5	316.2	20.0	-2195.2
20.0	1	20.0	25.5	1008.4	23.0L	0.0	25.0	326.2	20.0	-1901.3
20.5	1	20.5	26.0	865.2	23.0L	0.0	25.5	336.1	20.0	-1598.3
21.0	1	21.0	26.5	712.0	23.0L	0.0	26.0	346.1	20.0	-1287.8
21.5	1	21.5	27.0	548.9	23.0L	0.0	26.5	356.0	20.0	-971.1
22.0	1	22.0	27.5	375.9	23.0L	0.0	27.0	366.0	20.0	-650.0
22.5	1	22.5	28.0	192.9	23.0L	0.0	27.5	375.9	20.0	-325.7
23.0	1	23.0	13.5	0.0	18.5	-0.0	28.0	385.9	9.0	-0.0

NOTE:SHEAR values are calculated just to the
LEFT of Bridge or Span Dist(ance) for vehicles facing right and
RIGHT of Bridge or Span Dist(ance) for vehicles facing left.

Appendix C - MATLAB Alogrithm

B.1 Crack Growth Simulation

```
%%%%%ARCHPANELSIMLOGNORM.m%%%%%
% 'ARCHPANELSIMLOGNORM.m' simulates the stochastic lognormal CMOD process
% that describes the deterioration of first generation concrete ArchPanel bridge decks.
% NOTE: THIS IS A FIRST VERSION OF THIS PROGRAM AND AS SUCH HAS
% NOT BEEN THOROUGHLY TESTED.  November 8th 2004
%=========================================================
% The basic stochastic lognormal parameters:
%%%%%%%%%%%%%%%%%%%%%%%%%%%%%%%%%%%%%%%%%%%%%%%%%%%%%%%%
xi = 1.21052E-05;                  % Correlation coefficient: 1/(axle sets)
c = 5.02045E-22; m = 3.00;         % The ArchPanel deck concrete's coefficient and
                                   % exponent
var = 7.4825E-008;                 % Variance of normal Z = log(X) process
ainitial = 2.504e-004;             % Mean of initial CMOD distribution: meters
deltasigma1 = 2.35e+006;           % 'Standard' stress ranges applied to ArchPanel deck
deltasigma2 = 2.16e+006;
deltasigma3 = 2.01e+006;
deltasigma4 = 1.70e+006;
deltasigma5 = 1.54e+006;
sim_number = 23;                   % Number of lognormal simulations
maxmonths = 100;                   % Maximum number of months chosen for this
                                   % simulation
naxles = 185;                      % Number of axle sets crossing ArchPanel per month
filename = 'ArchPanel';
% Opening memory:
at = zeros(sim_number,naxles*maxmonths); dat =
zeros(sim_number,naxles*maxmonths);
dk = zeros(sim_number,naxles*maxmonths); p = zeros(sim_number,naxles*maxmonths);
%%%%%%%%%%%%%%%%%%%%%%%%%%%%%%%%%%%%%%%%%%%%%%%%%%%%%%%%
% Part 1:  Generation of the random numbers
%%%%%%%%%%%%%%%%%%%%%%%%%%%%%%%%%%%%%%%%%%%%%%%%%%%%%%%%
stdz = sqrt(var);                  % Standard deviation of Z's variance
randn('state',sum(100*clock))      % Reset of MATLAB's random number
                                   % generator
p = randn(sim_number,naxles*maxmonths); % Random numbers generated from the
                                   % standard
                                   % variate N(0,1) = N(mean,variance).
p = stdz*p;                        % Convertion to N(0,var) numbers for
                                   % normal Z
```

```
%%%%%%%%%%%%%%%%%%%%%%%%%%%%%%%%%%%%%
% Part 2: Generate sample functions of 'dk' and 'delta'
%%%%%%%%%%%%%%%%%%%%%%%%%%%%%%%%%%%%%
astdz = ainitial + exp(stdz) - 1.0;      % Upper truncation cut-off value of at
for sf = 1:sim_number
  at(sf,1) = ainitial + exp(p(sf,1)) - 1.0;
  if at(sf,1) <= astdz
    at(sf,1) == at(:,1);
  else
    at(sf,1) = ainitial;
  end
  if at(sf,1) >= 1.0e-020              % Lower truncation cut-off value of at
    at(sf,1) == at(:,1);
  else
    at(sf,1) = ainitial;
  end
  for mon = 1:maxmonths
    if mon == 1
      taum = 1 + ((mon - 1)*naxles);
    else
      taum = (mon - 1)*naxles;
    end
    for tau = (taum + 1):naxles*mon
      if tau <= taum + 3
        deltasigma = deltasigma1;
      else
        if tau <= taum + 35
          deltasigma = deltasigma2;
        else
          if tau <= taum + 110
            deltasigma = deltasigma3;
          else
            if tau <= taum + 157
              deltasigma = deltasigma4;
            else
              deltasigma = deltasigma5;
            end
          end
        end
      end
      dk(sf,(tau - 1)) = deltasigma*(sqrt(at(sf,(tau - 1))));   % Stress intensity range
      dat(sf,(tau - 1)) = exp(p(sf,(tau - 1)))*c*(dk(sf,(tau - 1))^m); % Random CMOD
                                                                        % growth
      at(sf,tau) = at(sf,(tau - 1)) + dat(sf,(tau - 1));       % Incremental growth in CMOD
      if at(sf,tau) >= 4e-003         % Cut-off number well above 'knuckle'
        at(sf,tau) = 4e-003;
```

```
        else
          at(sf,tau) = at(sf,tau);
        end
        p(sf,tau) = p(sf,(tau - 1))*exp(-xi); % Change in Z = p*exp(-xi*1);
      end
    end
  end
  M9614 = mean(at(:,9614))
  V9614 = (std(at(:,9614)))^2
  %%%%%%%%%%%%%%%%%%%%%%%%%%%%%%%%%%%
  % Part 3: Calculate mean and variance and store in: '< >.log_mean_var'
  %%%%%%%%%%%%%%%%%%%%%%%%%%%%%%%%%%%
  M = mean(at(:,:)); S = std(at(:,:)); V = S.^2;
  lmv = [M; V];
  fid = fopen([filename '.log_mean_var'],'w'); % Plotted by: 'PLOT_SIMLOG.m'
    fprintf(fid,'%e %e\n', lmv);            % and used by 'ARCHPANELRELIABILITY.m'
  fclose(fid);
  disp('The lognormal simulation is complete: the growth in CMOD may now be plotted')
  %%%%%%%%End of ARCHPANELSIMLOGNORM.m%%%%%%%%
```

A.2 The Reliability Assessment Algorithm

```
%%%%%ARCHPANELRELIABILITY.m%%%%%
% 'ARCHPANELRELIABILITY.m' takes the output from
ARCHPANELSIMLOGNORM.m,
% namely 'filename'.log_mean_var and establishes a reliability estimate for
% ArchPanel bridge decks. NOTE: THIS IS A FIRST VERSION OF THIS PROGRAM
% AND AS SUCH SHOULD BE THOROUGHLY CHECKED PRIOR TO FURTHER
% USE. November 8th 2004
%%%%%%%%%%%%%%%%%%%%%%%%%%%%%%%%%%%%
% Parameters establishing 'knuckle'
afailure = 957;        % (#) identifying knuckle CMOD state
da = 3.5e-006;         % meters
aknuckle = ainitial + afailure*da;
Rstar = 0.98;
%%%%%%%%%%%%%%%%%%%%%%%%%%%%%%%%%%%%
% Initial values of local arrays
MEAN = zeros(1,naxles*maxmonths); DEVIATION = zeros(1,naxles*maxmonths);
POF = zeros(1,naxles*maxmonths); RELI = zeros(1,naxles*maxmonths);
%%%%%%%%%%%%%%%%%%%%%%%%%%%%%%%%%%%%
% Reading the 'mean' and 'standard deviation' generated by
ARCHPANELSIMLOGNORM.m
fid = fopen([filename '.log_mean_var']);
  log_mean_var = (fscanf(fid,'%f',[2,inf]))';
fclose(fid);
MEAN(:) = log_mean_var(:,1);  DEVIATION(:) = log_mean_var(:,2).^0.5;
% MEAN & DEVIATION are [1,naxles*maxmonths] arrays
%%%%%%%%%%%%%%%%%%%%%%%%%%%%%%%%%%%%
% Step 1:  Generating the Type 1 ArchPanel deck reliabilities
%%%%%%%%%%%%%%%%%%%%%%%%%%%%%%%%%%%%
for T = 1:naxles*maxmonths
  MU = num2str(MEAN(T)); SIGMA = num2str(DEVIATION(T));
  delta = ainitial:da:(ainitial + naxles*maxmonths*da);
  FF = inline(strcat('normpdf(delta,',MU,',',SIGMA,')'));
  POF(T) = quadl(FF,aknuckle,(ainitial + naxles*maxmonths*da));
  RELI(T) = 1.0 - POF(T);
  if RELI(T) >= Rstar
    RELI(T) = RELI(T);
  else
    RELI(T) = 1.0;
  end
end
```

```
%%%%%%%%%%%%%%%%%%%%%%%%%%%%%%%%%%
% Step 2: Preparing files for plotting
%%%%%%%%%%%%%%%%%%%%%%%%%%%%%%%%%%
z = [t;RELI];
fid=fopen([ filename '.reli_prob'],'w');
  fprintf(fid,'%g\t %g\n', z);
  fclose(fid);
disp('The reliability of Type 1 ArchPanel decks is now established: please plot the
results.')
%%%%%%%%End of  ARCHPANELRELIABILITY.m%%%%%%%%
```